ABSTRACT

Title of Document: SULFUR ISOTOPE FRACTIONATIONS IN
                          BIOLOGICAL SYSTEMS: INSIGHT INTO
                          THE PROTEROZOIC BIOSPHERE

                          David T. Johnston, Ph.D. 2007

Directed By: Professor J. Farquhar, Department of Geology
                          and ESSIC

This study focuses on developing a framework for interpreting isotopic fractionations

in the four stable sulfur isotopes, with a special focus on microbial effects.

Calculations of low temperature equilibrium fractionations between various sulfur

species were performed and suggest a tightly constrained fractionation relationship

between the isotopes. This work was followed by conducting a series of batch culture

experiments with two prominent sulfur metabolisms: sulfate reduction and sulfur

disproportionation. The results of these experiments illustrate that measurable

deviations from the equilibrium predictions exist, and further serve to highlight the

ability of these measurements to differentiate between fractionations produced by

these two metabolisms. This is a distinction not possible from traditional isotope

measurements alone ($^{34}S/^{32}S$). In addition, models constructed to describe these

observations provide insight into the intra-workings of these metabolic pathways,

with the most recent experiments suggesting that the traditionally accepted model for

isotope fractionation produced by sulfate reducers be re-evaluated. The microbial

fractionations were also used to calibrate global sulfur cycle box models. These

models have been coupled with the measurement of natural samples to illustrate the

onset of microbial disproportionation ~800 million years earlier in Earth history than

previously thought and to describe the sulfur cycle of three Proterozoic marine basins.

SULFUR ISOTOPE FRACTIONATIONS IN BIOLOGICAL SYSTEMS:
INSIGHT INTO THE PROTEROZOIC BIOSPHERE

By

David T. Johnston

Dissertation submitted to the Faculty of the Graduate School of the
University of Maryland, College Park, in partial fulfillment
of the requirements for the degree of
Doctor of Philosophy
2007

Advisory Committee:

Professor James Farquhar, Chair
Professor Alan J. Kaufman
Professor William McDonough
Dr. Marilyn Fogel
Dr. Donald E. Canfield

Preface

Much of the work presented in this thesis was previously published as a collection of peer-reviewed journal articles. I am grateful to the efforts and comments of all my co-authors on those studies, as their contributions made the papers both stronger and broader in scope. Chapters 1, 3, 6, and 7 represent original contributions, and the references for the remaining chapters are listed below (though all chapters have been modified from their original published form). Copyright approval has been granted for the republication of this material, and is available upon request.

Chapter 5:
David T. Johnston, Simon W. Poulton, Philip W. Fralick, Boswell A. Wing, Donald E. Canfield, James Farquhar (2006). Evolution of the Oceanic Sulfur Cycle at the end of the Paleoproterozoic. *Geochimica et Cosmochimica Acta*. vol. 70, p. 5723-5739.

The final stages of this project were funded by the University of Maryland, Graduate School Dean's Dissertation Fellowship (Fall 2006).

Dedication

I dedicate this work in memory of Robert A. Miller: not only my grandfather, but also

a mentor, friend, and eternal fishing buddy.

In addition, this work is dedicated to my family. The never-ending support that they

have all provided has allowed me to pursue this degree with a focus that only comes

with true encouragement and support. To my Mom and Dad, I cannot begin to

express the debt that I owe you both for standing at my side during both the rainy and

sunny days. Even though you both thought it crazy when I expressed my interest in

pursuing my Ph.D., you quickly jumped on board. The respect that you had for my

decisions and goals has shaped me as a person and is a trait that I only hope I can

adopt. The love and friendship that you have both provided inspires me everyday,

and drives me to succeed and make you proud. And to Greg, my brother and best

friend. You were always my favorite outlet from the rigors of this degree. I would

have visited you wherever you landed, but I cannot thank you enough for your

hospitality during those long winter trips west. Those couple of weeks would keep

me working the rest of the year.

Acknowledgements

who passed through the doors of 407 Beech Ave, I also give my thanks. That house quickly, and as a function of the personalities that filled it, took on a personality of its own and was a fantastic place to live (and hide from the lab). Lastly, in my opinion, science is best done in a social and happy work environment. With this in mind, I would like to acknowledge and thank all the grad students who have come and gone during my time at Maryland. A special thanks to the early days of the Craig Hebert era. I am also very thankful for the friendship and constant source of amusement that was GEOL office 4105 from 2002-05 (Yes Courtney and Leah, we are <u>still</u> WE). From the long-haul folks (here is looking at you Ireland-Reno et al.) to those in the new school, I thank you.

Table of Contents

List of Tables

List of Figures

Chapter 1: Introductions and historical perspectives

Sulfur in the Earth system

The geologic sulfur isotope record represents one of the most robust and informative indicators of Earth surface change. This record carries a wealth of information because of the role and importance of sulfur, as an element, in surface processes. In part, sulfur serves as an effective tracer due to the wide range of reduction-oxidation (redox) states, spanning from the oxidized end-member sulfate (SO_4^{2-}: +6) to the reduced hydrogen sulfide (H_2S: -2). In addition, sulfur is poly-isotopic, which greatly contributes to the potential for this elemental system to carry information. The wide range of redox states promotes cycling in surface environments and catalyzes the production of a large range of isotopic fractionations, which span from +130‰ to -60‰ in $\delta^{34}S$ (Coplen et al., 2002). Further, if one considers the magnitude of an isotope effect (up to 190 ‰ in $\delta^{34}S$) and the analytical uncertainties on such a measurement (often ~ 0.20 ‰ using a SO_2 combustion technique), the interpretability and capability of this isotope system to record information is further revealed.

Before I can consider the details of the sulfur isotope system, I must understand the isotopes, their abundances, and their distribution in the Earth environment. Sulfur has four stable isotopes (^{32}S, ^{33}S, ^{34}S, ^{36}S). The stable isotopes vary greatly in abundance on Earth, with the following distribution: ^{32}S = 94.93, ^{33}S = 0.76, ^{34}S = 4.29, and ^{36}S = 0.02% (Coplen et al., 2002). The most heavily studied isotope relationship is the ratio between ^{34}S and ^{32}S, often described using $\delta^{34}S$ (delta notation is a measure of

the deviation of the ratio of ^{34}S to ^{32}S in a sample, compared to that of a standard, and

noted in parts per thousand or ‰: see Chapter 2 for full definition) due in large part to

the high relative abundances and subsequent analytical ease in their measurement.

The present study also includes analysis of ^{33}S and ^{36}S abundances, provides a

theoretical framework for their interpretation, and focuses on the use of these isotopes

in understanding natural systems.

Metabolic process	additional info.	e^- acceptor/donor	redox pair	‰	refs
Sulfate Reduction	dissimilatory	hydrogen	$SO_4 - H_2S$	37.8	1
		organics	$SO_4 - H_2S$	47	2
	assimilatory		$SO_4 - H_2S$	2.8	3
Sulfide Oxidation	phototrophic	light	$H_2S - S^o$	2	4
		light	$S^o - SO_4$	0	5
	non-phototrophic	O_2, NO_3	$H_2S - S^o$	1	3
		O_2, NO_3	$S^o - SO_4$	0	4
		O_2, NO_3	$SO_3 - SO_4$	0	4
Sulfur Disproportionation	elemental sulfur		$S^o - SO_4, H_2S$	38	6
	sulfite		$SO_3 - SO_4, H_2S$	55	7
	thiosulfate		$S_2O_3 - SO_4, H_2S$	11	7
	tetrationate		$S_4O_6 - SO_4, S_3O_6$	?	8

Table 1: A list of sulfur utilizing metabolic processes and the associated isotopic fractionation in $^{34}S/^{32}S$ (modified from Canfield, 2001). The fractionations represent the largest isotopic fractionation known for that process. Processes that are not included are thought to proceed through various intermediate reactions, most of which are included above. Values of zero suggest a fractionation < 1 ‰, whereas "?" represents a metabolism where isotope studies have not been conducted. References are: 1) Hoek et al. (2006), 2) Harrison and Thode (1958), 3) Kaplan and Rittenburg (1964), 4) Fry et al. (1986) 5) Fry et al. (1988), 6) Habicht et al. (1998), and 7) Wentzien and Sand (2004). This list is not exhaustive, and the reader is referred to Canfield (2001) for a more thorough review.

There are a variety of pathways and processes involved in the cycling of sulfur on the

Earth's surface, with some having a greater geologic relevance than others. The most

prominent of these processes are biological, as microorganisms play an important role

in the cycling of sulfur and impart large isotopic fractionations. These fractionations

are often used to track biological activity in an environment or through time. One

fate of sulfur in the biosphere is assimilation for biosynthesis. The organic sulfur

reservoir is generally taken to be quantitatively unimportant and is often disregarded.

The more commonly considered biological sulfur cycle is that of catabolic or

dissimilatory processes. These processes utilize the eight-electron sulfur redox

gradient to gain energy and fuel metabolic activity. Below I provide a general list of

the prominent metabolisms and associated isotopic fractionations.

To date, experimental studies with the above metabolisms indicate that sulfate

reduction and sulfur disproportionation produce the largest isotope fractionations.

This is in part due to the large change in the redox state of the reactants and products,

as both metabolisms cover the full range (8 electron transfer). Although equilibrium

isotope fractionations are also suggested to be capable of producing large

fractionations, they are generally not expressed (Ohmoto, 1986). Laboratory

experiments of natural sediments (cf. Canfield, 2001b) have extensively documented

the large metabolic fractionations, thus biology is used to explain the observed

geologic isotope record. Of these many different metabolic processes, sulfate

reduction is thought to be the most prominent process and have the deepest geologic

root (Shen et al., 2001). The terminal electron acceptor for this metabolism, sulfate, is

the second most abundant anion in the modern ocean at ~ 29mM (Jorgensen and

Kasten, 2006). From this, it is easy to understand how sulfate reduction has come to

play the role that it does, providing over 50% of the energy for organic carbon re-

mineralization in modern marine sediments (Jorgensen and Kasten, 2006).

Conversely, sulfur disproportionation reactions do not have as strong a link to the

carbon cycle, utilize more trace sulfur redox intermediates, and are thus relegated to a

less prominent role in the biogeochemistry of marine environments.

The geologic record, insights from $\delta^{34}S$:

The sulfur isotope record has long been targeted to pinpoint large-scale changes in the

global climate and redox state. A recent compilation of $\delta^{34}S$ record is presented in

Figure 1 (modified from Canfield, 2001). The $\delta^{34}S$ composition of the bulk Earth is

inferred to be approximately 0‰ (Thode, et al., 1961; Ohmoto, 1986) and is the

original input to the Earth surface environment. In Figure 1, the diamond symbols
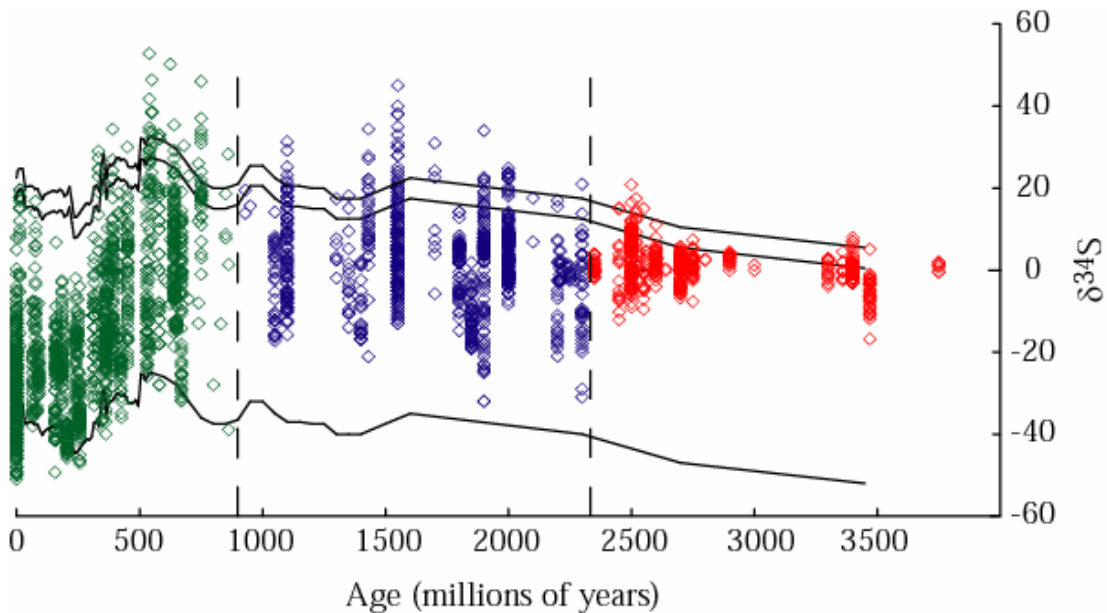
Figure 1: A compilation of sedimentary sulfide $\delta^{34}S$ versus time, modified from Canfield (2001). The definition of 'δ' is found later in the text. All the diamonds represent measurements of sedimentary sulfides. The two upper bounding lines represent model approximations for the isotopic composition of seawater sulfate, whereas the lower bounding line is a reference line offset by -55 ‰. The record is divided into three stages, separated by black dashed lines. The red data describes an anoxic Archean sulfur cycle; the blue data represents an intermediate (partially oxygenated) sulfur cycle, with the green data illustrating what is thought of as a modern sulfur cycle.

represent measurements of sedimentary sulfides. The uppermost two lines extending through the record represent model estimates of the seawater sulfate composition and bracket a 5‰ window. Offset by -55‰ is an additional line that is used for reference on the magnitude of deviation from seawater. This record is traditionally divided into three stages, which correspond to the three dominant stages, or redox conditions of the Earth's surface. I begin with a description of these subdivisions.

The first stage extends through the Archean and into the earliest Proterozoic, and is characterized by a small range of isotopic compositions. The isotopic difference between estimates of seawater sulfate and sulfide are generally less than ~ 10‰ and vary round a bulk Earth composition of ~ 0‰ (Canfield et al., 2000). Archean inputs into surface environments are thought to be dominated by volcanic and hydrothermal inputs of SO_2 and H_2S to the atmosphere and oceans. Many processes, including a range of inorganic mechanisms, are capable of producing the small fractionations seen in the Archean record. The small fractionations are also interpreted as providing information about relationship between the sulfur cycle and biosphere. Experimental evidence suggests that the range of fractionations seen in the Archean is indicative of the activity of sulfate reducing microorganisms operating under low oceanic sulfate concentrations (< 200 µM: Habicht et al., 2002). Further, evidence suggests that sulfate reduction was active back to 3450 Mya (Millions of Years Ago), corroborating this hypothesis (Shen et al., 2001). Shen and colleagues observed fractionations of ~ 24‰ between bedded evaporites and evaporite hosted pyrite crystals in the 3450 Ma Dresser Fm., North Pole Australia, suggesting both the

activity of sulfate reduction (to produce the observed fractionation) and elevated

sulfate concentrations (> 200uM), to allow for larger biological fractionations and as

a source for the evaporites. The interpretation of the Dresser Formation as recording

a biological signature has, however, been contested (for a review, see Shen and

Buick, 2004). Debate aside, the Archean δ^{34}S record does provide valuable insight

into the activity of the sulfur cycle at that time.

At ~ 2400 Mya, the range of sulfur isotope fractionation increased significantly from

< 10 ‰ to > 40‰. This change was in response to global climatic events and the

postulated "Great Oxidation Event" (see Holland, 2006 for a review). Widespread

geologic evidence now exists from multiple continents for this profound change in the

Earth environment (Karhu and Holland, 1996; Bekker et al., 2004; Kopp et al., 2005).

The most direct consequence of surface oxygenation on the sulfur cycle was the

activation of oxidative weathering, mobilizing terrestrial sulfides. Prior to 2400 Mya,

atmospheric oxygen levels are believed to have been too low to oxidize continental

sulfur (as pyrite). However, as a result of oxidative weathering, the marine reservoir

would have been flooded with igneous-derived sulfur. These events increased the

seawater sulfate reservoir to a level greater than 200 μM, resulting in larger isotopic

fractionations being expressed by sulfate reducers. For the following ~ 1400 Ma

(Million years), the observed range of isotopic fractionations bordered on an upper

limit of ~ 45‰, matching the experimental limit of sulfate reducing microorganisms.

The remarkable monotony of the observed Proterozoic record, and the consistency

with the observed limit for sulfate reducers led to the suggestion that sulfate reduction dominated the marine sulfur cycle during this period.

The increased size of the marine sulfur reservoir from oxidative weathering and the steady production of hydrogen sulfide (the by-product of sulfate reduction) may have driven a significant change in the chemistry of the deep ocean during the "monotonous" 1400 Ma following the GOE. The interplay between the production and burial of sulfide versus the production and re-oxidation of sulfide to sulfate, strongly influences (in addition to the carbon cycle) the amount of atmospheric oxygen over geologic timescales (Canfield, 2004). During the Archean and early Paleoproterozoic, evidence from expansive banded iron formations points to an anoxic and ferruginous (Fe^{2+} rich) deep-ocean. However, as Canfield (1998) suggested, the production of sulfide in the ocean slowly titrated the available iron, and once the iron pool became depleted, sulfide began to accumulate in the deep ocean water column. This condition may have characterized a majority of the Proterozoic. Using a new iron speciation approach (Poulton and Canfield, 2005), the transition from ferruginous to sulfidic deep-ocean conditions was identified in the 1840 Mya Animike Basin, North America (Poulton et al., 2004). Further support was given to the sulfidic ocean hypothesis with the basin analysis studies of Shen et al. (2002, 2003), which illustrated the presence of sulfidic conditions in the middle Proterozoic McArthur Basin of Australia.

The second increase in the observed range of fractionations is seen at ~ 800 Mya, recorded in sulfides from the Chuar Gp., Grand Canyon and extends through the entirety of the Phanerozoic. This transition precedes the first of the postulated Neoproterozoic snowball glaciations, suggesting that the biospheric change that promoted the production of larger $\delta^{34}S$ fractionations was not related to the ice ages, but could however, be related to the early emergence of an environmental condition that eventually resulted in glaciation. Association to climate aside, the increase in the magnitude of fractionation was originally thought to be associated with the oxidation of the deep ocean, the activation of non-photosynthetic sulfide oxidizing microorganisms, and the onset of sulfur disproportionation reactions (Canfield and Teske, 1996; Canfield, 1998). As indicated above (Table 1), disproportionation is capable of producing much larger fractionations than sulfate reduction alone. More recent studies track the coupled co-variation in sulfate and sulfide, which indicate that the isotopic difference between the two reservoirs may not have increased beyond ~ 47 ‰ until the terminal Neoproterozoic (Hurtgen et al., 2002, 2005; Fike et al., 2006; Canfield et al., 2007). The measurement of ^{33}S and ^{36}S is used to directly address the onset of disproportionation in Chapters 4-6.

Mass-dependent fractionations:

A vast majority of natural isotope fractionating processes result in mass-dependent fractionations. These fractionations are controlled by the relative mass difference between the isotopes, and the effects are observable in elemental systems with more than two stable isotopes. In the sulfur isotope system, which has four stable isotopes,
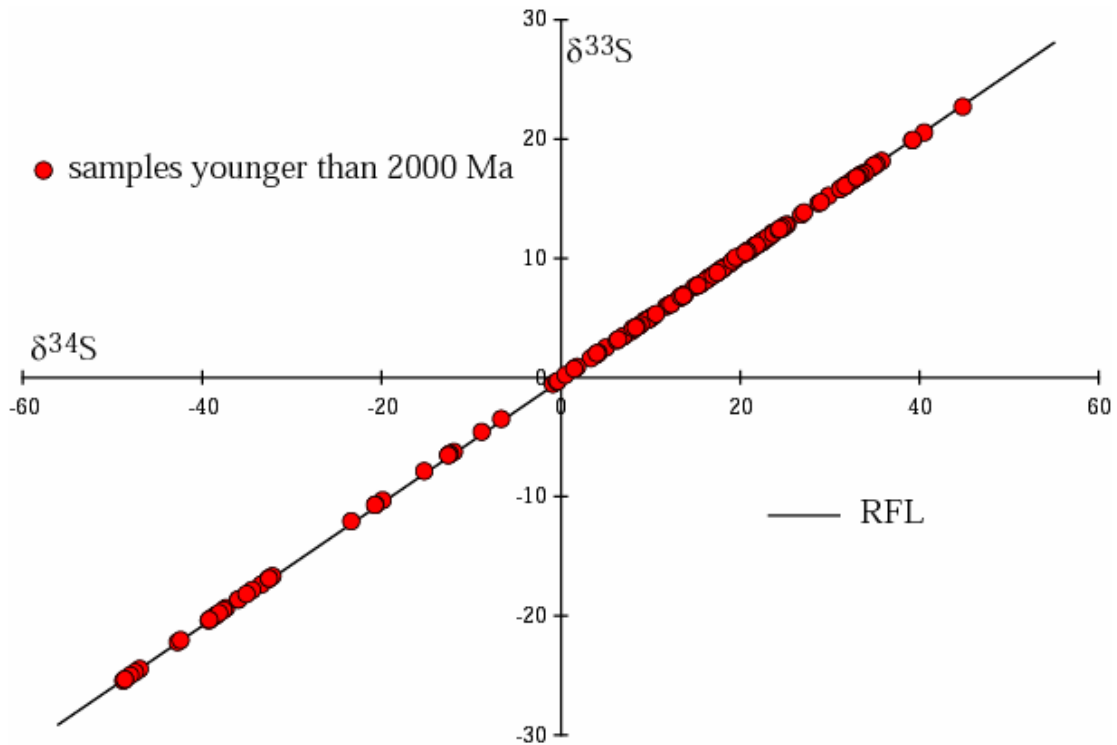
Figure 2: A plot of δ^{33}S versus δ^{34}S illustrating the principle of mass-dependent fractionation. Samples plotted are both from this dissertation and unpublished UMd data. Definitions of 'δ' are presented later in the text. Samples are from environments younger than 2000 Ma. All samples are from this study, with additional unpublished data from modern marine environments. The 'RFL' represents the *reference fractionation line*, which has a slope of 0.515. Though shown for δ^{33}S versus δ^{34}S, the same relationship could be illustrated in δ^{36}S versus δ^{34}S, which would plot along a RFL value of ~ 1.90.

the relative mass difference between ^{32}S and ^{33}S (^{32}S is the most abundant and therefore the reference isotope) is 1 atomic mass unit (AMU), whereas the difference between ^{32}S and ^{34}S is 2 AMU. When these differences are compared, the relationship between the magnitude of fractionation in δ^{33}S and δ^{34}S is roughly 1AMU/2AMU or 0.515. Figure 2 illustrates the mass-dependent fractionation relationship for δ^{33}S and δ^{34}S. The same principles hold for the other sulfur isotope relationship (^{34}S vs.^{36}S) and results in a line of slope ~ 1.90. Since these fractionations are controlled by mass and physical chemistry, they are tightly constrained. Even though there exists a tight isotopic correlation, some small-scale variability can be measured. The variability in

δ values generally occurs at the sub-percent level and can be a function of process (ie. kinetic, equilibrium, etc.) conditions (ie. temperature, molecules involved, etc.), or a combination of multiple factors. This variability can result in the production of isotope effects in ^{33}S and ^{36}S that deviate slightly from a single reference array (see Chapter 2 for details). These small deviations provide information about the process(es) and/or conditions that promoted the isotopic fractionation. It is these small, but resolvable, signatures that this dissertation sets out to better understand.

The minor isotopes (^{33}S and ^{36}S) enter the scene:

Until the late 1990's, the measurement and subsequent interpretation of the least abundant stable sulfur isotopes (^{33}S and ^{36}S) had been restricted to the field of cosmochemistry and the study of meteorites (Hulston and Thode, 1965; Thiemens 1999, 2006). Those pioneering works date back to the 1960's and provide a backdrop for all the work in this dissertation. Fast-forward three decades and in 1999, a post-doc working with Dr. Mark Thiemens at UCSD began measuring Archean rocks in hopes of finding the earliest signs of microbial sulfate reduction. Instead of finding a diagnostic inorganic biomarker, Dr. James Farquhar found the fingerprint of an anoxic atmosphere: mass-independent sulfur isotope fractionations, an effect that left its imprint on the geologic record until ~ 2400 Mya (Farquhar et al., 2000). The search for biological signatures continued however, with early measurements of laboratory experiments run with *Archeaglobus fulgidus* (a sulfate reducing microorganism) suggesting that the fractionations produced by biology were mass-dependent and differed from both that of equilibrium and the reference fractionation

array. This simple observation and the implications therein spurred much of the work included in this dissertation. With the presence of mass-independently fractionated sulfur in the Archean, the target environments for the application of mass-dependent systematics, such as shown in Figure 2, is the post-2400 Mya world (or Stage II and III of Figure 3).
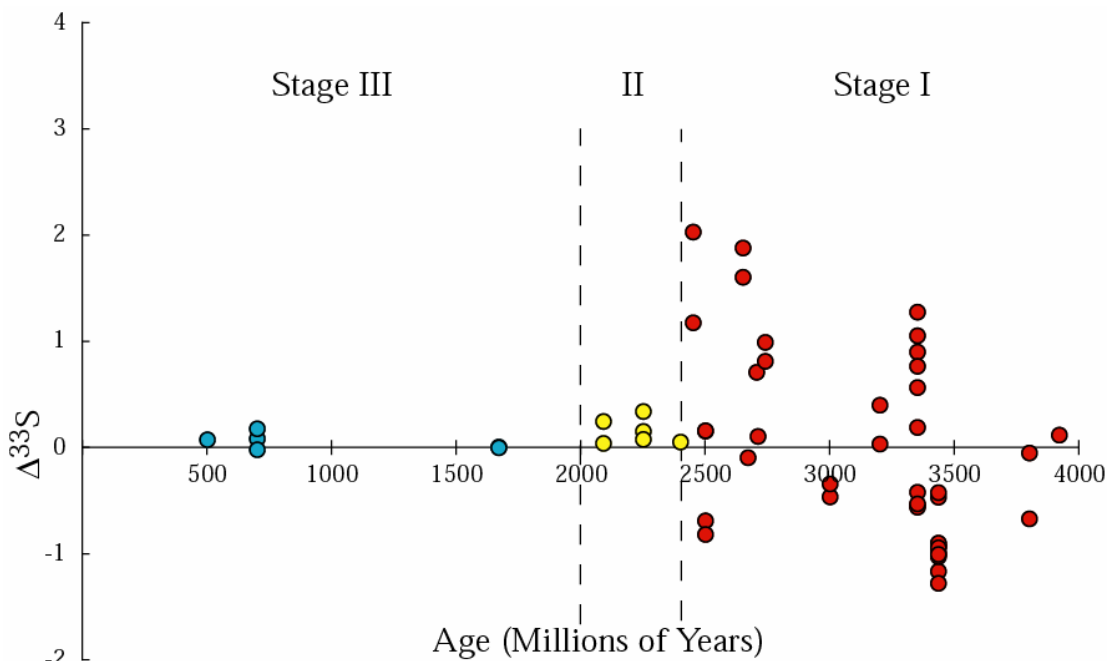
Figure 3: The record of Δ^{33}S versus time, modified from Farquhar et al. (2000). Capital delta notation is defined later in the text and errors are smaller than the symbols. All data is presented in Farquhar et al. (2000) and colored by Stage, which are also reviewed in Farquhar and Wing (2003, 2005). Stage I marks a period when mass-independent isotope effects dominate the sulfur isotope record. Stage II represents a transitional period preceding the establishment of a fully mass-dependent record (Stage III). These data were originally used to argue for an increase in the level of atmospheric oxygen at ~ 2450 Ma (Farquhar et al., 2000).

This study:

The primary goal of this study is to determine the quantitative character of biological isotope fractionations, namely sulfate reduction and sulfur disproportionation, for the four stable sulfur isotopes and to apply this information to natural systems. In addition, this work is done with the goal of identifying a unique, inorganic biomarker

11

that can be used later in studies of deep-time and astrobiological relevance. There are

two primary types of studies included. The first are experimental, where I test

different metabolisms and metabolic dependencies (Chapters 2-3). The second type

of study is environmental, where I use the results of the experimental studies to

constrain models of different natural systems and compare model predictions with

natural samples. These systems range in size and time, from large-scale changes

across the Proterozoic Eon to basin-scale variability covering millions of years. What

they all share is a diverse and complex biogeochemical sulfur cycle that can be

studied with the multiple sulfur isotopes.

This study begins with an experimental project examining the fractionation in ^{33}S for

sulfate reducing and sulfur disproportionating microorganisms (Chapter 2). The

second experimental study (Chapter 3) describes a set of focused sulfate reduction

temperature-block experiments that produced a large ^{33}S and ^{36}S data set, which I use

to test the correctness of different metabolic models. Chapter 4 describes the first

environmental application of this mass-dependent multiple isotope system, where I

used carbonate-associated sulfate (CAS) and evaporites from the Proterozoic to

pinpoint the evolutionary onset of sulfur disproportionating microorganisms. In

Chapter 5 I discuss another geological study that used sulfide minerals to reconstruct

a marine basin that captured the Paleoporterozoic transition from a ferruginous to

sulfidic deep-ocean. This basin-scale study of sulfide minerals is followed-up by an

examination of the Mesoproterzoic McArthur Gp. (Reward Fm.) and Roper Gp.

(Velkerri and McMinn Fms.), where I again use sulfide minerals to place quantitative

constraints on the isotopic composition of seawater sulfate, and to address whether

the oxidative sulfur cycle was active at this time (Chapter 6). Lastly, Chapter 7

synthesizes the results of this study, places this work in to greater context of the field,

and outlines goals and future areas of interest.

Chapter 2: Sulfur Isotope Fractionations in Biological Systems:
a case study with sulfate reducers and sulfur disproportionators

Introduction

Sulfur isotope (^{32}S, ^{33}S ^{34}S, and ^{36}S) measurements of sulfur compounds associated

with dissimilatory sulfate reduction, elemental sulfur disproportionation and sulfite

disproportionation indicate that different types of metabolic processes impart

different sulfur isotope signatures. An established network for sulfate reduction was

used previously to explain the isotope variability. Here, I revisit that treatment and

expand it to branching networks representative of biological sulfur

disproportionation, in an attempt to understand sulfur isotope fractionations

associated with that metabolism. This context is used to interpret experimental data

for both sulfate reducers and sulfur compound disproportionators. I explore the types

of information about material flow through these metabolic processes that can be

extracted by using isotope data. The different sulfur isotope relationships (Δ^{33}S and

λ) allow various metabolic processes to be distinguished from one another, even

when δ^{34}S fractionations are similar, providing a tool that can be used to interpret and

identify different types of biological sulfur fractionations in the geologic record.

Background

Dissimilatory sulfate reduction likely played an important role in determining the

isotopic composition of sedimentary sulfides and oceanic sulfate preserved in the

geologic record. It has been proposed that disproportionation of intermediate sulfur

species (that is the metabolic production of both an oxidized and reduced end-

member) has also played a role in determining the magnitude of the fractionation

within that record (Canfield and Thamdrup, 1994). The relative impact of these two

metabolisms on the global sulfur isotopic record, however, remains unknown.

Habicht and Canfield (2002) attempted to constrain the relative contribution of these

two metabolisms in a number of modern environments. Pinpointing a robust method

to differentiate between these metabolisms will make it possible to test models of

ocean chemistry and of microbial evolution. In this study, I examine the sulfur

isotope (^{32}S, ^{33}S, ^{34}S, and ^{36}S) signatures of products from experiments with

dissimilatory sulfate reducers and sulfur disproportionators, and then integrate these

results with models of material flow through metabolic networks as a first step toward

addressing these questions.

Experimental studies of sulfate-reducing bacteria under different physical and

chemical conditions have established a likely biochemistry for sulfate reduction

(Rees, 1973; Peck, 1959, 1961; Castro and others, 2000; Detmers et al., 2001;

Canfield, 2001). Rees (1973) described sulfate reduction using the network,

$$SO_{4(out)}^{=} \underset{2}{\overset{1}{\rightleftarrows}} \left(SO_{4(in)}^{=} \underset{5a}{\overset{4a}{\rightleftarrows}} APS \underset{5b}{\overset{4b}{\rightleftarrows}} SO_3^{=} \right) \overset{3}{\longrightarrow} H_2S \tag{1}$$
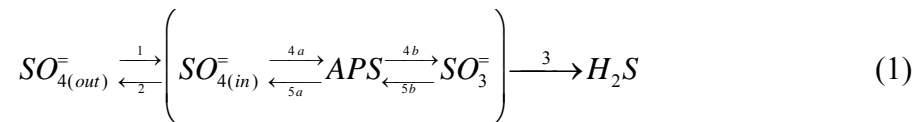
where the brackets represent the cell wall, APS is adenosine-5'-phosphosulfate, and

the numbers represent reaction pathways capable of fractionating material. The upper

net fractionation limit for this pathway is roughly 47 ‰ in δ^{34}S (Harrison and Thode,

1958; Kaplan and Rittenburg, 1986; Kemp and Thode, 1968; Chambers et al., 1976,

Canfield, 2001). Since sulfate reducing bacteria impart large sulfur isotopic

fractionations, and considering that dissimilatory sulfate reduction accounts for over

50% of the organic carbon remineralization in modern marine sediments, this process

is considered one of the most important controls on the sulfur isotope record

(Jørgensen, 1982; Thamdrup et al., 1996; Canfield, 2001; Habicht and Canfield,

2002).

Our understanding of sulfur disproportionation is less well developed.

Disproportionation uses various sulfur intermediates (elemental sulfur, sulfite, and

thiosulfate) and produces both oxidized (sulfate) and reduced (hydrogen sulfide) end-

members (Bak and Pfenning, 1987; Canfield and Thamdrup, 1994; Thamdrup et al.,

1994; Canfield and Teske, 1996; Finster et al., 1997; Habicht and Canfield, 1998;

Cypionka et al., 1998). In the case where sulfite is disproportionated, the reaction

proceeds as (Frederikson and Finster, 2003),

$$SO_3^= \underset{2}{\overset{1}{\rightleftarrows}} \underset{\substack{8 \downarrow \\ H_2S}}{SO_{3(in)}^=} \underset{5a}{\overset{4a}{\rightleftarrows}} APS \underset{5b}{\overset{4b}{\rightleftarrows}} SO_{4(in)}^= \underset{7}{\overset{6}{\rightleftarrows}} SO_{4(out)}^= \tag{2}$$
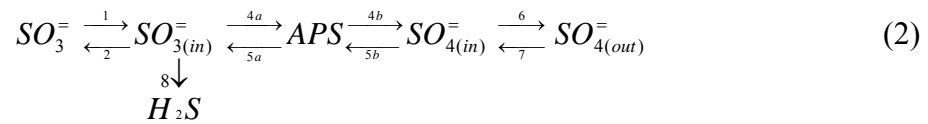
whereas when elemental sulfur is disproportionated,

$$S^0 \underset{2}{\overset{1}{\rightleftarrows}} \underset{\substack{10 \downarrow \\ H_2S}}{S_{(in)}^{0=}} \underset{5a}{\overset{4a}{\rightleftarrows}} SO_3^= \underset{5b}{\overset{4b}{\rightleftarrows}} APS \underset{7}{\overset{6}{\rightleftarrows}} SO_{4(in)}^= \underset{9}{\overset{8}{\rightleftarrows}} SO_{4(out)}^= . \tag{3}$$
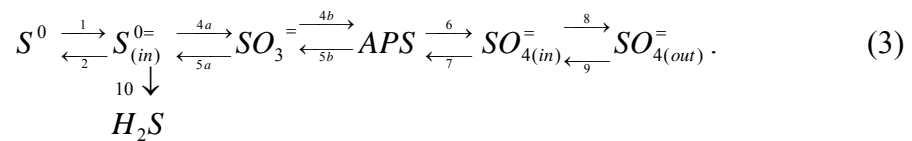
Fractionations in sedimentary sulfides that exceed those produced by sulfate

reduction have been attributed to the disproportionation of intermediate sulfur species

(Jørgensen 1990a, b; Jørgensen and Bak, 1991; Canfield and Thamdrup, 1996).

These intermediates are naturally present in low concentrations (Troelsen and

Jørgensen, 1982; Thamdrup et al., 1994), but when they are disproportionated, they

can impart large fractionations (up to 70‰ in δ^{34}S) between the product sulfate and

sulfide (Thamdrup et al., 1993; Canfield and Teske, 1996; Habicht and Canfield,

1998; Habicht and Canfield, 2002).

Studies of modern seafloor ecosystems have used both microbial and geochemical

techniques to examine the fractionation between product sulfides and residual pore-

water sulfate (Habicht and Canfield, 2002). This approach provides convincing

isotopic evidence for the influence of disproportionation in some modern

environments and further supports the argument that disproportionating bacteria

played an important role in the geological record of sulfur isotope fractionations.

However, it is not possible to apply this method directly to the ancient geological

record due to a lack of contemporaneous sulfide and pore water sulfate, and because

it is not possible to study cultures of indigenous sulfate-reducing bacteria in the same

way as Habicht and Canfield (2002).

Here, a new isotope tool is used to study the relative influences of dissimilatory

sulfate reduction and sulfur disproportionation on the sulfur isotope record. It is

demonstrated that abundances of ^{33}S (and ^{36}S) can be used in conjunction with ^{34}S to

differentiate the signatures of biological sulfate reduction and biological

disproportionation. In the geologic record it is suggested that these variations can be

distinguished from those produced by non-biological processes and hence provide

constraints on environmental evolution throughout the Proterozoic Eon. This

approach may allow for the evaluation of fractionation processes contributing to the

sulfur isotope record in ancient and modern systems.

Isotope Notation

Isotope ratios are used to determine the fractionation factor (α) between two

reservoirs, where

$$^{3x}\alpha_{AB} = \frac{\dfrac{^{3x}S}{^{32}S}_A}{\dfrac{^{3x}S}{^{32}S}_B} \tag{4}$$

and where A and B represent the two sulfur pools of interest and 3x is either 33, 34,

or 36. Specifically, $^{33}S/^{32}S$, $^{34}S/^{32}S$ and $^{36}S/^{32}S$ are reported using standard delta

notation (δ), where

$$\delta^{33}S = 1000 \times (^{33}\alpha - 1) , \tag{5}$$

$$\delta^{34}S = 1000 \times (^{34}\alpha - 1) , \tag{6}$$

and

$$\delta^{36}S = 1000 \times (^{36}\alpha - 1) . \tag{7}$$

The less abundant isotopes (^{33}S and ^{36}S) are reported using capital delta notation (Δ),

where

$$\Delta^{33}S = \delta^{33}S - 1000 \times \left[(1 + \frac{\delta^{34}S}{1000})^{0.515} - 1 \right] \tag{8}$$

and

$$\Delta^{36}S = \delta^{36}S - 1000 \times \left[(1 + \frac{\delta^{34}S}{1000})^{1.90} - 1 \right].$$ (9)

The exponents in these relationships (0.515 and 1.90) define the reference fractionation line (RFL) and approximate single-step thermodynamic equilibrium isotope exchange effects at low temperature (Hulston and Thode, 1965). All isotopic normalizations are discussed in Appendix 1.

Many fractionation processes depend strongly on the relative mass difference between the isotopes, resulting in highly correlated variations for $\delta^{33}S$ and $\delta^{34}S$ (Hulston and Thode, 1965; Farquhar et al., 2003). These variations are described by

$$^{33-34}\theta = \frac{\ln(^{33}\alpha)}{\ln(^{34}\alpha)},$$ (10)

which is a theoretical relationship between fractionation factors (α) and reflects a specific fractionation process. Current convention uses a mathematically equivalent, but functional definition that describes observed variations for $\delta^{33}S$ and $\delta^{34}S$ using

$$^{33-34}\lambda = \frac{\ln(1 + \frac{\delta^{33}S_A}{1000}) - \ln(1 + \frac{\delta^{33}S_B}{1000})}{\ln(1 + \frac{\delta^{34}S_A}{1000}) - \ln(1 + \frac{\delta^{34}S_B}{1000})},$$ (11)

where A and B represent different sulfur reservoirs (Miller, 2002). For simplicity, I note that when discussing a theoretically derived relationship θ is used, whereas when discussing an observation, λ is used.

In this study there is a distinction between isotopic fractionation *processes*, which are described using α and θ, and *observed* isotopic fractionations, which are described

using $\delta^{3x}S$ and λ (Mook, 2000; Farquhar et al., 2003; Angert et al., 2003). I use α and θ as input values in the modeling. Theta (θ) is largely a theoretical term because it is difficult to determine experimentally, however calculations presented in Farquhar et al. (2003) and Chapter 3 serve to approximate equilibrium processes. In this chapter, λ is used to describe both the fractionations observed in the experiments and the fractionations predicted from the modeling. $\delta^{3x}S$ and λ are "net" quantities that can include the effects of many processes and mass-balance (Hayes, 2001; Farquhar et al., 2003).

Mass-dependent isotope fractionation

Theoretical work by Urey (1947) and Bigeleisen and Mayer (1947) provides the foundation for the understanding of equilibrium mass-dependent isotopic fractionations. The predictions made using their formulae, and those of subsequent studies that describe other physical and chemical mass-dependent isotopic fractionations, have been applied to multiple isotope systems to learn more about the processes that operate in nature (Farquhar et al., 2003). Advancements in analytical precision allow for systems such as the four stable isotopes of sulfur to be more thoroughly studied experimentally.

Isotopic fractionation processes have been traditionally grouped into several overarching categories that include both equilibrium and kinetic processes. Equilibrium fractionations described by Urey (1947) and Bigeleisen and Mayer (1947) reflect the minimization of free energy associated with isotopic exchange

reactions. Kinetic fractionations comprise a much larger group of processes that are characterized by unidirectional reactions and transport. Transition state theory has been applied to kinetic fractionations by Bigeleisen and Wolfsberg (1958), who describe chemical kinetic isotopic fractionations in terms of the vibrational energies of the transition state, those of the reactants, and also the reaction path and its relationship to the potential energy surface that describes the different states. Other authors describe kinetic fractionations in terms of the relationship between velocity and kinetic energy for isotopically substituted species (Craig et al., 1988; Matsuhisa et al., 1978; Mook, 2000; Young et al., 2002; Schauble, 2004). It is important to recognize that each of these treatments applies in a different physical-chemical situation, and that each of these treatments has different implications for the isotopic fractionations. Further, some studies have referred to metabolic fractionation processes as kinetic fractionations (Kaplan, 1975). I prefer to make a distinction between fractionation effects that are produced by multi-step metabolic and biogeochemical processes and those that are intrinsic to individual chemical and physical processes (cf. Urey, 1947; Bigeleisen and Mayer, 1947; Bigeleisen and Wolfsberg, 1958; Matsuhisa et al., 1978; Craig et al., 1988; Mook, 2000; Young et al., 2002; Schauble, 2004).

The possibility of different mass-dependent fractionations arising from different equilibrium and kinetic fractionation processes is well documented (Bigeleisen and Wolfsberg, 1958; Matsuhisa and others, 1978; Mook, 2000; Young and others, 2002; Schauble, 2004, Young and Galy, 2004). Values of θ produced by equilibrium

isotopic exchange of sulfur between sulfur species have been constrained using the theoretical treatment of Urey (1947) and are generally near 0.515 for $^{33}\theta$ and 1.90 for $^{36}\theta$. Determinations of $^{3x\text{-}34}\theta$ produced by kinetic processes are more variable, falling between 0.500 and 0.515 for the example of $^{33}\theta$, and depend on the nature of the fractionation process responsible for the isotopic fractionations.

Values of λ produced by multi-step metabolic processes described by Farquhar et al. (2003) depend on the structure of the network, the relative amounts of material transferred through the metabolic network, and on the isotopic fractionations (α and θ) of its constituent steps. Because of the dependence on material transfer and network structure, the values of λ can be more variable than the values of θ for *all* constituent steps within any given network. All of the modeling efforts presented in this chapter assume a $^{33}\theta = 0.5145$ ($^{36}\theta = 1.89$), which is an equilibrium value for exchange between sulfate and hydrogen sulfide at 20 °C (Farquhar et al., 2003). It is recognized that the calculations may later be refined with more precise assignments of $^{33}\theta$ (and $^{36}\theta$) for each of the constituent network steps, but do not explore this aspect in the present study. Data for ^{36}S is presented for experiments described in this chapter, but interpretations based on those measurements are discussed in Chapter 3.

The term λ_{SR} is calculated using Equations 2 and 5, and is thus designated to describe sulfate reduction. Although describing a single process, λ_{SR} does not necessarily represent a single reaction. For example, a net fractionation relationship could be calculated for the sulfate reduction metabolism (α_{net} and λ_{net} or α_{SR} and λ_{SR}), which

encompasses a series of biochemical reactions with their own unique α and λ (such as α_{diff} and λ_{diff} for diffusion, or α_{enz} and λ_{enz} for an enzymatic processes). In the case where there is a theoretical understanding for a well-defined process, such as for temperature-dependent equilibrium isotope exchange, θ is used. Otherwise, when describing a transformation that is thought or known to encompass many steps, λ is used.

The variations of interest here are the net biological signatures. These signatures originally have the added effects of material balance in the system (due to the batch culture experimental design), and thus deviate from the situation whereby $\lambda_{obs} = \lambda_{SR}$ (where λ_{obs} is the observation). If the experiments were run in a chemostat (steady-state bioreactor), closed system effects would not be expected in the experiments and λ_{obs} should equal λ_{SR}. The data is corrected to remove the isotopic effects of the closed system batch experiments using standard Rayleigh equations presented later in the chapter (also see Appendix 2). This allows for the manipulation and discussion of isotopic signatures thought to reflect the sulfate reduction process. In addition to generating non-zero $\Delta^{33}S$ and $\Delta^{36}S$ due to contributions from specific processes, there is also a mass-balance contribution, which is more fully discussed in Appendixes 1 and 5.

Modeling isotope networks

In a recent study, Farquhar et al. (2003) examined how the flow of sulfur through simple metabolic networks can affect the isotopic fractionations in systems with three or more stable isotopes of the same element. These authors took a previously published metabolic network that describes sulfate reduction (Rees, 1973) and adapted it to describe the isotopic fractionations involving the four sulfur isotopes. These predictions are represented by a flow-net that is contoured by a pair of relative flux terms, f_3 and f_5. $f_3 = \varphi_3/(\varphi_3 + \varphi_2)$ and $f_5 = \varphi_5/(\varphi_5 + \varphi_3)$, where φ_j is a term quatifying the amount of material moving along pathway j. f_3 indicates the relative amount of material leaving the cell as hydrogen sulfide (pathway 3 in Equation 1) as opposed to leaving the cell as sulfate (pathway 2 in Equation 1), whereas f_5 represents the relative internal backflow of sulfur (pathways 5a and 5b in Equation 1). These flow-nets illustrate the dependence of λ (and $\Delta^{33}S$) on the intercellular recycling of sulfur (f_5) and the internal/external exchange of sulfate (f_3).

An important result from this treatment is that values for λ will be less than θ for all values of f other than 0 and 1 if the fractionation factors (α) are less than 1.00. The converse is true when the fractionation factors are greater than 1.00. In more complex networks with multiple fractionation factors, some of which are greater than 1 and some that are less than 1, λ can be greater than or less than θ depending on the values of f. When values of $f = 0$ or 1, $\lambda = \theta$. Another consequence from this treatment is that the solution to progressively more and more complex networks can be obtained by nesting the solutions for simple networks (see also Rees, 1973). In

other words, the fractionation factors for multiple steps are multiplicative.

Modeling disproportionation networks can be undertaken by adapting a similar treatment to the disproportionation network structure. Farquhar et al. (2003) examined a very simple branching network component without backflow and noted that the mass-dependent factor, λ, between the products of this network would be a weighted average of the θ's for each of the branches. This treatment can be expanded to branching networks with backflow by applying the ideas above. If the fractionation factors along a branch are greater than 1.00, such as is the case along oxidative branches for sulfur disproportionation, the net λ values have the potential to be greater than the constituent θ values for all values of f other than 0 and 1. For example, to produce λ values greater than 0.5145 for a branching network with all $\theta =$ 0.5145, a back reaction along the oxidative branch of the network (similar to those seen in Equations 2 and 3) must be employed. These principles are used below to interpret the experimental results.

Biological and modeling methods

Pure cultures of sulfate reducing bacteria were grown according to media recipes recommended by Deutsche Sammlung von Mikroorganismen, Braunschweig, Germany (DSM strain # 3382 and 10085 respectively below). Inoculated solutions were prepared under anaerobic conditions with a N_2 atmosphere and without the initial addition of sulfate or substrate. *Desulfobacterium autotrophicum* was grown under a H_2/CO_2 atmosphere where atmospheric pressure was monitored, whereas

Desulfospira jorgensenii was provided an organic substrate (Na-pyruvate). Cultures were grown in batch and harvested during the late exponential growth phase. Samples were fixed and metabolic activity terminated through the addition of a 20% Zinc Acetate solution.

Sulfide concentrations (± 5% 1σ) are determined photometrically using a methylene blue technique (Cline, 1969), and later distilled using 6N HCl, liberating H_2S, which was then reacted with $AgNO_3$ to produce Ag_2S. Sulfate and thiosulfate concentrations (± 1% SD) were determined via ion chromatography after the addition of a bicarbonate buffer. Sulfates were originally precipitated as $BaSO_4$ and then further reduced (Thode, 1961; Forrest and Newman, 1977) to CdS, and then finally to Ag_2S (see Appendix 3 for general chemical methods).

Cell growth was monitored through optical density measurements at 670nm. Optical density was calibrated to cell numbers by staining cells with DAPI and counting them under UV light. As published by Detmers et al. (2001), cell specific reduction rates (csSRR) during exponential phase growth are represented by,

$$csSRR = \frac{SO_4^{2-}{}_{(2)} - SO_4^{2-}{}_{(1)}}{\frac{(cn_{(1)} + cn_{(2)})}{2} \times (T_{(2)} - T_{(1)})} \qquad (12)$$

where subscripts 1 and 2 represent different sampling times. Here, '$SO_4^{2-}{}_{(2)}$' is the sulfate concentration at time (2), 'cn' is cell number and 'T' is time. The samples used for the disproportionation experiments were generated in the studies of Canfield et al. (1998) for elemental sulfur disproportionation and Habicht et al. (1998) for

sulfite disproportionation. Product ratios (SO_4:H_2S) included in these publications

serve as mass-balance parameters when interpreting isotope results.

Our modeling technique is presented in Farquhar et al. (2003), and outlined earlier in

this dissertation. The model network used for dissimilatory sulfate reduction is

presented in Rees (1973) and can be seen in Equation (1). In the case of dissimilatory

sulfate reduction, I solved for the relationship between the initial sulfate and product

hydrogen sulfide. For sulfur disproportionation, I use the networks presented in

Equations (2) and (3) and a stoichiometry of $4SO_3^{2-} + 2H^+ \rightarrow H_2S + 3SO_4^{2-}$ for sulfite

disproportionation and $4S^o + 4H_2O \rightarrow 3H_2S + SO_4^{2-} + 2H^+$ for elemental sulfur

disproportionation to solve for both end-members (sulfate and sulfide) as well as the

composition of the reactant pool (either elemental sulfur or sulfite) (Thamdrup et al.,

1993; Finster et al., 1998; Canfield, 2001). All reactions are modeled with $^{33}\theta$ values

at 0.5145. The individual fractionation factors for the sulfate reduction pathway are

taken as $\alpha = 1.003$ for diffusion of sulfate into the cell, and $\alpha = 0.975$ for both the

internal conversion of sulfate to sulfite and the enzymatic reduction of sulfite to

hydrogen sulfide (Rees, 1973). Fractionation factors for the disproportionation

networks were taken partly from the sulfate reduction literature (Rees, 1973), with the

remaining α values being provided by theoretical calculations presented in Table 2 of

Farquhar et al. (2003).

Cell specific reduction rates (measured in *f*mol/cell*day) for both sulfate reduction

experiments match well with those published in Detmers et al. (2001) for exponential

phase growth. Bacterial populations during the experiments reached cell densities of

the same magnitude as seen previously with these strains. Concentrations of the

sulfate and sulfide pools were monitored and co-vary (Figure 4). Isotopic

compositions for the stable isotopes of sulfur as well as the cell-specific metabolic
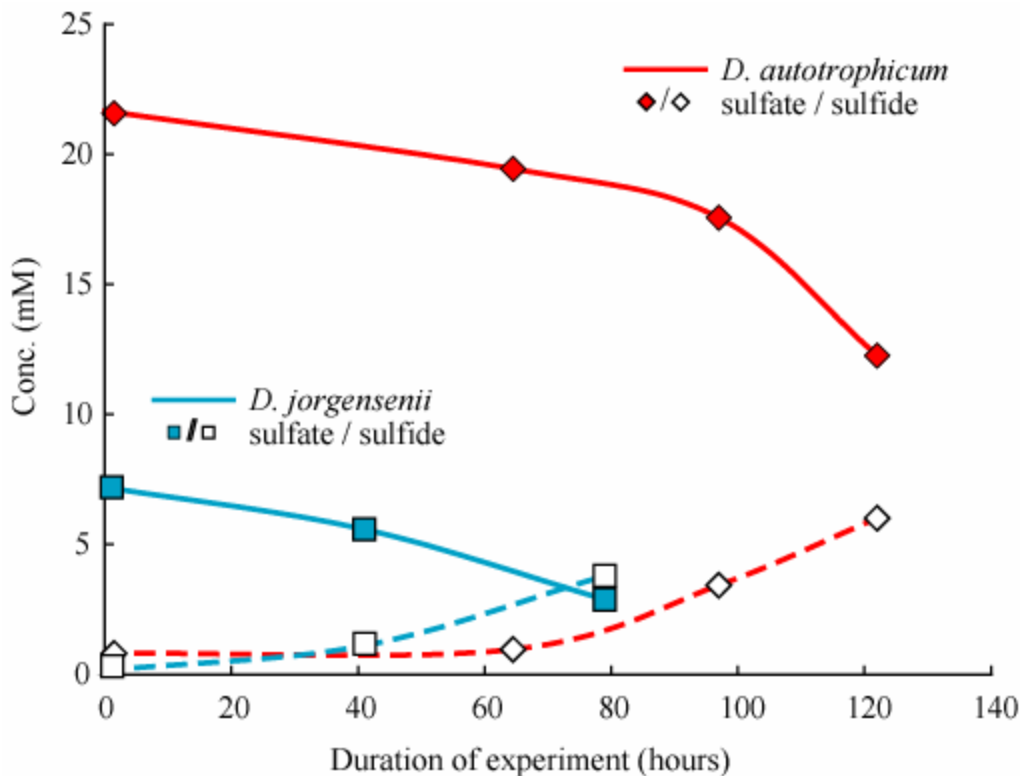
Figure 4: Concentrations of sulfates and sulfides for sulfate reduction experiments with *D. autotrophicum* and *D. jorgensenii* are plotted against the duration of the experiment. Each symbol represents a time when the experiment was sampled. I note the stoichiometric depletion of sulfate and accumulation of sulfide. Experiments were run until ~ 50 % of the initial sulfate was consumed. Due to a low csSRR and a low tolerance for H$_2$S, *D. jorgensenii* was started at a lower sulfate concentration. This concentration is still large enough not to effect the fractionation produced by the organisms (Habicht et al., 2002).

rates and concentration data from sulfate reduction experiments are listed in Table 2.

The net fractionation between the reactant sulfate and the product sulfide for sulfate

reduction experiments is reported (Table 2: sulfate – sulfide). Additionally, Table 3

presents the fractionations from sulfur disproportionation experiments. In the case of

disproportionation, the isotopic composition of the products (sulfate and sulfide) are

first reported relative to the isotopic composition of the starting material, with the net

fractionation (sulfate - sulfide) reported in gray. Calculated values of $\Delta^{33}S$, $\Delta^{36}S$, $^{33}\lambda$

and $^{36}\lambda$ are further reported for each sample. The isotopic compositions of the sulfate

reduction experiments were normalized to the starting sulfate composition and, when

possible, sulfur disproportionation experiments were normalized to the composition

of the starting sulfur compound. In the case of the Golfo Dulce samples, where no

initial sample was available, values were normalized to house UMd SF_6, whose value

is reported in Appendix 1.

Sulfate reducing microorganisms

For *Desulfospira jorgensenii*, the product sulfide was depleted in $\delta^{34}S$ and the

residual sulfate was enriched with respect to the $\delta^{34}S$ values for the starting sulfate.

For longer duration experiments, $\delta^{34}S$ fractionation between sulfate and sulfide

($\delta^{34}S_{H2S-SO4}$) increased slightly. The $\Delta^{33}S_{H2S-SO4}$ values did not change much with

time, but did record a larger initial change (between time = zero and the first data

recorded). The $\lambda_{H2S-SO4}$ values for this experiment ranged from 0.5102 to 0.5103.

Mixing lines between product sulfide and the residual sulfate intersected the initial

sulfate composition, therefore satisfying mass balance.

Results for experiments run with *Desulfobacterium autotrophicum* illustrate a sulfide reservoir with depleted $\delta^{34}S$ values and with an enriched $\delta^{34}S$ composition in the sulfate reservoir, when compared to the starting material. As the reaction proceeds, the net $\delta^{34}S$ fractionation ($\delta^{34}S_{H2S-SO4}$) increases significantly. The $\Delta^{33}S_{H2S-SO4}$ values record a slight variability, but overall do not record a statistically significant change. Net $\lambda_{H2S-SO4}$ for this experiment evolved from 0.5102 to 0.5120. Mixing lines between the residual sulfate and product hydrogen sulfide intersect the starting composition of the initial sulfate and the data are therefore consistent with isotopic mass balance.

Exp. Duration (hours)	csSRR (fmol/cell*day)	Sulfate (mM)	Sulfide (mM)	$\delta^{34}S$	$\Delta^{33}S$	$\Delta^{36}S$	$^{33\text{-}34}\lambda$	$^{33\text{-}34}\sigma_\lambda$	$^{36\text{-}34}\lambda$	$^{36\text{-}34}\sigma_\lambda$
D. autotrophicum	30									
64.5		19.44	0.97	-14.22	0.068	NA	0.5102	0.0006	NA	NA
97		17.56	3.43	-18.90	0.058	-0.083	0.5120	0.0004	1.905	0.011
122		12.26	6.01	-21.99	0.072	-0.250	0.5117	0.0004	1.912	0.009
D. jorgensenii	0.4									
41		5.58	1.11	-19.21	0.090	-0.625	0.5103	0.0004	1.933	0.011
79		2.88	3.79	-22.01	0.105	-0.107	0.5102	0.0004	1.905	0.009

Table 2: Isotopic and biochemical data from sulfate reduction experiments with *D. autotrophicum* and *D. jorgensenii*. Note that isotopic compositions for time = 0 in Figure 4 are not listed, as that represents innoculum material. Isotopic data was calculated as the net fractionation between the sulfide and sulfate in an experiment, at the time listed. Isotopic uncertainties are fully discussed in Appendix 1. Cellular rates were calculated according to Detmers et al. (2001) and are for exponential phase growth. Isotopic results and calculations are discussed in the text, whereas the calculation of   is presented in Appendix 4.

Sulfur disproportionating microorganisms

Two experiments with freshwater sulfite disproportionator *Desulfocapsa thiozymogenes* yielded fractionations of up to ~31 ‰ for $\delta^{34}S_{H2S-SO4}$ (Table 3). The

sulfide pool showed strong $\delta^{34}S$ depletions of ~23 ‰, whereas the sulfate pool was only enriched by ~7 ‰. The $\Delta^{33}S$ values of the two reservoirs are more positive than the starting sulfite by up to 0.15 ‰ and the average $\lambda_{SO4\text{-}H2S}$ was 0.5163.

Two sulfite disproportionating experiments with *Desulfovibrio sulfodismutans* produced large fractionations for $\delta^{34}S$, with an average $\delta^{34}S_{H2S\text{-}SO4}$ of ~50 ‰ between the sulfides and sulfates (Table 3). Longer duration experiments produced sulfides that were less depleted in $\delta^{34}S$ whereas the sulfates became less enriched in $\delta^{34}S$. The $\Delta^{33}S$ values in both pools recorded significant enrichments of up to 0.16 ‰, relative to the starting sulfite. The average observed $\lambda_{H2S\text{-}SO4}$ for this experiment was 0.5147.

	S-intermeadiate			Sulfate			Sulfide		
	$\delta^{34}S$	$\Delta^{33}S$	$\Delta^{36}S$	$\delta^{33}S$	$\delta^{34}S$	$\delta^{36}S$	$\delta^{33}S$	$\delta^{34}S$	$\delta^{36}S$
D. thiozymogenes									
(hours) 99.25	-2.95	-5.52	-11.18	1.01	1.88	2.96	-15.04	-28.99	-55.00
99.25				1.17	2.20	3.44	-14.34	-27.65	-52.29
D. sulfodismutans									
(hours)1149.5	0.52	1.18	1.85	5.77	11.15	20.52	-22.87	-44.05	NA
1149.5				4.63	9.00	16.22	-18.85	-36.32	-68.29
Golfo Dulce									
A	NA	NA	NA	15.06	29.28	NA	2.27	4.41	7.31
B				17.17	33.48	75.30	2.17	4.21	6.86

		$\delta^{34}S$	$\Delta^{33}S$	$\Delta^{36}S$	$^{33\text{-}34}\lambda$	$^{33\text{-}34}\sigma_\lambda$	$^{36\text{-}34}\lambda$	$^{36\text{-}34}\sigma_\lambda$
Totals (sulfate-sulfide)	*D. thiozymogenes*	-30.82	0.048	0.05	0.5165	0.0003	1.902	0.004
		-29.79	0.032	-0.30	0.5161	0.0003	1.889	0.005
	D. sulfodismutans	-54.60	-0.027	NA	0.5145	0.0001	NA	NA
		-44.91	-0.010	-0.45	0.5148	0.0002	1.889	0.003
	Golfo Dulce	-24.16	0.090	-0.07	0.5187	0.0003	1.897	0.006
		-28.33	0.059	NA	0.5171	0.0003	NA	NA

Table 3: Isotopic results obtained for sulfur and sulfite disproportionation experiments. Data for every experiment, except those with the Golfo Dulce culture, which is normalized to UMd house SF$_6$, are referenced to the isotopic composition of the starting material (listed under "S-intermediate"). The numbers listed under the organism name are the time intervals (in hours) that the experiment was run. Time intervals 'A' and 'B' for the Golfo Dulce samples represent different experiment durations with A preceding B. For all, the raw data is listed above and the total fractionations are boxed and presented in italics.

Two experiments with an elemental sulfur disproportionator from Golfo Dulce, Costa Rica produced smaller $\delta^{34}S_{H2S-SO4}$ fractionations, with an upper limit of ~29 ‰ (Table 3). I observe $\delta^{34}S$ sulfide values of ≈ 4 ‰, with the complimentary sulfate pool recording a $\delta^{34}S$ enrichment of ~30 ‰. The $\Delta^{33}S$ values were depleted by up to 0.09 ‰ in the sulfates, and with $\lambda_{SO4-H2S}$ of up to 0.5187. Measurements of $\delta^{34}S$ highlight the large fractionations between products sulfide and sulfate that are produced by sulfur disproportionation (Thamdrup et al., 1993; Canfield and Teske, 1996; Habicht et al., 1998). The addition of minor isotope data also indicates variations in $\Delta^{33}S$, most notably between initial compositions and the products. When coupled, very large fractionations in $\delta^{34}S$ and measurable $\Delta^{33}S$ allow for more precise determinations of λ, and hence greater resolution from λ_{RFL} than for the sulfate reduction experiments.

Discussion/Conclusions

Interpretation of experimental data using flow networks

The sulfur isotopic fractionations between product hydrogen sulfide and source sulfate in a biological network depend on the structure of the network, the transfer of sulfur within the network, and the isotopic fractionations associated with the transfer pathways. Using the published network for dissimilatory sulfate reduction of Rees (1973), Farquhar et al. (2003) demonstrated that it is possible to account for variability in both λ and the $\delta^{34}S_{H2S-SO4}$ produced during the reduction of sulfate by *A*.

fulgidus. In this study, multiple sulfur isotope data from experiments with two other

sulfate reducers (*D. autotrophicum* and *D. jorgensenii*) are additionally presented

(Figure 5). The ranges of isotopic variations produced by these organisms yields

$\lambda_{H2S-SO4}$ from 0.5102 to 0.5120, which can also be represented by non-zero and

negative Δ^{33}S values, as is seen in Figure 5. These λ values are significantly less than
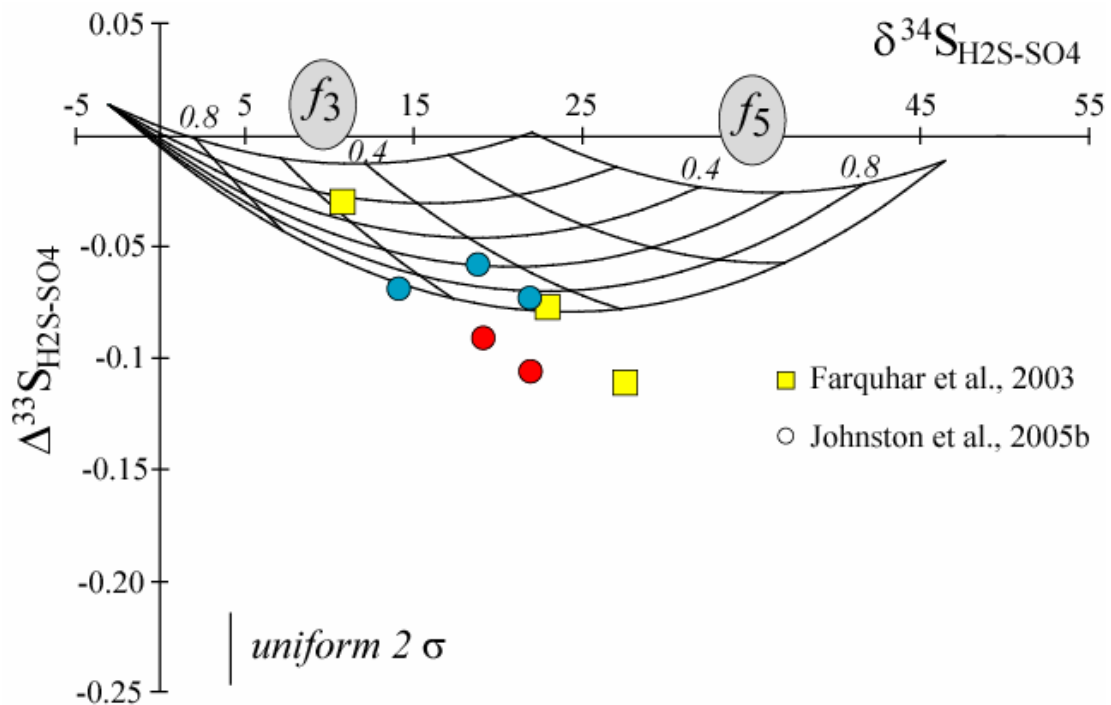
Figure 5: Plot of Δ^{33}S versus δ^{34}S$_{H2S-SO4}$ illustrating the effect of the Rees (1973) biosynthetic network (Equation 1 in text) on multiple isotopic fractionations between hydrogen sulfide and sulfate. Division of flow within the network is compactly described by f_3, which represents the interaction between the enzymatic reduction of sulfite and the sulfate leaving the cell and f_5, which is the proportion of back reaction from sulfite to sulfate. Relative fluxes (from 0 to 1 are noted by 0.4 and 0.8 on both the f_3 and f_5 contours. I include data from Farquhar et al. (2003) along with new data from this study, where the blue circles note *D. autotrophicum* and red circles are from *D. jorgensenii*. Assumptions in the construction of the model are values of 0.5145 for relating the fractionation in ^{33}S to ^{34}S. This value was selected on the grounds that it represents a low temperature equilibrium process. Fractionation factors used were taken from Rees (1973). See text and Farquhar et al. (2003) for further discussion of the modeling.

those predicted for equilibrium exchange between hydrogen sulfide and sulfate

between 0 and 120 °C (0.5146-0.5150), but similar to those predicted for

dissimilatory sulfate reduction (0.512) (Farquhar et al., 2003). The relationship between λ and the $\delta^{34}S_{H2S-SO4}$ reflects changes in the flow parameters of the sulfate reduction network (Equation 1). As described previously (Farquhar et al., 2003), the isotopic composition of experiments with *A. fulgidus* (culture grown as a continuous culture within a bioreactor) evolved along a contour that defines constant proportions of sulfur diffusion into and out of the cell ($f_3 \approx 0.4$) and variable proportions of internal back reactions between sulfite, APS, and sulfate (f_5 varies from 0.2 to 1.0) (see Figure 5). In Figure 5 I translate these arguments and data from both Farquhar et al. (2003) and this chapter to a $\Delta^{33}S$ versus $\delta^{34}S$ coordinate system.

Experiments with *D. jorgensenii* grown in batch culture produced $\delta^{34}S$ fractionations typical of other sulfate reducing bacteria. This experiment evolved in a similar way to *A. fulgidus* along an extension of f_3 (approximately 0.6), but produced fractionations that required f_5 values slightly greater than 1.0 (Figure 5). Since it is not possible for f_5 to exceed 1, these experiments suggest that at least one of the input fractionation factors associated with the internal network steps is slightly incorrect. For instance, it is possible to account for the data using the Rees (1973) network by increasing the fractionation factor for the internal back reaction ($SO_3^=$ to $SO_4^=_{(in)}$) to 35 ‰ in $\delta^{34}S$ (originally at 25 ‰). One possible explanation for the evolution along the f_3 contour is that this organism is known to metabolize very slowly, as seen by the low specific rates calculated earlier. This may indicate a less dynamic sulfate exchange mechanism.

The isotopic relationships produced by *D. autotrophicum* evolve in a different way than *A.fulgidus* and *D. jorgensenii*, but the δ^{34}S fractionations are still consistent with sulfate reduction. This experiment follows a contour that defines a range of f_5 from 0.6 to 1.0 and f_3 that varies from 0.45 to 0.65 (Figure 5). I interpret variations in f_3 as a response to the changes in the external sulfate concentration during the batch culture experiments, which is further investigated in Chapter 3.

This analysis illustrates the potential applications for this approach. Experimental data provides a critical check of the validity of the structure, the fractionation factors, and the flow parameters used in the proposed biological networks. At present, the data do not allow us uniquely to constrain these parameters in the networks, but future work that includes experimental determination of the isotopic compositions of intermediate sulfur pools has the potential to provide this information.

Experiments with elemental sulfur and sulfite disproportionating microorganisms

A similar approach is used to understand the sulfur isotopic fractionations produced by disproportionation networks. In the case of sulfur disproportionation, we interpret the relationship between the products (sulfide and sulfate) rather than between reactant and product. The modeling treatment of these disproportionation networks (see Equations 2 and 3) describes the general features that are observed in the experiments, but the calculations can be sensitive to the input parameters, such as α and θ, which remain to be further constrained.

Sulfur isotope measurements from the disproportionation experiments produced $\delta^{34}S$

fractionations that range from 23 to 55 ‰, consistent with the understanding of

disproportionation. The experiments yield λ values between product hydrogen

sulfide and product sulfate that range from 0.5145 to 0.5187 and $\Delta^{33}S$ from 0.09 to

-0.027 (Figure 6). The sample pairs with the lowest values of $\Delta^{33}S$ (and λ) produced

the largest $\delta^{34}S$ fractionations. The models of Farquhar et al. (2003) produce similar

values when there is insignificant back reaction (unidirectional flow) after the
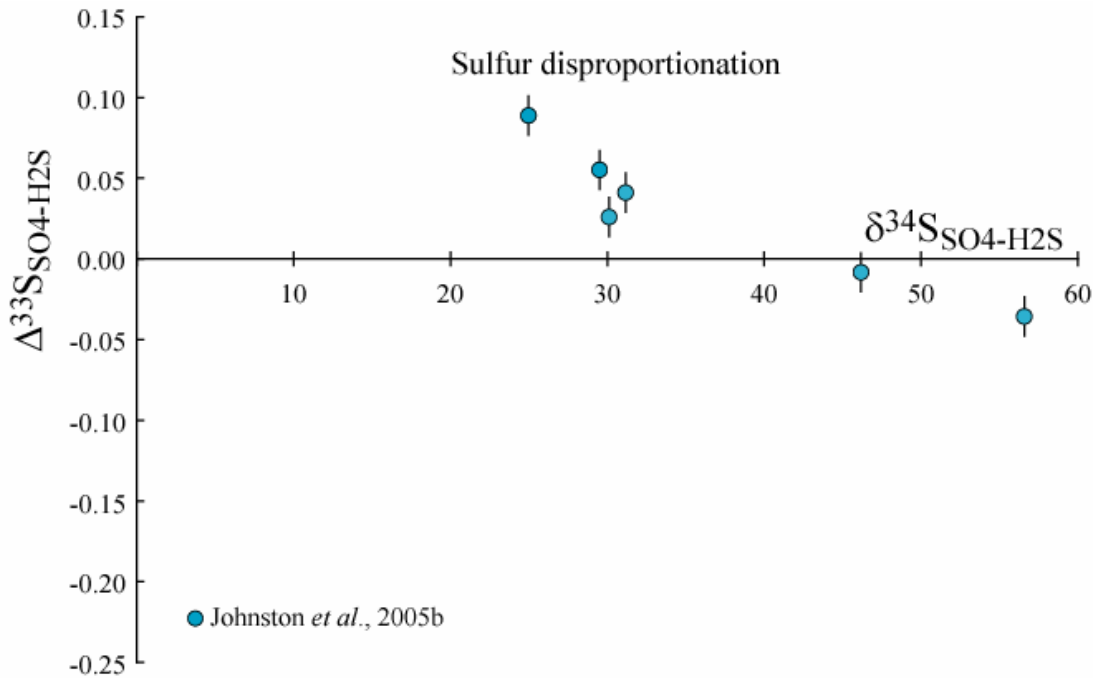
Figure 6: Plot of $\Delta^{33}S$ versus $\delta^{34}S_{H2S-SO4}$ for disproportionation data from experiments with *D. thiozymogenes*, *D. sulfodismutans*, and a culture from Golfo Dulce, Costa Rica. Large ^{34}S fractionations are typical of disproportionation reactions. Error bars represent 2 σ uncertainties. Values of $\Delta^{33}S$ greater than zero are interpreted to reflect back flow along the oxidative branch of the disproportionation network (see text for discussion).

disproportionation branching point. For sample pairs with more positive $\Delta^{33}S$ values,

the $\delta^{34}S$ fractionations are smaller. I interpret these larger $\Delta^{33}S$ values, in the context

of the Farquhar et al. (2003) model, as indicating a back reaction in the oxidative

branch (pathways 5 and 7 in Equation 2 and pathways 5, 7, and 9 in Equation 3) of

the disproportionation network. Although I view $\theta = 0.516$ as a natural upper limit

for mass-dependent processes, branching networks have been shown to produce

inverse fractionation effects, or in this case $\lambda > 0.516$, associated with one product of

a branching network (Fry, 2003). Back flow along the reductive branch of the

disproportionation network conversely reduces the λ (yielding more negative $\Delta^{33}S$)

values in a similar fashion to that of sulfate reduction (see Figure 5). The large range

in λ values may indicate that internal back flow, primarily along the oxidative branch,

is a highly variable characteristic of disproportionation biochemistry. Although the

modeling approach provides insight into the first-order fractionation effects, I have

been unable to reproduce the data using fractionations similar to those in the sulfate

reduction network. The model can be forced to reproduce the data, but requires large

(~10‰ in $^{34}S/^{32}S$) fractionations associated with sulfite transport into the cell, and

very large (40-50‰ in $^{34}S/^{32}S$) fractionations associated with the sulfite-APS-sulfate

steps. I feel that the modeling methodologies are resilient, and the focus of future

work rests on determining the appropriate network for these metabolisms.

Geological and biological applications

Our experiments and their evaluation in the context of metabolic networks

demonstrate that it is possible to distinguish between signatures produced by

dissimilatory sulfate reducers and sulfur disproportionators, even when the magnitude

of the isotopic fractionation is similar. Figure 7 illustrates the relationship between

$\Delta^{33}S$ values and $\delta^{34}S$ fractionations for hydrogen sulfide-sulfate pairs for experiments

involving dissimilatory sulfate reducers as well as sulfite and elemental sulfur

disproportionators. Biological disproportionation processes produce $\Delta^{33}S$ values that

converge on equilibrium values for hydrogen sulfide-sulfate exchange ($\Delta^{33}S \sim 0$)
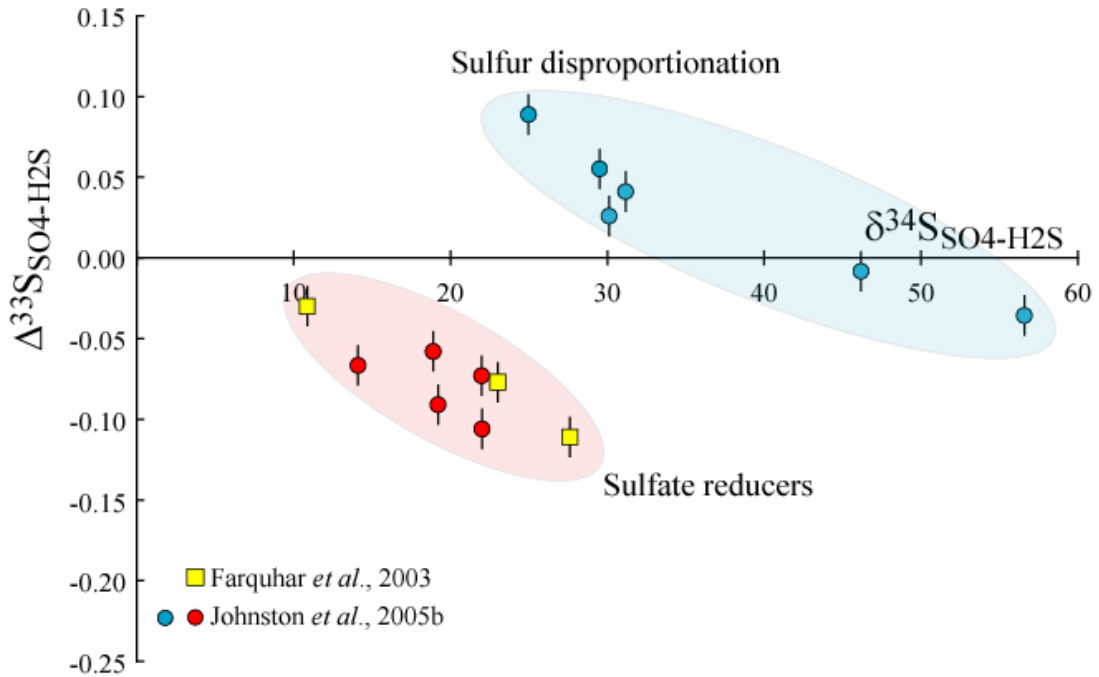
Figure 7: Plot of $\Delta^{33}S$ versus $\delta^{34}S_{H2S\text{-}SO4}$ that includes data from all experiments and the *A. fulgidus* experiment from Farquhar et al. (2003). Data from experiments with sulfate reducers plot at values of $\Delta^{33}S$ that are between -0.12 and -0.02, while data from experiments with sulfite disproportionators and elemental-sulfur disproportionators plot at values of $\Delta^{33}S$ from -0.06 to values greater than 0.05. At low $\delta^{34}S$ fractionations, such as those seen here, the X-axis is similar to that of equilibrium exchange between H_2S and SO_4 (Farquhar and Wing, 2003). Figures 6 and 7 illustrate two fundamental points. First, most metabolic fractionation processes cannot be approximated by equilibrium isotope exchange. Further, isotope fractionations by sulfur disproportionation are often resolvable from fractionations by sulfate reduction only by considering ^{33}S in addition to ^{34}S.

when $\delta^{34}S$ fractionations are large, but trends to $\Delta^{33}S > 0$ when $\delta^{34}S$ fractionations are

less than approximately 35 ‰. Fractionations between H_2S and SO_4 that are

produced by dissimilatory sulfate reduction yield negative $\Delta^{33}S$ values (λ values

between 0.5125 and 0.5103), significantly different from that produced by either

equilibrium exchange (0.5147-0.5150) or biological disproportionation (0.5147) at

the same magnitude $\delta^{34}S$ fractionation, as both result in near zero $\Delta^{33}S$.

Under certain conditions, some sulfur disproportionating bacteria can operate as facultative sulfate reducers. In this scenario, I expect that the λ associated with reduction be similar to that of the obligate sulfate reducers. Primary disproportionators will only reduce sulfate as a means of survival under conditions where disproportionation is less favorable. In interpreting the geologic record, a sulfur disproportionating bacteria reducing sulfate should be just as diagnostic of the environmental conditions as a sulfate reducing bacteria reducing sulfate.

The ability to distinguish isotopic fractionations produced by dissimilatory metabolisms from those produced by disproportionation metabolisms has potential application for testing hypotheses about the changing role of sulfur metabolisms in the terrestrial sulfur cycle over the course of Earth's history. For instance, Shen et al. (2001) have argued that large $\delta^{34}S$ fractionations between pyrite and host barite in 3450 Mya samples of the Pilbara group of northwestern Australia reflect dissimilatory sulfate reduction by early bacteria. Moreover, it has been suggested that after 2450 Mya, the record of sulfur isotopes on a global scale cycle bears the signature of sulfate reducing bacteria and that the imprint of disproportionation did not become significant until after approximately 1000 Mya (Canfield, 2001; Canfield, 1998; also see Chapter 4). It has also been suggested that the large positive excursions for $\delta^{34}S$ following Neoproterozoic glaciations were caused by distillation of sulfur by sulfate reducing bacteria (Hurtgen et al., 2002). The findings suggest that determination of the multiple isotope fractionations for these and related samples may

39

provide a new test of these hypotheses as well as potential tests for evidence of metabolic activity and sulfur fractionations in samples relevant to astrobiological studies.

Chapter 3: Sulfur Isotope Fractionations Produced by Sulfate Reducing Bacteria: *insight into isotope systematics and metabolic models*

Introduction

Metabolic models for fractionations produced by sulfate reducing bacteria and archea derived from experimental observations are the cornerstone of the interpretation of ancient and modern biogeochemical cycles. Although recent studies have called into question a traditionally accepted model, experimental evidence has been lacking for such a claim. I present data from all four sulfur isotopes that suggest that the internal fractionations associated with the sulfate reduction network are larger than previous estimates. Models of both a traditional sulfate reduction network, as well as a more recent incarnation of the sulfate reduction network (with multiple sulfur intermediates) are constructed to aid in the understanding of new experimental data. These data also allow for the further development of additional minor isotope relationships, one which is easily measurable in geologic settings and accurately depicts the net effect of an environment, whereas the other is more applicable to modern environments and may better illuminate the specific process(es) controlling the fractionation in those environments. This approach illustrates the uses of systems containing more than two isotopes.

Conventional sulfur isotope fractionation models for microbial sulfate reduction

underpin the interpretation of the geologic sulfur isotope record and in turn, the

history of Earth surface oxidation (Berner, 1991, Claypool et al., 1981; Canfield,

2001). The antiquity of sulfate reduction has been traced into the early Archean

(Shen et al., 2001), and sulfate reduction is thought to have played a critical role in

shaping the Earth's surface sulfur cycle. Estimates on the magnitude of sulfur isotope

fractionation produced by sulfate reducers rest on experimental observations (Peck,

1959, 1961; Castro and others, 2000; Detmers and others, 2001; Canfield, 2001) and

decades-old theoretical frameworks (Harrison and Thode, 1958; Kaplan and

Rittenburg, 1964; Kemp and Thode, 1968; Rees, 1973; Chambers and others, 1976,

Canfield, 2001). The traditionally applied limit, which has been used in models of

the Precambrian and Phanerozoic sulfur cycles (Berner 1991; Canfield and Teske,

1996; Canfield, 1998; Habicht et al., 2002), is ~ 47 ‰ in $^{34}S/^{32}S$ (Rees, 1973;

Canfield, 2001). However, recent measurements of natural environments (Rudnicki

et al., 2001; Wortmann et al., 2004) and new models (Brunner and Bernasconi, 2005)

suggest that the prior estimate may underestimate the fractionation associated with

sulfate reduction by as much as 30‰. If valid, a recalibration of most conventionally

accepted sulfur cycle models might be in order. Here, I use a recently developed

approach (Chapter 2; Farquhar et al., 2003; Johnston et al., 2005) to investigate

isotopic fractionations associated with sulfate reduction. While this approach does

not provide new limits for the total fractionation a sulfate reducer can produce, it does

provide a way to place limits on the magnitude of fractionation for the internal steps within the metabolic networks.

In the present study, I analyze and interpret new measurements of the sulfur isotopes (^{32}S, ^{33}S, ^{34}S, ^{36}S) from sulfate and sulfide associated with pure culture sulfate reduction experiments. This study, therefore, builds on previous research, which has highlighted the use of ^{33}S for differentiating fractionations produced by sulfate reducing and sulfur disproportionating microorganisms (Chapter 2; Farquhar et al., 2003; Johnston et al., 2005). The experiments were designed to highlight temperature-induced physiological shifts driving the magnitude and pathways of fractionation. These results, when coupled with the associated modeling, allow us to explore the maximum isotopic fractionation capability of the sulfate reduction metabolic network. In addition, the present study will: (1) provide insight into biochemical implications of different sulfate reduction models, (2) pinpoint, and make predictions about future research experiments that can further address the questions discussed/raised in this study, and (3) elucidate the character of the mass-dependent relationship between ^{33}S and ^{36}S.

More on mass-dependence

Multiple isotope signatures, like those examined in this study, are a function of mass-balance (mixing) and the specific processes producing the fractionation, each of which contribute to the observed effect. What determines whether a signature is mass-dependent (or non mass-dependent) is the specific process that is producing the

fractionation. In the present study, microorganisms are responsible for the observed

fractionations, and similar to most Earth surface processes, they produce mass-

dependent isotope effects. To describe the exponent that characterizes the mass-

dependent fractionation in a system, I again use λ, as defined in Chapter 2, which

describes the observed relationship between a pair of samples (Mook, 2000; Farquhar

et al., 2003; Johnston et al., 2005). This expression can also be modified to describe

a suite (more than two) of samples. These values fluctuate around the reference

exponents (0.515 and 1.9 for ^{33}S-^{34}S and ^{36}S-^{34}S respectively) for a number of mass-

dependent processes. For instance, variability in this term (on the order of a few

tenths of a percent) arises for equilibrium isotope exchange at a range of geologically

relevant temperatures, whereas other processes, like diffusive isotope separation and

chemical kinetic isotope exchange (ie. going through a transition state), may deviate

from the reference values by a few percent (Mook, 2000; Miller, 2002; Young et al.,

2002; Farquhar et al., 2003; Farquhar and Wing, 2003). All of the above listed

fractionations are still considered to be mass-dependent. The primary interest in this

study is isolating the mass-dependent fractionations directly attributable to the

catabolic reduction of sulfate. To do so, I quantify and subtract the effects associated

with overall mass-balance in the batch experiments, leaving behind the fractionation

directly attributable to sulfate reduction (see Appendix 2). Since the variability in λ

is small, I carefully describe uncertainties associated with these calculations using

standard error propagation techniques (see Appendix 4).

Metabolic models

A common approach to understanding the complex fractionation paths and processes within biological systems is through the construction of steady-state box models (Chapter 2; Hayes, 2001; Farquhar et al., 2003; Johnston et al., 2005). In contrast to traditional isotope studies that use two isotopes ($\delta^{13}C$, $\delta^{18}O$, $\delta^{34}S$), consideration of multiple (>2) isotopes of the same element can provide better constraints on how material flows through a system. For example, Farquhar et al. (2003) and Johnston et al. (2005) (Chapter 2) used the multiple sulfur isotopes to describe material cycling in both sulfate reducers and sulfur disproportionators. The treatment here will expand on those studies, specifically the sulfate reduction model, with the calculation of new sulfate reduction networks and the inclusion of ^{36}S. All of the fractionation results presented below were normalized to the isotopic composition of sulfate (ie. the co-existing sulfate always plots at the origin).

Predictions from Rees (1973): The classic biological pathway employed for dissimilatory sulfate reduction, as reviewed below, was originally proposed by Harrison and Thode (1958) and expanded upon by Rees (1973) and is discussed in Chapter 2:

$$SO_{4(out)}^{=} \underset{2}{\overset{1}{\rightleftharpoons}} \left(SO_{4(in)}^{=} \underset{5a}{\overset{4a}{\rightleftharpoons}} APS \underset{5b}{\overset{4b}{\rightleftharpoons}} SO_3^{=} \right) \overset{3}{\longrightarrow} H_2S. \tag{13}$$
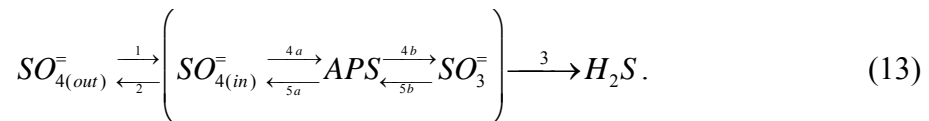
The four primary steps and $\delta^{34}S$ fractionations within this model are 1) transport of sulfate across the cellular membrane ($^{34}\alpha_1$=1.003), 2) the activation of inorganic sulfate to adenosine 5' phosphosulfate (APS), 3) the reduction and subsequent

45

cleavage of the sulfate bound in APS ($^{34}\alpha_{4b}$=0.975), and 4.) the reduction of sulfite to

hydrogen sulfide ($^{34}\alpha_3$=0.975). If I take these fractionations as additive, this network

results in an upper estimation of the $\delta^{34}S$ fractionation capability of sulfate reduction

at $\delta^{34}S \sim 47‰$. This estimate is consistent with observations of fractionations

produced in pure culture and natural population experiments (Harrison and Thode,

1958; Kaplan and Rittenburg, 1964; Kemp and Thode, 1968; Habicht and Canfield,

2002; Canfield, 2001; Detmers et al., 2001).

Predictions for a trithionate pathway: Recent work (Rudnicki et al., 2001;

Wortmann et al., 2004) suggests that the fractionation capability of sulfate reduction

may exceed the 47‰ upper limit proposed by Rees (1973). Explanations for higher

fractionations typically involve the inclusion of the "trithionate pathway" (Kobayashi

et al., 1974; Fitz and Cypoinka, 1990; Agaki, 1995; Cypoinka, 1995), whereby the

reduction of sulfite is not unidirectional and complete, but proceeds through a series

of sulfur intermediate species (S_2O_3, S_3O_6). These steps are described as reversible,

and according to some models are viewed as incomplete. Further, one study

(Brunner and Bernasconi, 2005) includes the presence of an internal hydrogen sulfide

reservoir, which could either react back towards sulfite or be transported out of the

cell[1]. These considerations result in a variety of potential flow networks, one of

which is:

---

[1] Although shown without transport of external sulfide back into the cell, this pathway was included in Brunner and Bernasconi (2005). If there is no fractionation associated with the back reaction, as was suggested by Brunner and Bernasconi (2005), the modeling can simplify to the network shown in equation 14.

$$SO_{4(out)}^{=} \underset{2}{\overset{1}{\rightleftarrows}} \left(SO_{4(in)}^{=} \underset{5a}{\overset{4a}{\rightleftarrows}} APS \underset{5b}{\overset{4b}{\rightleftarrows}} SO_3^{=} \underset{7}{\overset{6}{\rightleftarrows}} S_{int} \underset{9}{\overset{8}{\rightleftarrows}} H_2S_{(in)} \right) \overset{3}{\longrightarrow} H_2S_{(out)}. \quad (14)$$
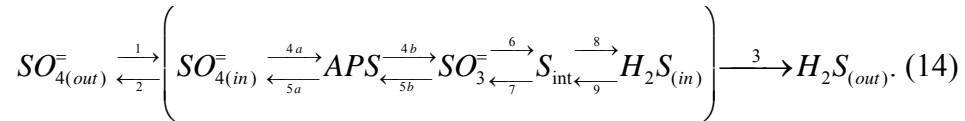
Brunner and Bernasconi (2005) suggest a different fractionation for the reduction of

$SO_3^{=}$ to $H_2S_{(in)}$, and use equilibrium isotope exchange calculations presented in

Farquhar et al. (2003) to suggest $\delta^{34}S$ fractionations of $^{34}\alpha_1=1.003$, $^{34}\alpha_{4b}=0.975$,

$^{34}\alpha_6 = 0.947$ and $^{34}\alpha_7 = 1.005$. This network would allow an upper $\delta^{34}S$ fractionation

limit of ~ 75‰, far exceeding those observed in pure culture and natural population

experiments. From a modeling perspective, the expansion of the model network

requires the introduction of a third flux term, which monitors the back reaction along

pathway 7 ($f_7=$ [flux 7]/[flux 6]) (see Chapter 2). Similar to the modeling presented

above, the flux terms vary from zero to one, and for this network are f_3, f_5, and f_7 and

are defined as before.

Biological methods

A pure culture of *D. autotrophicum* (DSM strain # 3382) was obtained from Deutsche

Sammlung von Mikroorganismen, Braunschweig, Germany and grown according to

recommended media recipes. Media solutions were prepared anaerobically with a N_2

atmosphere and at sulfate and butyrate concentrations of 28 mM and 20 mM

respectively. All cultures were grown in batch. Cell growth was monitored through

optical density measurements at 670 nm. Calibration of optical density measurements

was performed by staining cells with DAPI (4', 6-diamidino phenylindole) and

counting under UV light. Cell-specific rates of sulfate reduction (csSRR: see Chapter

2) during the exponential phase were determined according to Detmers et al. (2001).

New experiments were inoculated from growing cultures in the late exponential growth phase, as determined by earlier establishment of reproducible growth curves and subsequent optical density measurements.

Experiments were run in a temperature gradient block (2-38°C) and in quadruplicate (time series of four). Metabolic activity was terminated and sulfide captured through the addition of a 20% Zinc acetate solution. Samples were then frozen until the necessary chemical extractions could be performed. Sulfate concentrations (± 1 % 1σ) were determined via ion chromatography with the addition of a bicarbonate buffer. Sulfate was precipitated out of solution as $BaSO_4$, through the addition of 1mL 1M BaCl. Sulfide concentrations (± 5 % 1σ) were measured photometrically using a methylene blue technique described in Cline (1969). Sulfide was later distilled using 3N HCl to liberate H_2S, which is captured in an $AgNO_3$ trap as Ag_2S. All isotopic methods, uncertainties, and normalizations can be found in Appendix 1.

Results

Concentrations of sulfate and sulfide were monitored in the experiments and co-varied. Cell specific sulfate reduction rates vary as a function of temperature (between 2 and 38ºC), with rates slowing to near zero (> 15 *f*mol/cell*day) as the end-member temperatures were approached. The maximum cell specific reduction rate was ~ 150 *f*mol/cell*day at 22°C. After the effects of Rayleigh distillation are removed (Appendix 2), a range in the net sulfur isotope fractionation ($\delta_{sulfide} - \delta_{sulfate}$) is observed, from -36.36 to -16.03‰, 0.062 to 0.204‰, and -2.13 to -0.11‰ for $\delta^{34}S$,

T (°C)	series	csSRR	δ³⁴S (‰)	Δ³³S (‰)	Δ³⁶S (‰)	λ³³S	σλ33 (1 σ)	λ³⁶S	σλ36 (1 σ)
2.1	a		-22.39	0.162	-0.989	0.5077	0.0004	1.946	0.009
	b	22.9	-23.78	0.147	-1.122	0.5088	0.0003	1.949	0.009
4.2	a		-27.43	0.149	-1.482	0.5096	0.0003	1.956	0.008
	b	32.9	-30.19	0.144	-2.130	0.5102	0.0003	1.974	0.007
6.2	a		-29.76	0.174	-1.648	0.5092	0.0003	1.958	0.007
	b	36.5	-26.87	0.162	-1.212	0.5090	0.0003	1.947	0.008
8.3	a		-25.24	0.138	-1.138	0.5095	0.0003	1.947	0.008
	b	41.7	-27.51	0.117	-1.722	0.5108	0.0003	1.965	0.008
10.3	a		-36.36	0.204	-1.388	0.5094	0.0002	1.940	0.006
	b	47.4	-27.83	0.130	-1.183	0.5103	0.0003	1.944	0.007
12.3	a		-29.95	0.108	-1.889	0.5114	0.0003	1.966	0.007
	b	56.2	-21.41	0.083	-0.110	0.5111	0.0004	1.905	0.010
14.3	a		-30.73	0.121	-1.176	0.5111	0.0003	1.940	0.007
	b	64.0	-28.19	0.168	-1.394	0.5090	0.0003	1.952	0.007
16.3	a		-25.12	0.119	-0.948	0.5103	0.0003	1.939	0.008
	b	68.8	-21.90	0.089	-1.123	0.5109	0.0004	1.953	0.009
18.3	a		-21.11	0.097	-0.779	0.5104	0.0004	1.938	0.010
	b	123.2	-25.65	0.147	-1.213	0.5093	0.0003	1.949	0.008
20.3	a		-22.17	0.110	-0.853	0.5100	0.0004	1.940	0.009
	b	147.9	-27.10	0.133	-1.175	0.5101	0.0003	1.945	0.008
21.3	a		-28.83	0.102	-1.563	0.5114	0.0003	1.957	0.007
	b	147.1	-26.97	0.113	-0.982	0.5108	0.0003	1.938	0.008
22.3	a		-24.85	0.138	-1.301	0.5094	0.0003	1.954	0.008
	b	135.3	NA	NA	NA	NA	NA	NA	NA
23.2	a		-27.21	0.135	-1.166	0.5100	0.0003	1.945	0.008
	b	110.1	-23.36	0.086	-0.969	0.5113	0.0003	1.943	0.009
24.2	a		-23.89	0.087	-0.845	0.5113	0.0003	1.937	0.009
	b	121.3	-24.39	0.126	-0.883	0.5098	0.0003	1.938	0.008
25.2	a		-25.48	0.130	-1.426	0.5099	0.0003	1.958	0.008
	b	98.8	-23.32	0.085	-1.087	0.5113	0.0003	1.948	0.009
26.3	a		-25.95	0.115	-1.108	0.5106	0.0003	1.944	0.008
	b	112.5	NA	NA	NA	NA	NA	NA	NA
27.3	a		-23.09	0.123	-1.579	0.5097	0.0003	1.971	0.009
	b	93.4	-21.67	0.096	-1.160	0.5106	0.0004	1.955	0.010
28.3	a		-19.44	0.103	-1.034	0.5097	0.0004	1.955	0.011
	b	95.1	-26.00	0.124	-1.160	0.5102	0.0003	1.946	0.008
29.3	a		-25.26	0.130	-1.258	0.5099	0.0003	1.952	0.008
	b	75.2	-16.03	0.108	-0.469	0.5083	0.0005	1.930	0.013
30.3	a		-21.21	0.132	-0.350	0.5088	0.0004	1.917	0.010
	b	75.2	-19.51	0.102	-0.301	0.5097	0.0004	1.916	0.011
32.3	a		-24.53	0.084	-1.148	0.5116	0.0003	1.948	0.008
	b	72.7	-23.60	0.094	-1.056	0.5110	0.0003	1.946	0.009
34.4	a		NA	NA	NA	NA	NA	NA	NA
	b	25.2	-18.77	0.083	-0.921	0.5106	0.0004	1.950	0.011
36.4	a		-24.54	0.062	-1.233	0.5125	0.0003	1.952	0.008
	b	22.6	-22.98	0.081	-0.802	0.5115	0.0003	1.936	0.009

Table 4: Experimental sulfate reduction net fractionations. Points "a" and "b" represent a time series, with point "a" preceding "b." Rates are calculated according to Detmers et al. (2001) and reported in units of *f*mol/cell*day. Isotopic fractionations are determined by relating the ratio of sulfide to sulfate (Equation 4) and then converting to isotopic compositions (Equations 2-4). Raw data is presented in Table A1. Samples labeled as 'NA' represent temperatures where isotopic data (for either sulfate or sulfide) was unavailable. Uncertainties are listed in the text and further discussed in Appendixes 1 and 2.

$\Delta^{33}S$ and $\Delta^{36}S$ respectively (Table 4; Appendix 2). The minor isotope relationships of 46 pairs of samples range from $^{33}\lambda_{SR} = 0.5077$-$0.5125$ and $^{36}\lambda_{SR} = 1.905$-$1.974$. I further present the data as $\Delta^{33}S$ vs. $\Delta^{36}S$, where the data are defined by: $\Delta^{36}S = -8.98$ (± 0.47) $*\Delta^{33}S$ -0.029 (± 0.041).

Discussion

Cell growth and sulfate reduction rates: The cell specific rates reported here are slightly higher than the one value reported in Detmers et al. (2001) for *D. autotrophicum* grown on an organic substrate, but still well within the range reported for other sulfate reducers. Previously reported optimal growth temperatures for strains of *D. autotrophicum* extend from 25-28°C, whereas this culture grew optimally at 22°C. Metabolic activity and cell growth continued above this temperature (to 34°C), as is typical (cf. Hoek et al. 2006). The data follow the empirical relationship between csSRR and fractionation observed in previous studies (cf. Habicht and Canfield, 1997; Hoek et al., 2006) where csSRR and fractionation are inversely related. This is noted below as the "conventional relationship". The data from Detmers et al. (2001) also falls within the values reported in this study. The conventional relationship (Figure 8) is thought to be indicative of the degree of material transfer through the cell, with high rates suggesting near quantitative transfer through the cell (small net fractionations) and low rates giving way to a more restricted flow path, that would allow for the more complete isotopic expression of the internal fractionations (higher net fractionations). This relationship has been

shown not to be universal, however (Canfield et al., 2006), and the data from the most

extreme, and two optimal temperatures within the gradient block do not fit this model

(see ellipses in Figure 8).
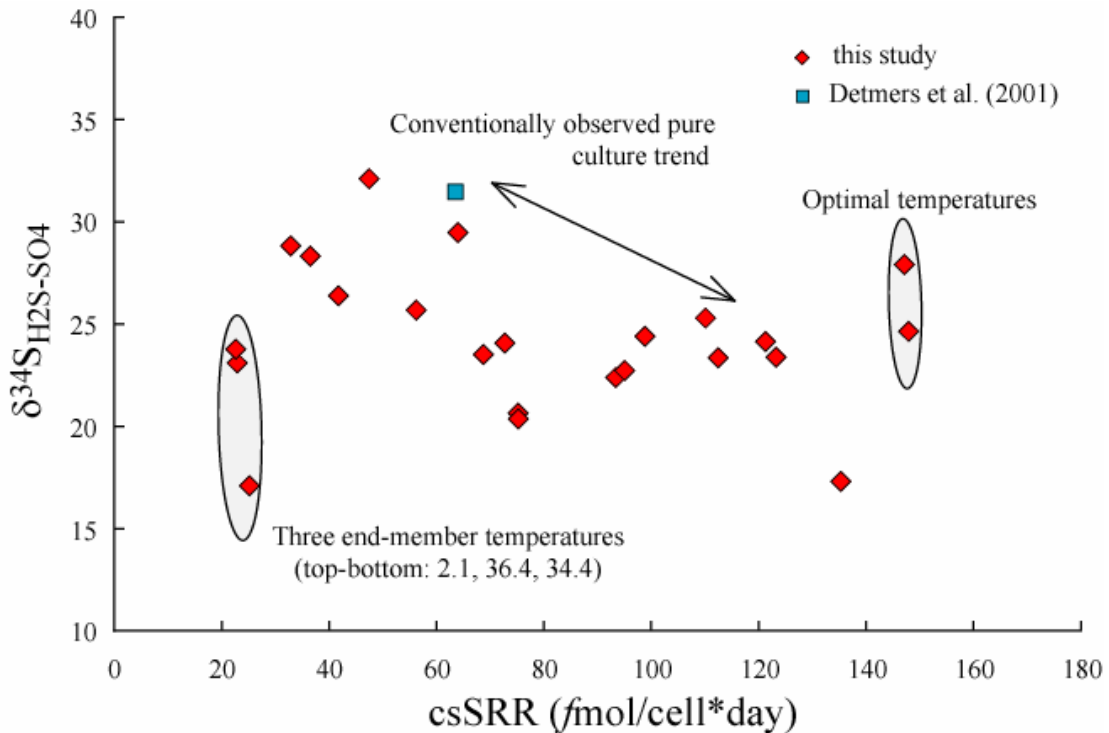
Figure 8: A plot illustrating the relationship between fractionation (δ^{34}S) and the cell specific rate of sulfate reduction (csSRR, *f*mol/cell*day). Isotopic errors are smaller than the symbols. The data is consistent with a previous observation (Detmers et al., 2001) and shows the inverse relationship thought to exist for pure cultures between these parameters. However, samples from the upper two most and lower most temperature, as well as two optimal temperature points, stand in marked opposition to this trend. Studies of natural environments (Habicht et al., 2001) and a recent experimental study (Canfield et al., 2006) have challenged the universality of the inverse relationship between δ^{34}S and reduction rate. The outlying data support the lack of uniformity to this relation, and point to a physiological response in the cell as causing the deviation from the inverse trend, which is observed in the remainder of the data.

Towards the end-member temperatures (and in more extreme conditions in general),

the ability for the cell membrane to stabilize is thought to be a function of the relative

saturation and chain length of the fatty acids comprising the cell membrane (Scherer

and Newhouse, 2002; Canfield et al., 2006). In bacteria, higher temperature generally

results in saturation, whereas colder temperatures begin to favor unsaturated bonds. Thus, as temperatures increase and membrane bound proteins become more loosely retained; the cellular response is to increase the proportion of saturated fatty acids in order to stabilize the membrane (Rabus et al., 2002). Organisms can also modify the chain lengths of the membrane fatty acids in order to maximize membrane fluidity.

Temperature-dependent rate and fractionation: A capability of a cell to fractionate isotopes is likely variable (cf. Harrison and Thode, 1958; Kaplan and Rittenburg, 1964; Kemp and Thode, 1968; Habicht and Canfield, 1998; Canfield, 2001; Detmers et al., 2001), as may also be the dependence of fractionation on rate (as suggested by the "conventional" trend noted in Figure 8). As purely a thought experiment, each of these relationships is considered in turn, where we first address the relationship between csSRR and temperature (Figure 9a). As is expected, the rate calculated from the experiments increased with temperature, reaching a maximum at ~ 22ºC. Above this temperature, the reduction rates begin to fall and approach zero at the upper temperature of 36.4ºC. Figure 9b illustrates the relationship between fractionation (in $\delta^{34}S$) and temperature. This figure presents the calculated average fractionation measured at each temperature (average of points 'a' and 'b'; Table 4). No systematic relationship between temperature and fractionation is observed (the slope of the trend line is not resolvable from horizontal), as the fractionation remains constant throughout. These experiments thus differ from the expectation, which suggests temperature dependence. Of interest is also trying to understand how these two parameters (fractionation and rate) are related. In order to investigate this

relationship, the average fractionation (δ: Figure 9b) is combined with the measured

reduction rates (csSRR: Figure 9a). The goal of this new expression is to examine the

co-variation of these parameters (Figure 9c).

If the thought experiment is continued, the relationship plotted in Figure 9c can be

used to try and better understand the outlying samples from Figure 8. First, the

fractionation/rate term is interpreted as follows. When no change is observed in this

ratio (a horizontal line in Figure 9c), the two variables can be seen to be changing in

concert (positively correlated). This could also be interpreted as a condition where

the machinery responsible for the changes in rate are associated with steps that

fractionate isotopes. The converse would also hold true. As seen in Figure 8, there

are two areas where the conventional relationship is not upheld: at the temperature

extremes and at the optimal growth temperature (though the optimal growth

temperatures could loosely be agued to be within the trend established by the

remainder of the data). Comparing Figure 8 and 9c allows for an interesting

distinction to be made. The optimal temperature samples fall slightly outside the

Figure 8 trend, but fit well with the trend observed in Figure 9c in which they show

no variation. Conversely, at the temperature extremes where the trend in Figure 8 is

also not met, the relationship in Figure 9c shows a great deal of variability.
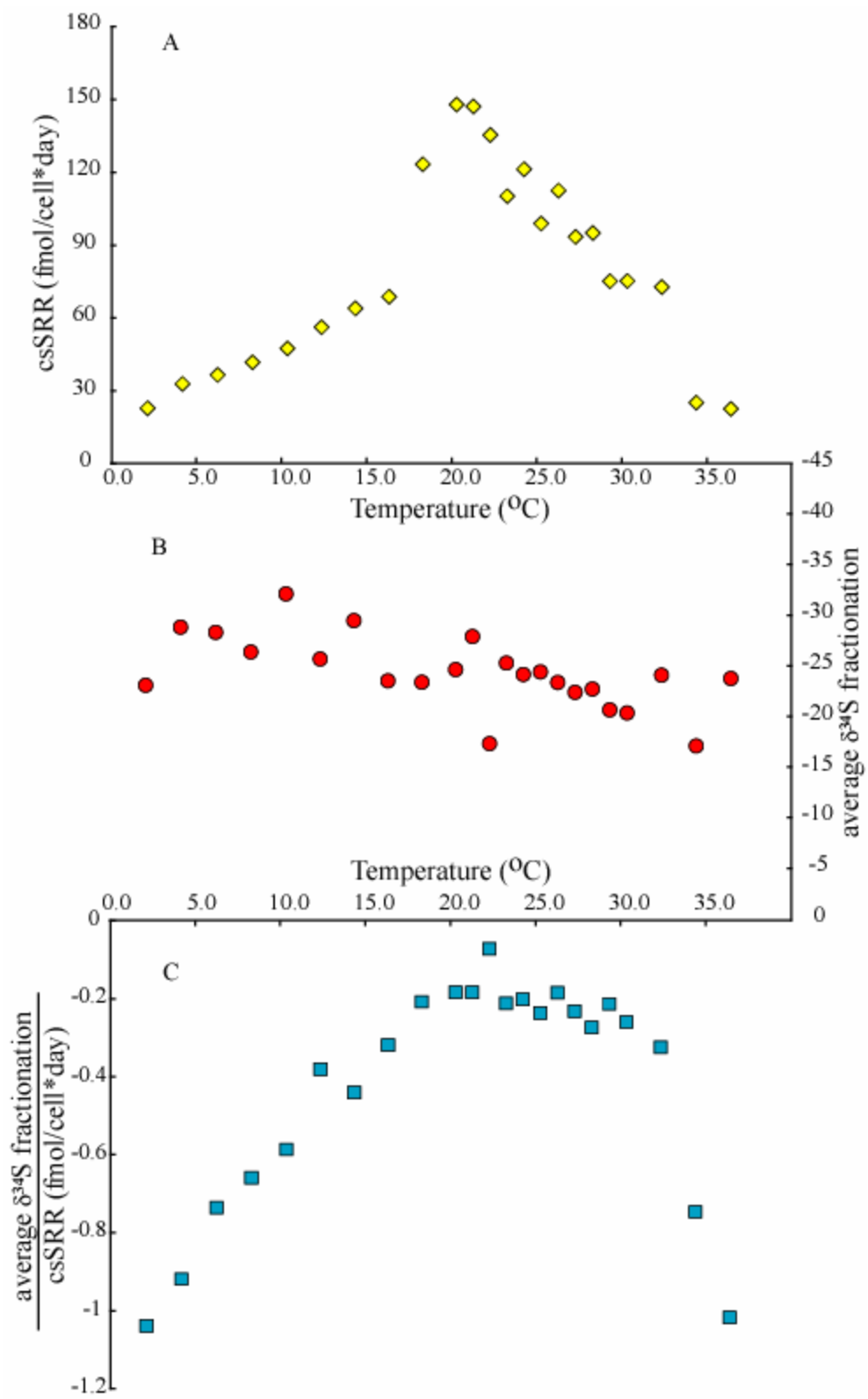
Figure 9: A series of figures illustrating the relationship between temperature and csSRR (A), fractionation (B), and a ratio of the two symbols (C). A) A plot of temperature versus cell specific sulfate reduction rate, which is calculated during the exponential phase of growth at each temperature. The data follow the expected distribution, with lower rates towards the extreme temperatures and a maximum rate towards the upper end of the growth range (~ 22°C). Maximum rates are similar to those reported in Detmers et al. (2001). B) A plot of temperature versus average fractionation (in $\delta^{34}S$). Here, I average the isotopic composition of points 'a' and 'b' seen in Table 1. I do not observe a temperature dependence of isotopic fractionation. C) Temperature plotted against a new relationship, the ratio of the average isotopic fractionation ($\delta^{34}S$) over csSRR. This relationship allows for investigation directly into the co-variation of rate and fractionation.

I take this simple observation to suggest two preliminary conclusions. First, the cause of the deviation from the conventional trend at the extreme temperatures is *different* than that at the optimal temperatures (one trend is flat in Figure 9c, whereas the other is highly variable). The positive co-variation implied by the horizontal trend in Figure 9c suggests that at the optimal temperatures, the machinery controlling sulfate reduction is tied to one (or more) of the significant fractionation steps (perhaps an enzymatic response). Conversely, at the temperature extremes where the relationship between fractionation and rate is not steady (a non-horizontal trend in Figure 9c), the deviation is likely related to a biochemical change not directly dependent on the fractionation steps associated with sulfate reduction. This may again point to a cell membrane dependency (or metabolic component completely unrelated to the dissimilatory process) at these temperatures. Though this application and these results are preliminary and perhaps speculative, I feel that this style of treatment, coupled with a detailed molecular approach (for instance, tracking gene regulation), should be considered in future studies.
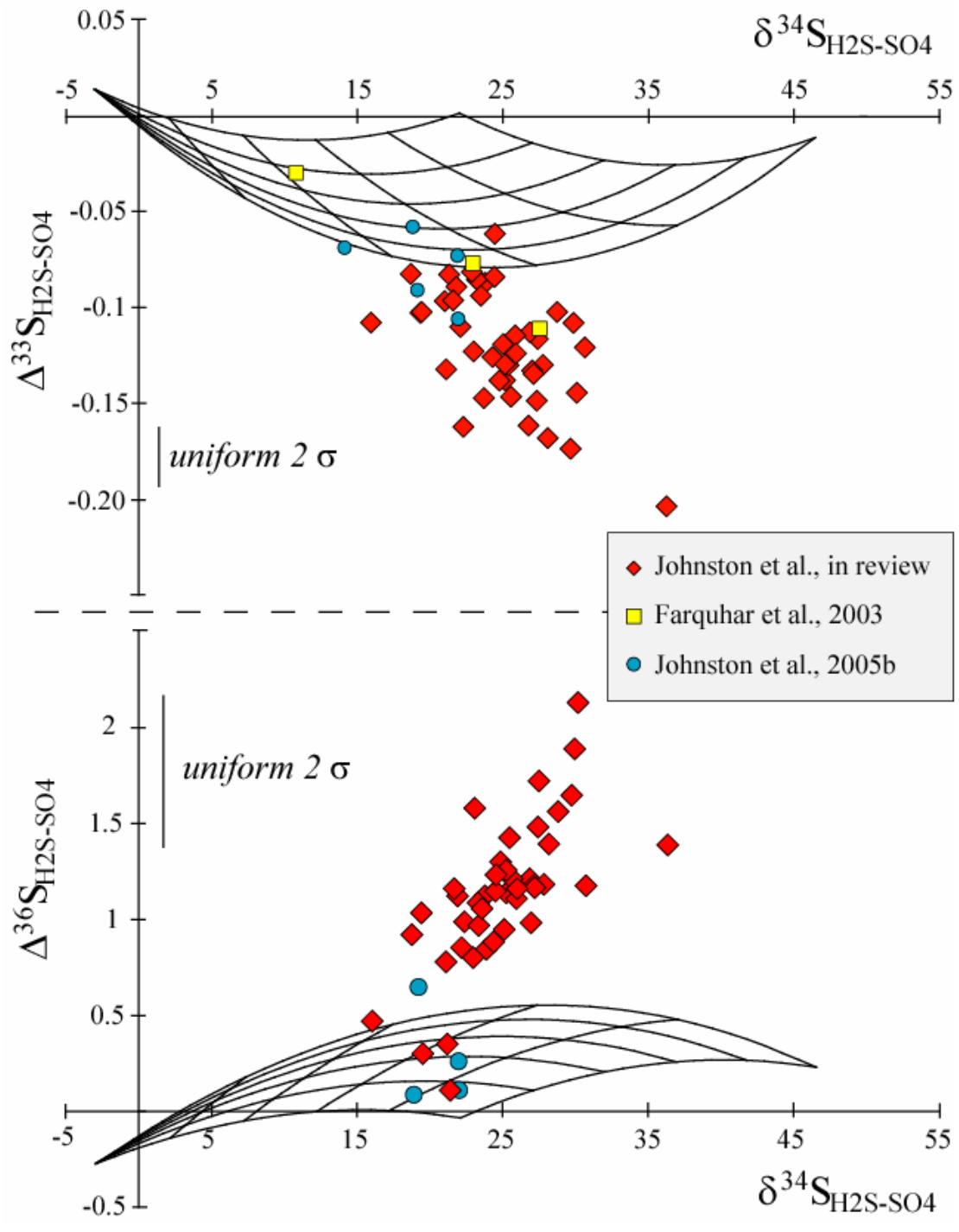
Figure 10: Sulfur isotope model for the consequences of the Rees (1973) network for dissimilatory sulfate reduction (Equation 9). The flux terms seen in these models are described and defined in the text, with f_3 representing mass balance on the entire cell, whereas f_5 constrains the backflow of material from sulfite to sulfate. See Figure 7. a.) The model cast in $\Delta^{33}S$ vs. $\delta^{34}S$ (taken from Farquhar et al., 2003; Johnston et al., 2005) with the new experimental data (red diamonds) and the recalculated previously published data (see Appendixes 1 and 5; squares = Farquhar et al., 2003; circles= Johnston et al., 2005b). The new data illustrates the inconsistency with the model prediction. b.) Same model cast in terms of $\Delta^{36}S$ vs. $\delta^{34}S$. Previous experimental data has been included where ^{36}S data is available (see Appendix 4). As was seen in Figure 9a, the model does not fit the observation.

Evaluating metabolic models

The Rees (1973) model: The standard model (Rees, 1973) for dissimilatory sulfate reduction entails a variety of enzymatically catalyzed steps and fractionations and suggests a uni-directional, single step reduction of sulfite to sulfide. Previous work (Farquhar et al., 2003; Johnston et al., 2005) used the Rees (1973) network to describe the anticipated fractionation in ^{33}S. Those authors presented a model and illustrated a consistency between the model prediction and the previously collected fractionation data. In Figure 10a and 10b I model the predicted isotopic compositions for the Rees (1973) network and include the data from this and previous studies. The new fractionation data, which demonstrate larger $\delta^{34}S_{H2S-SO4}$ fractionations than previous experimental data, fall outside the field calculated using the Rees (1973) network and the assumption that $^{33}\lambda$ and $^{36}\lambda$ for the internal sulfur cycling steps are 0.5145 and 1.90 respectively. This observation suggests that the assumption that the λ values for the internal fractionation steps can be approximated by equilibrium is not appropriate. The new data then suggest that either 1) the Rees (1973) network does not adequately represent the sulfate reduction metabolism, 2) one or more of the assumptions in the isotope model are invalid, or 3) a combination of both. The Rees (1973) model provides both the network and the $\delta^{34}S$ fractionations that I use here.

The changeable free parameters in the model, which may be adjusted to fit the data are the input major and minor isotope fractionations (α, λ) and the network structure. This treatments uses input $^{34}\alpha$'s assigned by Rees (1973) and λ values that represent low temperature thermodynamic equilibrium. Variations in λ have been proposed for some processes, such as diffusion and chemical kinetics (Craig, 1968; Young et al., 2002), but no single set of λ values can account for the ranges observed in Δ^{33}S and Δ^{36}S. This means that, if $^{34}\alpha$ is held constant, no one single set of λ values defining the internal fractionation steps can satisfy all the data. In order for the data to be satisfied with the Rees (1973) $^{34}\alpha$ values, the input λ values would have to vary within the experiments, perhaps as a function of temperature. I suggest that at least one of the internal fractionation steps (either one of the enzymatic steps, the diffusion step, or some component of both) may be underestimated in $^{34}\alpha$ and/or has a temperature-dependence in λ, which could explain the observation.

A modified Rees (1973) model: The "modified Rees (1973)" network consists of the Rees (1973) network structure, but the fractionation factors ($^{34}\alpha$) are modified to reflect low temperature equilibrium processes rather than those fractionations selected by Rees. Following in the spirit of Brunner and Bernasconi (2005), I have assigned equilibrium fractionation values calculated from vibrational spectra (for ^{33}S, Farquhar et al., 2003 is used, however all values are listed in Table 5). The changes from the Rees (1973) fractionations are in the steps associated with both the reduction of sulfate to sulfite, and sulfite to sulfide. I adopt fractionation for these steps using equilibrium values at 0, 10, 20 and 30°C. These values were chosen since they span

58

the temperature range of the experiments. I am not proposing a new fractionation

regime for sulfate reduction, but rather illustrating how the models respond to

different assumptions about the internal fractionations.

T	SO_4^{2-} - SO_2			SO_4^{2-} - SO_3^{2-}		
(°C)	$^{34}\alpha$	$^{33\text{-}34}\lambda_{int}$	$^{36\text{-}34}\lambda_{int}$	$^{34}\alpha$	$^{33\text{-}34}\lambda_{int}$	$^{36\text{-}34}\lambda_{int}$
0	1.04416	0.51444	1.9003	1.02727	0.51408	1.9028
10	1.04169	0.51449	1.8999	1.02595	0.51414	1.9023
20	1.03941	0.51455	1.8995	1.02473	0.51420	1.9019
30	1.03730	0.51460	1.8992	1.02360	0.51426	1.9016
40	1.03536	0.51465	1.8988	1.02253	0.51431	1.9012
65	1.03107	0.51477	1.8980	1.02016	0.51444	1.9003
90	1.02749	0.51488	1.8973	1.01814	0.51455	1.8995
115	1.02447	0.51497	1.8966	1.01639	0.51466	1.8988

	SO_3^{2-} - SO_2			SO_4^{2-} - H_2S		
(°C)	$^{34}\alpha$	$^{33\text{-}34}\lambda_{int}$	$^{36\text{-}34}\lambda_{int}$	$^{34}\alpha$	$^{33\text{-}34}\lambda_{int}$	$^{36\text{-}34}\lambda_{int}$
0	1.01689	0.51501	1.8964	1.08255	0.51457	1.8994
10	1.01573	0.51507	1.8959	1.07807	0.51461	1.8991
20	1.01468	0.51514	1.8955	1.07392	0.51465	1.8988
30	1.01371	0.51520	1.8950	1.07008	0.51470	1.8985
40	1.01282	0.51526	1.8946	1.06652	0.51474	1.8982
65	1.01091	0.51539	1.8937	1.05867	0.51483	1.8976
90	1.00935	0.51551	1.8930	1.05207	0.51492	1.8970
115	1.00808	0.51560	1.8923	1.04647	0.51500	1.8964

Table 5: Listed are $^{34}\alpha$, $^{33}\lambda$ and $^{36}\lambda$ values calculated between common sulfur compounds at low temperatures. Values of $^{34}\alpha$ and $^{33}\lambda$ are expanded from Farquhar et al. (2003), where they are noted as θ. All additional values are calculated in the same fashion as described in Farquhar et al. (2003) and are thus based on low temperature gas phase equilibrium.

As presented in Figures 11a and 11b, these larger fractionation factors allow a

majority of the data to be explained.   As the temperature increases, the net

fractionation prediction becomes smaller in $\delta^{34}S_{H2S\text{-}SO4}$, as well as in $\Delta^{33}S_{H2S\text{-}SO4}$ and
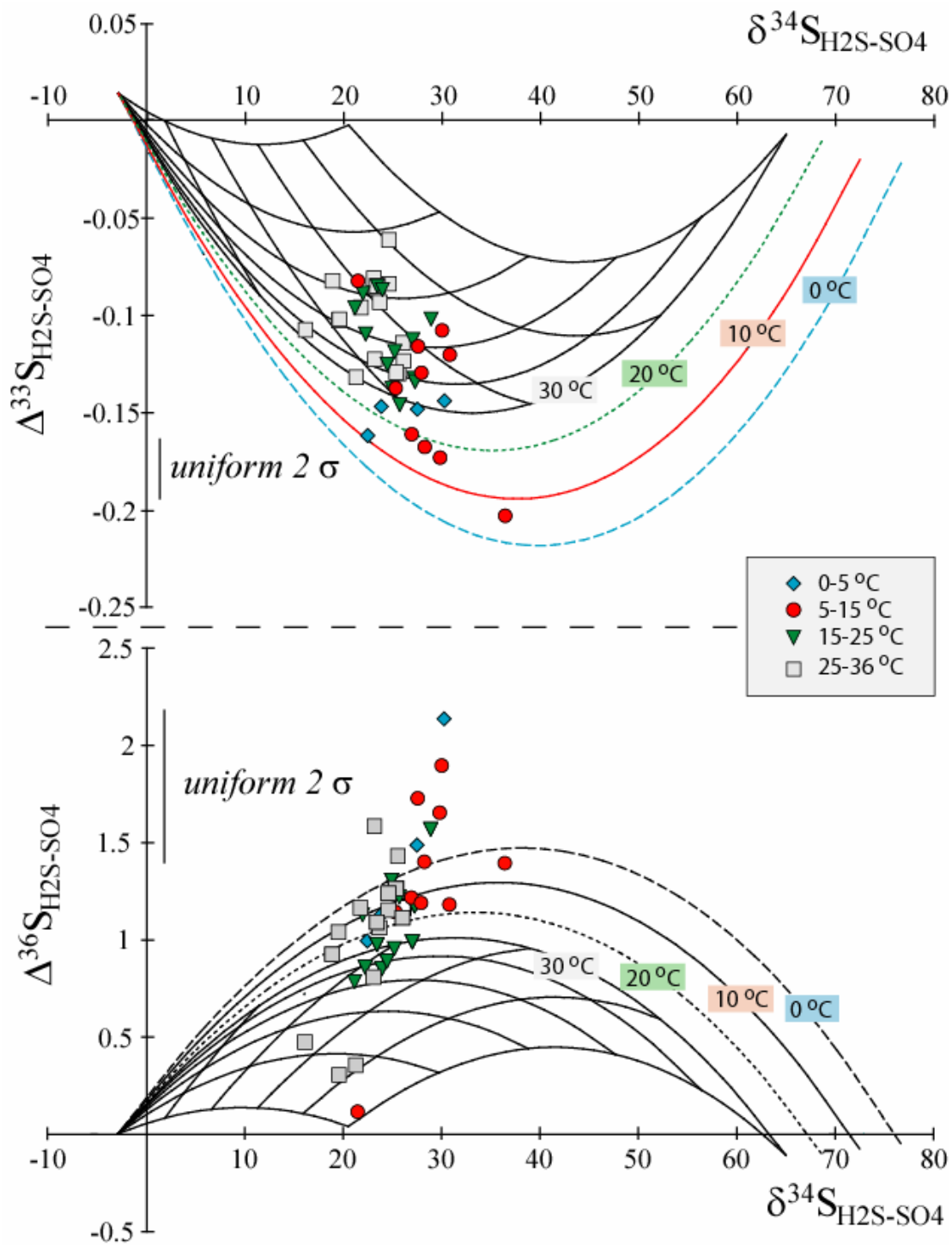
Figure 11: Here I present a model for a modified Rees (1973) network that adopts the structure seen in Equation 9, but using equilibrium fractionations associated with low temperature thermodynamic equilibrium calculations (see Farquhar et al., 2003 for ^{33}S, this study, Table 5, for ^{36}S). The definition of the flux terms is the same as seen in Figure 5. I plot the entire model for fractionation values at 30°C, but include the limits at temperatures of 0, 10, and 20°C. The data are grouped to match these temperature choices. a.) The model cast in Δ^{33}S vs. δ^{34}S. The increased δ^{34}S consequences of this model allow for a majority of the data to be described, with a δ^{34}S limit of ~ 70‰. b.) Same model cast in terms of Δ^{36}S vs. δ^{34}S. Previous experimental data has been included where ^{36}S data is available (see Appendix 4). As was seen in ^{33}S, this model can account for most of the ^{36}S fractionations observed in the experimental data. I note, however, that most of the data is within 2σ of the model prediction but the locus of points falls outside the proper field. This modified network is presented to illustrate a point, and not to propose a modification of the Rees (1973) network.

Δ^{36}S $_{H2S-SO4}$. In Figures 11a and 11b, the data has been binned by temperature to demonstrate the match (or mismatch) between these specific fractionation predictions and the effect of temperature in the experiments. The match between the data and the theoretical temperature prediction is fairly robust, as the grouping of data generally follows the temperature predictions. Only the lowest temperature data (0-5°C) do not fit this trend. Overall, this exercise presented a better fit in ^{33}S than ^{36}S. In Figure 11a, 100% of the data fall within the model prediction whereas in Figure 11b, only 81% are consistent within the prediction, but 95% fall within 2σ. While there is no indication of an analytical artifact that is biasing the ^{36}S measurement, this isotope is difficult to measure and all possible explanations are still considered. Longer-term studies between multiple labs will help to address this issue. The modified Rees (1973) network illustrates that, to a degree, all which is required to satisfy the data are larger internal fractionations as mass-balance can account for much of the observed variability (see Appendix 1 for more details). The requirement is that the ^{34}S fractionation be larger (if $^{33}\lambda$ is ~ 0.515) in order to produce the observed Δ^{33}S signature, even though the large δ^{34}S fractionation implicit in such a situation may go

unexpressed (holding $^{33}\lambda$ constant, the larger the $\delta^{34}S$ fractionation the larger the potential $\Delta^{33}S$).

An active trithionate model: Discussions of the metabolic pathway employed by dissimilatory sulfate reduction have long included the potential presence of sulfur intermediate species (cf. Kobayashi et al., 1974; Fitz and Cypoinka, 1990; Agaki, 1995; Cypoinka, 1995). In particular, the trithionate pathway suggests a step-wise reduction from SO_3 to H_2S (Equation 14). In Figures 12a and 12b I compare model predictions for an active trithionate pathway with the data. As can be seen, when I incorporate fractionation factors suggested by Brunner and Bernasconi (2005), this model easily satisfies the ^{33}S measurements and a majority of the ^{36}S data. This calculation of the pathway ascribes the "trithionate associated fractionations" between sulfite and the sulfur intermediate pool (fluxes 6 and 7 in Equation 14). A different formulation in Brunner and Bernasconi (2005) suggests that the tritionate-associated fractionation should be split equally between the sulfite to sulfur intermediate step (fluxes 6 and 7 in Equation 14) and the sulfur intermediate to sulfide step (fluxes 8 and 9 in Equation 14). The consequence of this change on the model is in the shape of the lower limit (boundary nearest the x-axis). This boundary line would shift such that a new cusp (convergent point of concave down bounding lines) would form with spacing directly related to the size of the two new fractionation steps. In short, the overall magnitude (in ^{34}S) of the predicted field would not change, but the shape of the lower boundary line would. It can be seen that the predictions for the isotopic consequences of an active trithionate pathway are similar to that of the "modified

62

Rees" network, further illustrating that the primary parameter controlling the model

bounds and accounting for the data is $^{34}\alpha$.

The consistency between the data and the trithionate pathway model is encouraging,

and warrants a more detailed examination into both the model implications and the

biochemical consequences. Ideally, the data would provide a diagnostic indication of

the presence of this pathway, however, I am only left with the observation that a

pathway with larger fractionations than Rees (1973) can satisfy the data. The

adoption of the trithionate pathway, or any network with larger net fractionations, is

met by a formidable body of pre-existing experimental evidence on pure cultures and

natural populations of sulfate reducers illustrating fractionations that do not exceed

$\delta^{34}S_{H2S-SO4} = 47$ ‰. As written here and presented in Brunner and Bernasconi (2005),

the sulfate reduction network should be capable of producing fractionations up to

$\delta^{34}S_{H2S-SO4} \sim 75$ ‰. It remains to be seen whether the specific flow conditions

required to produce these large fractionations occurs (or are possible) in natural

settings or communities. This is a target for future study.

Similar to a treatment presented in Canfield et al. (2006), the model approach that this

study uses provides a means of directly testing one portion of the trithionate

prediction: the reversibility and presence of an oxidative sulfur intermediate pool

(such as thiosulfate). The present data set is not ideal for such a treatment, but to

make a prediction and demonstrate the application of such an approach, this test is

outlined. It would be expected that as sulfate reduction proceeds, the electron donor
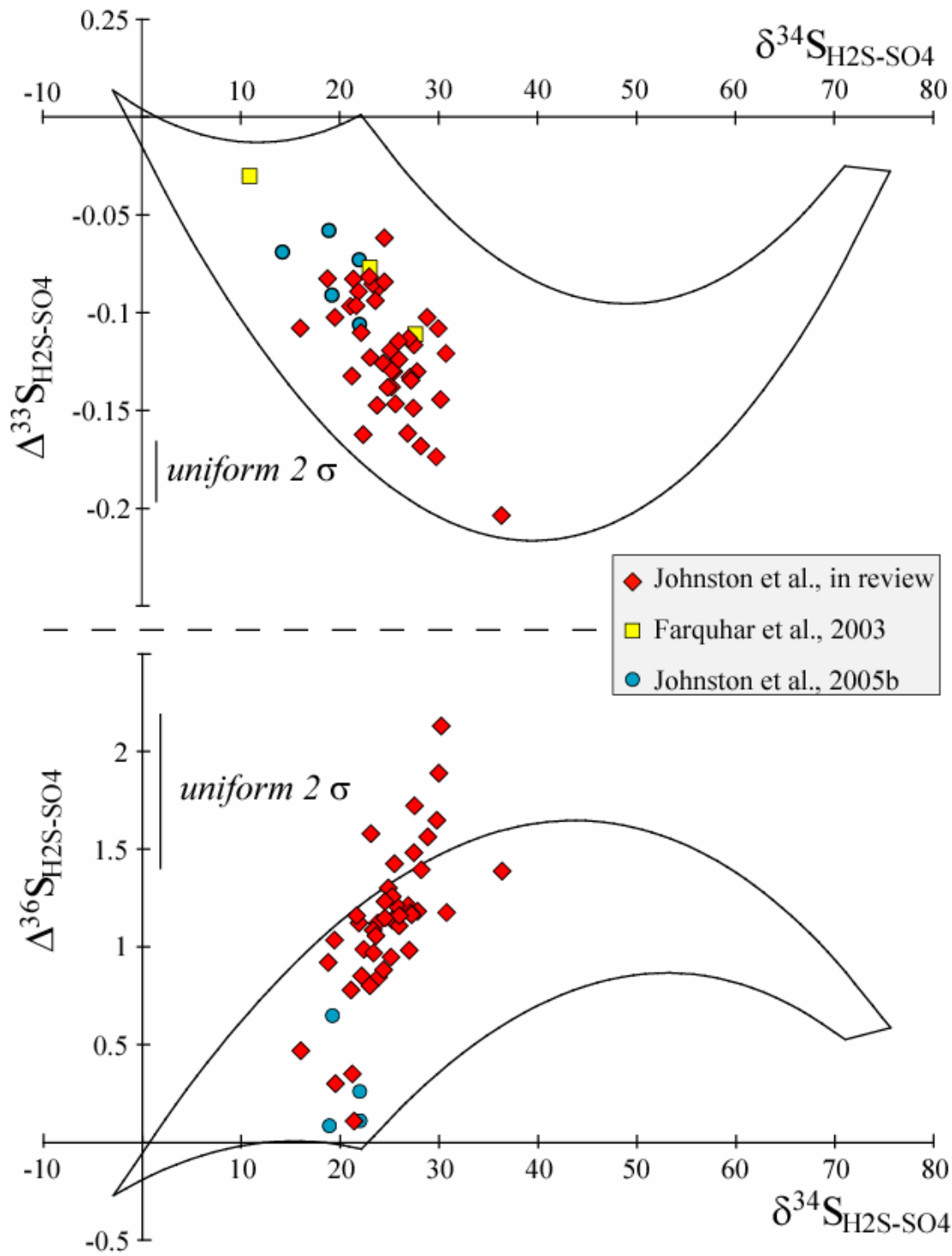
Figure 12: Sulfur isotope model for the consequences of a sulfate reduction network with an active trithionate pathway, as presented in Brunner and Bernasconi (2005) (Equation 14). The new experimental data (red diamonds) along with previously published data (yellow squares = Farquhar et al., 2003; blue circles= Johnston et al., 2005b). a.) The model cast in Δ^{33}S vs. δ^{34}S. This model can describe all the experimental data, and extends to a much larger δ^{34}S limit of ~ 75‰. b.) Same model cast in terms of Δ^{36}S vs. δ^{34}S. Previous experimental data has been included where ^{36}S data is available (see Appendix 4). As was seen in ^{33}S, this model can account for a majority of the ^{36}S fractionations observed in the experimental data (within error).

for the reaction (in this case butyrate) would become depleted. Experimental evidence suggests that as the electron donor becomes more limiting, the concentration of sulfur intermediate species increases (Chambers and Trudinger, 1978; Fitz and Cyponkia, 1990). If true, it would be expected that with the increased concentrations of S-intermediates, the back reaction from the intermediate to sulfite would become more likely.

The same principle would hold true for the presence of an internal hydrogen sulfide pool. For the model presented in Equation 14, the back reaction from the S-intermediate to sulfite has an associated 5 ‰ effect in δ^{34}S, which would suggest that as the intermediate accumulates and begins to back react, the net fractionation would increase by 5 ‰. The increased fractionation in the model is represented by the variable f_7, which constrains the material flow along the back reaction. So, as f_7 varies from 0 (no back reaction) towards 1 (full back reaction), there is an isotope effect of 5 ‰. Future experiments could be designed to target the expression of this biochemical step in the sulfate reduction process as a test of the presence of a trithionate pathway.

Comparing metabolic models: While the data do not uniquely support one or another network structure, if it were possible to extend the measurements of the four sulfur isotopes to the internal sulfur reservoirs, I might be able to construct a framework for evaluating the different networks. Figure 13 illustrates the predicted isotopic compositions of the internal sulfur pools (sulfite and sulfate) within the Rees (1973) network and defines a testable hypothesis for the validity of this network, provided that the isotopic composition of one internal sulfur species can be obtained. Similar predictions were made for ^{34}S by Canfield et al. (2006). Although Rees (1973) is the only network considered, this approach can, in principle, be applied to any network and for any internal species. To illustrate this point, plotted are the predictions for $f_3 = 0.6$ and $f_5 = 0.8$, with the external sulfate constrained to the origin. Predictions for internal species in an active trithionate pathway are more difficult to uniquely constrain given that the model has three independent parameters.

A number of noteworthy points can be derived from the example given in Figure 13. First, the compositions of sulfide and sulfite track one another, always offset by $\delta^{34}S_{SO3-S} = 25‰$ on a slope ($^{33}\lambda_{SO3-S}$) of ~ 0.5145. One example of this is demonstrated through the example included on the model fields, which are offset by 25‰ on a slope of 0.5145. This reflects the input network structure, where the sulfite is assumed to be uni-directionally reduced to sulfide via the sulfite reductase enzyme. Conversely, the relationship between internal sulfate and sulfite is not constant, due to the reversibility of this reaction and the added flux and fractionation of sulfur moving

into and out of the cell as sulfate. As shown in Figure 13, the $\delta^{34}S_{SO4(int)-SO3} \sim 20\text{‰}$
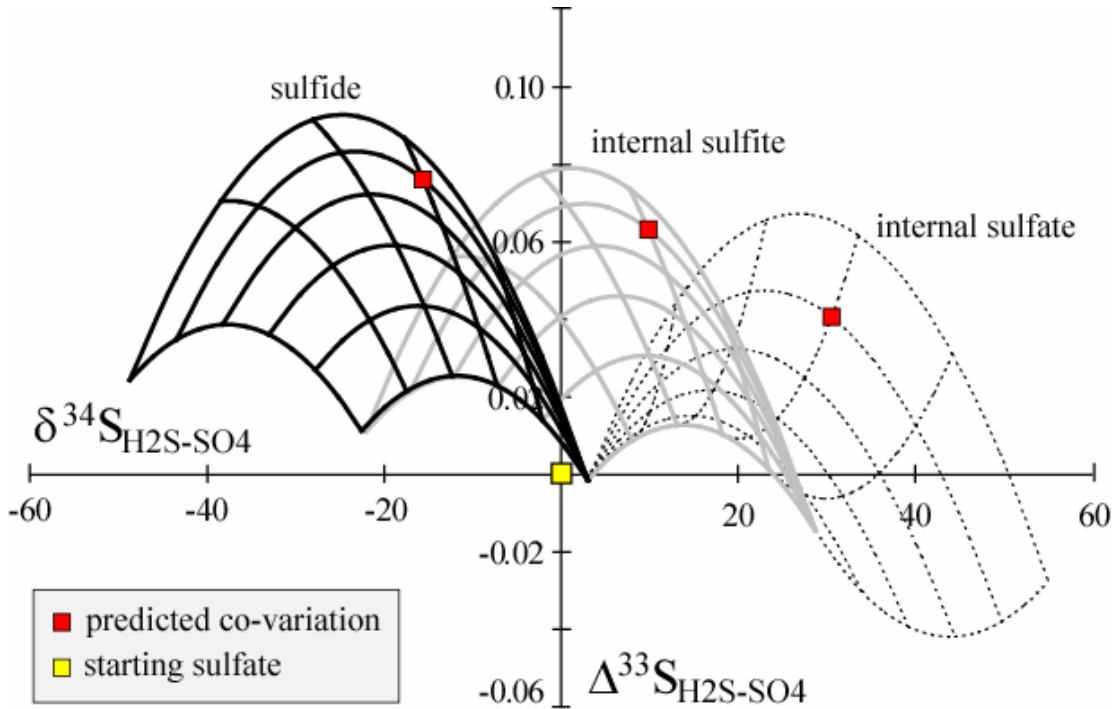
Figure 13: Modeling treatments also allow for the prediction of the isotopic composition of the internal sulfur pools in a network. Plotted are the solutions for the Rees (1973) network (seen in terms of ^{33}S) where the composition of the external sulfate (plotted at origin), internal sulfate (dashed field), internal sulfite (gray field) and external sulfide (black field) are predicted. The contours within the model fields present relative fluxes, similar to that presented for the Rees (1973) network. As an example, plotted are the prediction for $f_3 = 0.6$ and $f_5 = 0.8$ to illustrate how the composition of the three fields should co-vary. The measurement of these reservoirs is an ideal target for future assessments of the sulfate reduction network.

with $^{33}\lambda_{SO4(int)-SO3} \sim 0.5138$. All the $^{33}\lambda$ values for the relationship between the

internal pools vary around a value of ~ 0.5145, consistent with the original definition

of $^{33}\alpha$ ($= {}^{34}\alpha^{0.5145}$) in the model. The relationship between the external sulfate

reservoir and the internal pools varies more widely, since all these relationships

incorporate a variety of steps and influences. This is largely due to internal recycling

of material, and predicts a range of $^{33}\lambda$ values from $^{33}\lambda_{SO4(ex)-SO3} = 0.521$ to the net

sulfate reduction fractionation of $^{33}\lambda_{SO4(ex)-S}$ (or $^{33}\lambda_{SR}$) $= 0.510$.

The relationship between ^{33}S and ^{36}S

Defining (or developing) a tool to distinguish between two (or multiple) processes contributing to a common natural record would greatly increase the understanding of natural systems. I look to the relationships of all four isotopes to provide this tool, and pose two questions: *Does the fractionation observed in ^{33}S and ^{36}S vary in a predictable fashion?* and, *If there is variability in these signatures, is it related to process?* Until now, the difficulty in addressing these questions has been two-fold: analytical precision has been insufficient for the task and there has been a lack of data. Recent advancements in analytical capabilities now allow for precise measurements of ^{36}S, and this, coupled with the feasibility of collecting large data sets (98 measurements in the current chapter), allows these questions to be examined. I approach this problem from two directions. First, I evaluate the relationship between Δ^{33}S and Δ^{36}S, which is dependent on the minor isotope fractionation and on the magnitude of fractionation of ^{34}S/^{32}S. Second, I examine the relationship between $^{33}\lambda$ and $^{36}\lambda$, which are the exponents that describe the fractionations. These terms are calculated independent of the magnitude of the δ^{34}S fractionation and this approach may allow for the character of different fractionation mechanisms to be directly compared.

Δ^{33}S vs. Δ^{36}S: Recent studies have suggested that relationships relating Δ^{33}S and Δ^{36}S may preserve information about mass-dependent geochemical cycling (Ono et al., 2006; Johnston et al., 2006: Chapter 5). Models incorporating single-step equilibrium fractionations and mixing/distillation have been presented to argue for a linear

relationship with $\Delta^{36}S = -6.85*\Delta^{33}S$ (Ono et al., 2006). Modeling of Paleoproterozoic

sediments with multi-step mixing and distillation processes indicate that the

relationship between $\Delta^{33}S$ and $\Delta^{36}S$ cannot be described by a single line, but that the

approximation of $\Delta^{36}S \sim -7*\Delta^{33}S$ may be reasonable (Johnston et al., 2006: Chapter

5). The interest here is to define the character of the co-variation between $\Delta^{33}S$ vs.

$\Delta^{36}S$ for a single process rather than entire environment. In addition, the goal is to

determine whether there exists a unique relationship for sulfate reduction that differs

from or is similar to that previously established for global or basin scale geochemical

systems, and in doing so to define a range of values that can be compared to other

biological, chemical, and physical fractionation processes.

Our first attempt to define a range of proposed predictions begins with the results of

the modeling treatments discussed above, meaning that I can cast the models seen in

Figure 10-12 in terms of $\Delta^{33}S$ vs. $\Delta^{36}S$. All of these models are built with the *a priori*

assignment of the relationship between ^{33}S and ^{36}S (the input exponent values of

0.5145 and 1.9 respectively), which reflects low temperature equilibrium

fractionation. As can be seen in Figure 14a (model prediction for the trithionate

pathway), the model does not predict a single line, but instead reveals a narrowly

defined region. The choice of 0.515 (rather than 0.5145) would result in the $\Delta^{33}S$ vs.

$\Delta^{36}S$ model prediction collapsing onto a single line, since 0.515 and 1.90 are the

values used in the definition of the Δ values. The model results then indicate that

values other than $\Delta^{36}S = -6.85 \Delta^{33}S$, the theoretical prediction of Ono et al. (2006),

can be produced when either a non 0.515 (or 1.90) exponent (or process reflected by

69

the exponent) or mass-balance effect, such as those described in Appendixes 1 and 2, are present.
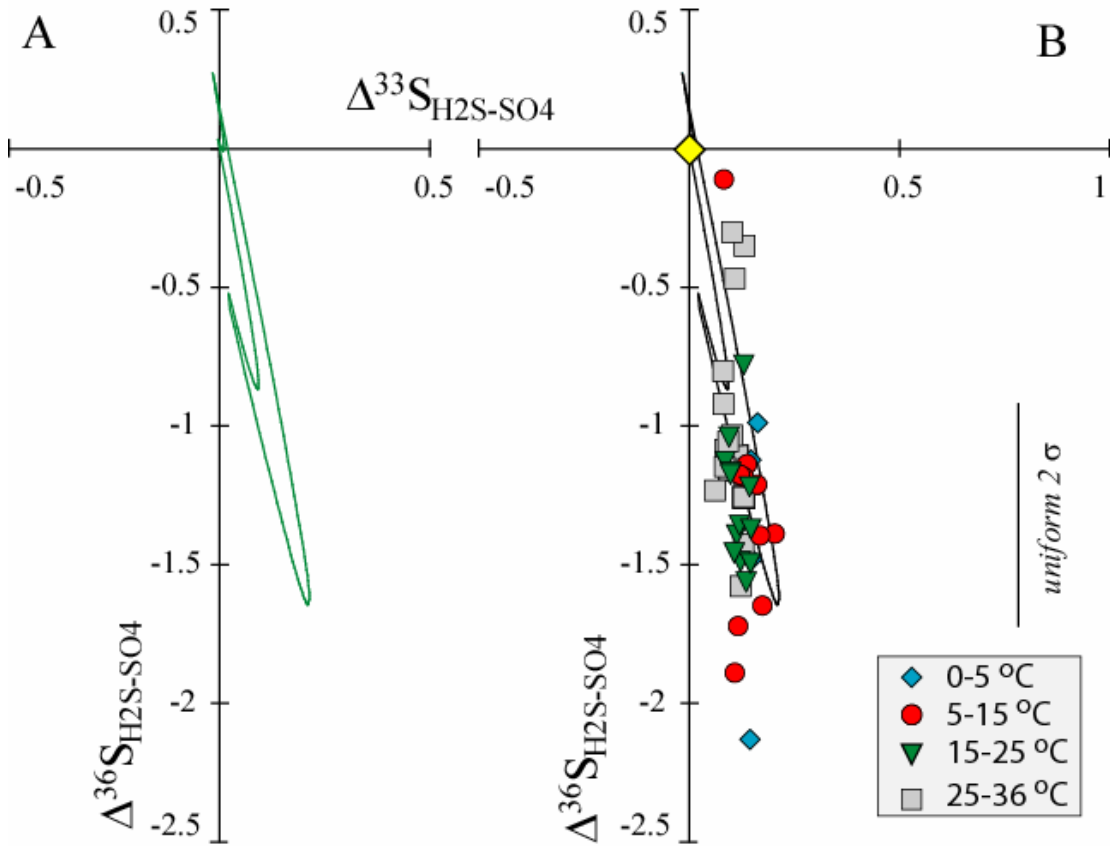
Figure 14: Plotted is the model solution for the active trithionate pathway (A) and the data from this study (B), in terms of $\Delta^{33}S$ and $\Delta^{36}S$. Uncertainties in $\Delta^{33}S$ are smaller than the symbols. The models do not suggest much variability due to the *a priori* determination of the relationship (see text), and generally follow a slope suggested by equilibrium (-6.85). Although a majority of the data falls near this model prediction (or even within uncertainty), the fit is not ideal as the general trend of the data and model differ.

Figure 14b and Figure 15 present all the data in terms of $\Delta^{33}S$ and $\Delta^{36}S$ (Table 4).

Each data point represents a sulfate-sulfide pair, such that for every data point on the

figure there is an accompanying data point at the origin. The array extending through

the data follows the net relationship: $\Delta^{36}S = -8.98 \,(\pm 0.47)\, \Delta^{33}S -0.029 \,(\pm 0.041)$,

which is $> 2\sigma$ from the equilibrium prediction ($\Delta^{36}S = -6.85\, \Delta^{33}S$). If broken down in

more detail, the slope values for each of the different temperature clusters falls within

1σ of the net relationship defined above, and ranges from -8.74 to -9.27. It is taken

from this observation that the net sulfate reduction signature (or small change in

slopes) deviates slightly from equilibrium predictions and is independent of

temperature. I postulate that the slope defined by the data represents the net process

of sulfate reduction, rather than a single physiological step within the sulfate

reduction network. This is suggested because the data cover a range of temperatures

(2-38°C), ruling out the possibility of a single physiological condition controlling the

signature. The overall fit of the model predictions is not perfect, (cf. Fig 14) but does

illustrate how natural variability, like that seen in the experiments, can arise (cf.

changing internal λ).

In addition, Rayleigh effects (see Appendix 4) can alter the observed relationship

between $\Delta^{33}S$ and $\Delta^{36}S$. Prior to the removal of the Rayleigh effects, the $\Delta^{33}S$ and

$\Delta^{36}S$ co-variation was significantly different, and suggested a value of $\Delta^{36}S = -10.32$

$\Delta^{33}S$. I document, therefore, that closed system effects can drive the $\Delta^{33}S$ vs. $\Delta^{36}S$

slope towards more negative values, as is demonstrated in the experiments. This

suggests that both process and mass-balance can contribute to the overall observed

$\Delta^{33}S$ vs. $\Delta^{36}S$ slope. This lesson should be carried into studies of natural basins and

marine settings, where contributions are more difficult to distinguish and where the

possibility of closed system behavior is more prevalent. In addition to providing

valuable insight into the role of closed system behavior, this allows us to use this data

to begin to place limits on the anticipated range of values measured in natural settings

as extending up to $\sim$ -11 (similar to the observed, uncorrected data).
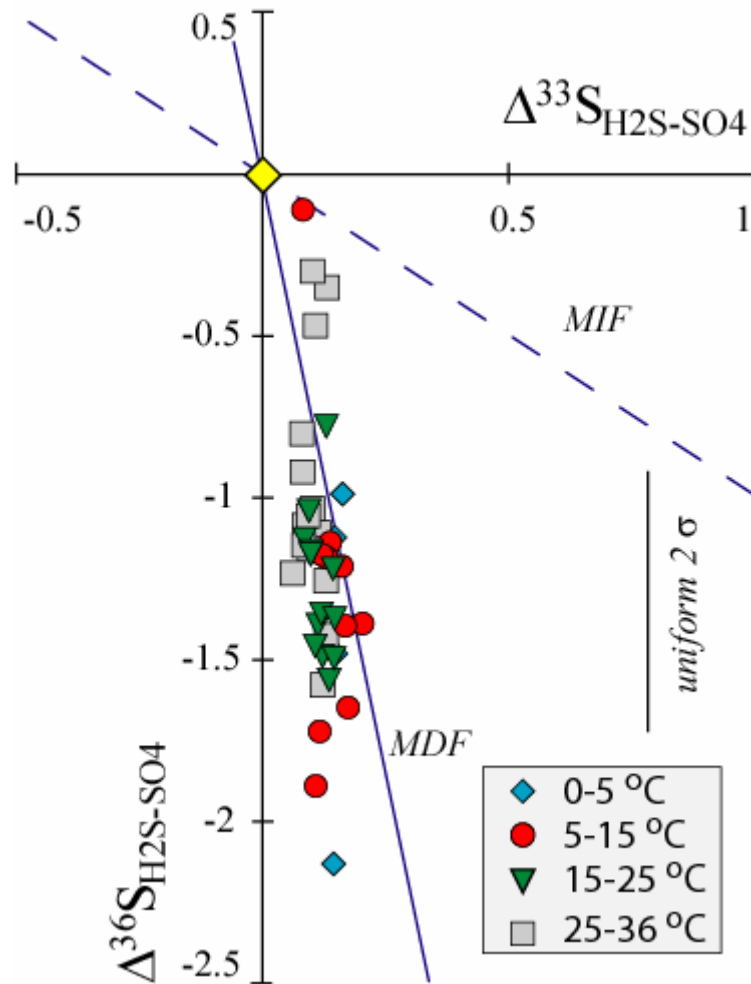
Figure 15: All the data plotted as a function of the minor isotope composition ($\Delta^{33}S$ and $\Delta^{36}S$). A mass-dependent (MDF) prediction from Ono et al. (2006) as well as a mass-independent (MIF) prediction (from Farquhar et al., 2000) are included for reference. The data all fall to the lower right (quadrant 4), with an equal number of samples plotting at (0, 0) due to the normalization. The slope of the line determined by the data is statistically resolvable from that of theoretical equilibrium predictions (Ono et al., 2006). This is taken to suggest a process-specificity to the signature.

It is acknowledged that little is known about the ^{36}S fractionation associated with oxidation processes, and speculate that they will produce slopes < -6.85 and expand the range proposed above. On its own, it is also intriguing that the sulfate reduction data define a well-constrained relationship that differs from a single -6.85 equilibrium line. This suggests that there may exist a predictable, linear, and process-

specific relationship between $\Delta^{33}S$ and $\Delta^{36}S$. Future studies of both natural and experimental systems are needed to aid in this understanding.

$^{33}\lambda$ vs. $^{36}\lambda$: The second relationship that I examine is between $^{33}\lambda$ and $^{36}\lambda$. In Figure 16 I plot all the sulfate reduction data in terms of $^{33}\lambda$ vs. $^{36}\lambda$. I observe that a majority of the data falls away from the reference fractionation coordinate of (0.515, 1.90). Although plotting away from the reference coordinate, the sulfate reduction data does cluster with $^{33}\lambda < 0.515$ and $^{36}\lambda > 1.90$. I take this to suggest that the fractionations associated with ^{33}S and ^{36}S may be coupled (clusters in Figure 16), but follow a relationship different than that of low temperature equilibrium (origin of the reference values). This suggests that what is expressed may be a *process-specific* relationship between ^{33}S and ^{36}S that describes sulfate reduction. Limited data for sulfur disproportionation experiments is also included in Figure 16 (see Table 3). These data suggest that the $^{33}\lambda$ vs. $^{36}\lambda$ for sulfur disproportionation experiments differ from the sulfate reduction experiments. Although preliminary, I propose this approach as a means of deciphering between the influences of sulfate reduction and sulfur disproportionation, especially when trying to understand complex environments. These data would suggest that a modern marine environment, where both sulfate reduction and sulfur disproportionation are active, would plot between the two established fields. The $^{33}\lambda$ vs. $^{36}\lambda$ relationship could provide great insight into the processes contributing to both modern marine isotope records, and also ancient records where the presence of different microbial processes is unknown or disputed.
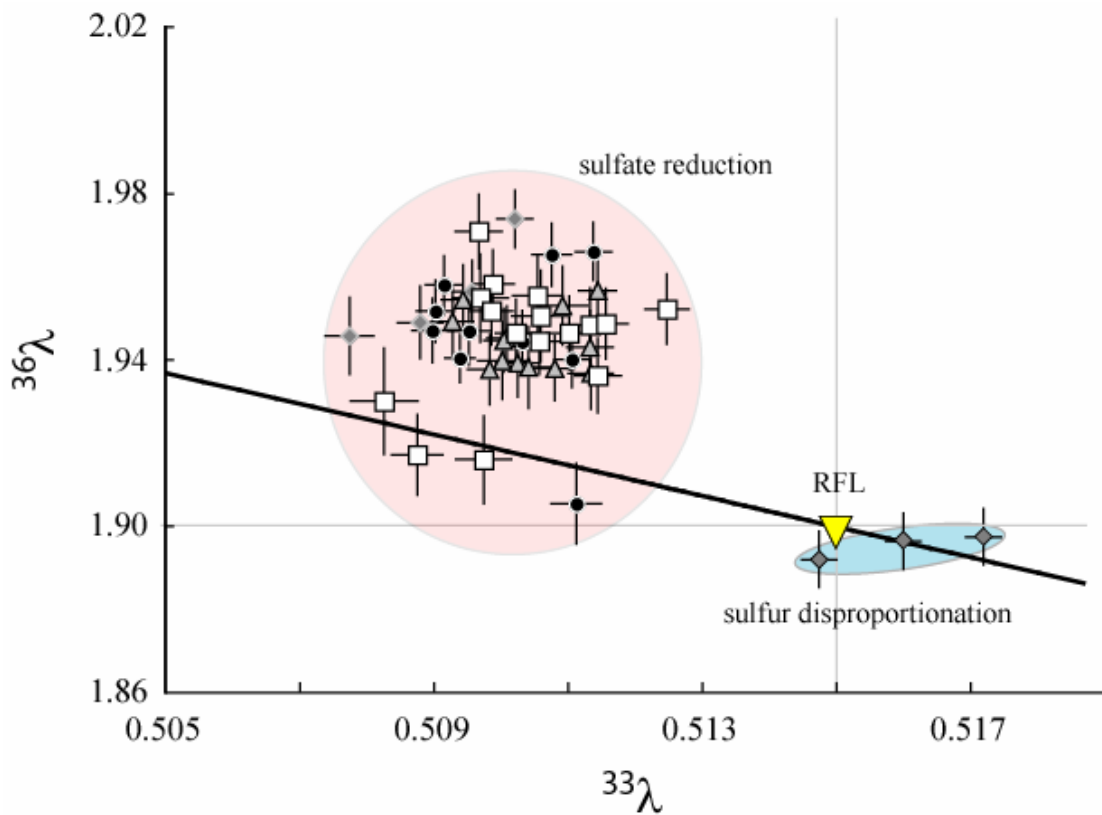
Figure 16: The normalized data plotted as a function of $^{33}\lambda$ and $^{36}\lambda$, a general measure is independent of the magnitude of $\delta^{34}S$ fractionation. Errors are 2 σ. The giant yellow triangle represents the accepted RFL value (0.515 and 1.90), whereas the sulfate reduction data plots in the field defined by the four temperature suites listed. Symbol shapes are defined in Figure 15, with the addition of gray squares, which represent data from Chapter 2. Limited sulfur disproportionator data (from Chapter 2) is also included to illustrate the potential application of this measure as a means to distinguish between contributions from different sulfur utilizing metabolisms.

Conclusions

The investigation of sulfur isotope fractionations for all four sulfur isotopes by sulfate

reducing microorganisms has allowed for the traditional model of dissimilatory

sulfate reduction (Rees, 1973) to be re-evaluated, indicating that the internal

fractionations are larger than those assigned by Rees (1973). While the data require

larger internal fractionation factors, they do not uniquely support (or rule out) the possibility of an active trithionate pathway with reverse flow from a sulfur intermediate (or internal sulfide) to sulfite. The identification of this network using this approach would require lab experiments that produce larger $\delta^{34}S$ fractionations than have been observed and very specific $\Delta^{33}S$ and $\Delta^{36}S$. In my opinion, studies targeting the isotopic composition of the four isotopes and concentration of internal sulfur species (namely internal sulfate and sulfite) and the fractionation associated with key enzymes (sulfite reductase) will be required to provide the information necessary to define an updated sulfate reduction isotopic fractionation pathway.

Other trace isotope relationships have also aided in the understanding of mass-dependent fractionations and potential environmental applications of the lessons learned from this study. I suggest that the application of the $\Delta^{33}S$ vs. $\Delta^{36}S$ relationship in mass-dependent systems and post 2.0 Ga environments can be a powerful means of addressing the presence of different metabolic processes or the presence of closed-system behavior in larger-scale systems, such as sedimentary basins or oceanic settings. Further, the data suggest a sulfate reduction specific slope of ~ -9, which statistically differs from the slope presented for single-step equilibrium fractionation effects (Ono et al., 2006). I also investigated a relationship between ^{33}S and ^{36}S that is independent of the magnitude of fractionation ($\delta^{34}S_{H2S-SO4}$), $^{33}\lambda$ vs. $^{36}\lambda$. The difference in $^{33}\lambda$ vs. $^{36}\lambda$ for sulfate reduction and sulfur disproportionation suggests that this relationship may be very useful in studies of natural environments, where the relative contribution from these two metabolisms is poorly constrained.

The results of this study suggest that the sulfate reduction metabolism has larger internal fractionation steps than previously proposed. If all the fractionations associated with the sulfate reduction metabolism could be fully expressed, the data require that net fractionations would exceed 47 ‰. However, these large net fractionations have not been observed in laboratory experiments or natural population studies, suggesting that the conditions necessary to produce such effects are difficult to achieve or unlikely in nature. The question then becomes, what is the feature limiting the expression of the larger internal fractionation steps? A similar dependence has been illustrated for the relationship between isotopic fractionation and sulfate concentrations (Thode et al., 1951; Habicht et al., 2002), and the results raise the tantalizing possibility that the lack of the full isotopic expression of sulfate reduction may actually be providing information about paleo-environmental limitations or limits for the cycling of sulfur within a sulfate reducing microorganism.

Chapter 4: Active Sulfur Disproportionation in the Mesoproterozoic

Introduction

The environmental expression of sulfur compound disproportionation has been placed between 640 – 1050 Mya and linked to increases in atmospheric oxygen. These arguments are based on temporal changes in the magnitude of $^{34}S/^{32}S$ fractionations between sulfate and sulfide. Here, I present a Proterozoic seawater sulfate isotope record that includes the less abundant sulfur isotope, ^{33}S. These measurements imply that sulfur compound disproportionation was an active part of the sulfur cycle by 1300 Mya, and that progressive Earth surface oxygenation may have characterized the Mesoproterozoic.

Background

There is a strong link between the oxidation state of the Earth's surface environment and the microbial sulfur metabolisms that influence the sulfur cycle (Canfield and Teske, 1996; Canfield, 1998; Shen et al., 2001). This link is revealed through sulfur isotope studies where different microbial metabolisms contribute to the final isotopic composition of sulfur species preserved in the geologic record (Thode et al., 1961; Holser et al., 1988; Canfield, 2001). The relationship between isotopic fractionation

due to sulfate-reducing microorganisms (SRB[2]; $SO_4^{2-} \rightarrow H_2S$) and seawater sulfate

concentration has been the primary tool for interpreting the sulfur isotope record of

Earth surface oxidation (Perry et al., 1971; Hattori et al., 1983; Ohmoto et al., 1993;

Habicht et al., 2002; Kah et al., 2004). For example, the isotopic record of

sedimentary sulfides reveals that SRB may have dominated the global sulfur cycle

until the Neoproterozoic. After this, greater $^{34}S/^{32}S$ fractionations cannot be explained

by sulfate reduction alone (Canfield and Teske, 1996), and they likely reflect the

added contribution of sulfur compound disproportionating microorganisms (SDB;

$S^0/SO_3^{2-}/S_2O_3 \rightarrow SO_4^{2-}+H_2S$). As sulfide oxidation is responsible for the intermediate

sulfur compounds used by SDB (Troelsen and Jorgensen, 1982; Bak and Pfenning,

1987; Thamdrup et al., 1993; Canfield and Thamdrup, 1998), the widespread activity

of SDB has been interpreted to indicate increased atmospheric oxygen content

(Canfield and Teske, 1996). New data, however, suggests that the isotopic

fractionation between seawater sulfate and sulfide in the Neoproterozoic may have

been smaller than previously estimated (Hurtgen et al., 2002, 2005). This raises the

prospect that the $\delta^{34}S$ record may not uniquely reveal the activities of SDB during the

Neoproterozoic.

Recent experiments illustrate that SRB and SDB produce resolvable $^{33}S/^{32}S$

fractionations for similar magnitudes of $^{34}S/^{32}S$ fractionations (Chapters 2-3; Farquhar

et al., 2003; Johnston et al., 2005b). In those experiments, the compositions of sulfate

associated with SDB were more ^{33}S enriched than sulfate associated with SRB. The

---

[2] I chose to keep the traditional shorthand of SRB (sulfate reducing bacteria) to represent sulfate
reducing microorganisms (Bacteria and Archea). Similarly, I use SDB to represent sulfur
disproportionating microorganisms.

fractionations preserved in the sulfur isotope record largely reflect the combined influence of these two metabolisms (Canfield, 2001). I propose that by considering both the fractionations associated with $^{33}S/^{32}S$ and $^{34}S/^{32}S$, as preserved in ancient marine sulfide and sulfate minerals, I can elucidate the significance of SRB and SDB on the global sulfur cycle. Here I combine a steady-state, open-system isotope mass-balance model with data from sediments deposited between ~2000 and ~500 Ma to constrain how sulfur isotope signatures are transferred through a global sulfur cycle that includes SRB and SDB (Figure 17). The model tracks the sulfur isotopic composition of the seawater sulfate and reactive sulfide reservoirs as sulfur is microbially cycled between them. A fundamental assumption in the model is that any re-oxidation flux from reactive sulfide to seawater sulfate ultimately occurs through disproportionation reactions.

Sulfur cycle models

Our model has a similar structure to other isotope mass-balance models of the S-cycle with two exceptions: (1) the model tracks ^{33}S as well as ^{34}S and ^{32}S; and (2) it explicitly includes pathways through a sulfur reservoir of intermediate oxidation state to account for the isotopic consequences of disproportionation (Figure 17). The model was constructed with conventional approximations that result from the trace distribution of minor isotopes (^{33}S, ^{34}S). It was calibrated with experimentally derived fractionation factors (see Chapters 2-3) for microbial sulfate reduction and microbial sulfur disproportionation. A series of model calculations were run incorporating the whole range in $^{33}S/^{32}S$ and $^{34}S/^{32}S$ fractionations observed in pure

and enriched culture experiments (Chapters 2-3). The limits from over 200 individual

models runs are represented by the fields presented in Figure 18. Inputs to the model

are: 1) the experimentally calibrated $^{33}S/^{32}S$ and $^{34}S/^{32}S$ fractionations associated SRB

and SDB, 2) the isotopic composition of the sulfate entering the model through the
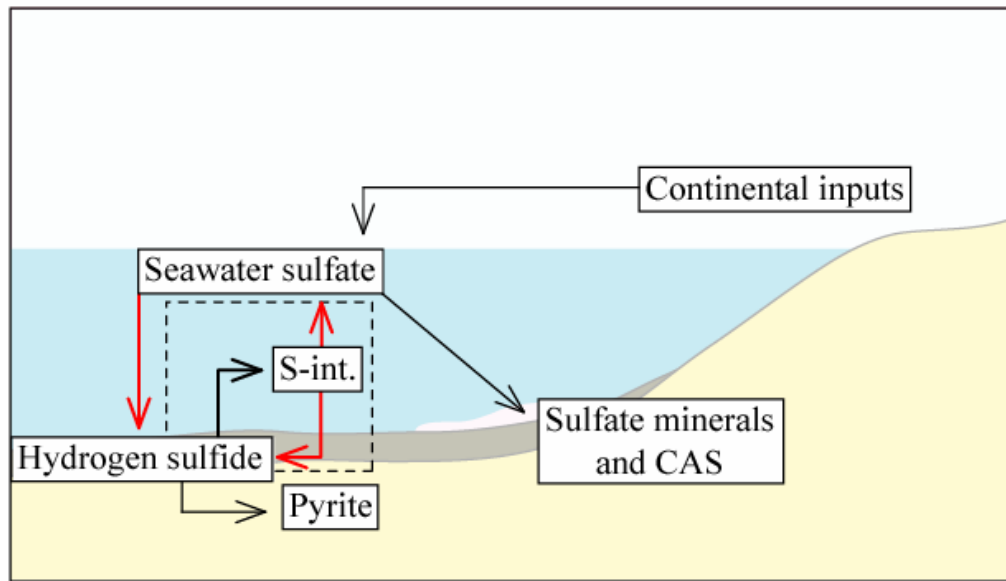
Figure 17: Illustration of the box model used to constrain the isotopic composition of seawater sulfate. The arrows represent fluxes of material between reservoirs. Biologically mediated reactions are shown as red arrows, with both the reduction of sulfate to sulfide (by sulfate reducing microorganisms) and the oxidation and reduction of sulfur intermediates (by sulfur disproportionating microorganisms) involving significant fractionations. Contributions from volcanism are thought to be negligible, or contribute sulfur that is isotopically similar to continental weathering.

seawater sulfate reservoir (the origin in Figures 18-20), 3) the proportion of sulfate

entering the model through the seawater sulfate reservoir that leaves the model as

pyrite rather than as sulfate minerals (f_{py}), and 4) the proportion of sulfur entering the

reactive sulfide pool that is completely re-oxidized to sulfate (f_{r-o}). I began each

calculation by choosing fractionations for SRB and SDB, and by varying f_{py} and f_{r-o} a

unique array of relationships between the $\delta^{34}S$ and $\Delta^{33}S$ of model seawater sulfate

was produced.
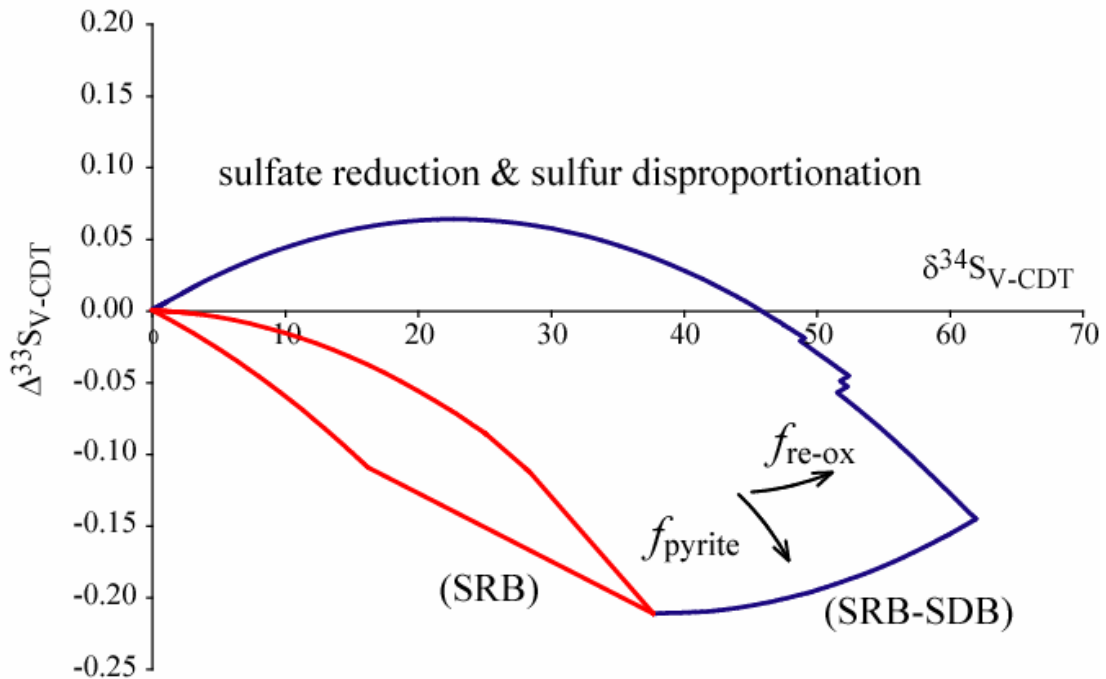
Figure 18: $\Delta^{33}S$ vs. $\delta^{34}S$ values for seawater sulfate predicted from an open-system steady-state S-cycle model. The discrete curves are calculated for a sulfur cycle that includes only SRB. Different curves are calculated for different values of experimentally constrained isotopic fractionations by SRB. The field bound by a solid red line is accessible to a strict SRB S-cycle (SRB-system). The field bound by a solid blue line is accessible to a combined SRB-SDB microbial S-cycle (SRB/SDB-system). The inset shows the direction that $\Delta^{33}S$ vs. $\delta^{34}S$ trajectories evolve as f_{py} and f_{r-o} increase. The different $\Delta^{33}S$ vs. $\delta^{34}S$ regions accessed by the SRB- and SRB/SDB-systems are used to assess the microbial contribution to the oceanic sulfur cycle at the time of sulfate deposition.

As f_{py} increases in a model system including only SRB, the composition of seawater

sulfate becomes ^{34}S-enriched relative to the sulfate entering the model (Figure 18;

Garrels and Lerman, 1981; Kump and Garrles, 1986; Berner, 1987; Holser et al.,

1988; Kah et al., 2004). In this case, the $\Delta^{33}S$ values of model seawater sulfate

become more negative as $\delta^{34}S$ values increase (Farquhar et al., 2003). This is

reflected in the orientation of the curves that outline the field of $\Delta^{33}S$ and $\delta^{34}S$ in

Figure 18 labeled "SRB". When the model S-cycle is expanded with a re-oxidative

sub-cycle that allows for microbial sulfur disproportionation, increasing $f_{r\text{-}o}$ leads to seawater sulfate that is more enriched in ^{34}S and has more positive $\Delta^{33}S$ than when only SRB is included. This is reflected by the field labeled "SRB-SDB" (Figure 18). These model results form the basis for using the isotopic composition of proxies for seawater sulfate to distinguish the significance of microbial sulfur disproportionation within the global sulfur cycle.

This study

I measured the sulfur isotopic composition of 49 Proterozoic to Cambrian sulfate samples from either carbonate associated sulfate (CAS: 35 in total) or sulfate minerals (14 in total; Table 6). Although I report ^{36}S data in Figure 6, I save the discussion of this data until Chapter 7. CAS was extracted from powdered rock samples using a modified version of standard techniques (Burdett et al., 1989) and then reduced to Ag_2S (Thode et al., 1961). Sulfate minerals were powdered and directly reduced to Ag_2S. In Figure 19, the $\Delta^{33}S$ and $\delta^{34}S$ values of these samples are plotted relative to fields for the modeled SRB-system and the modeled SRB-SDB-system. The model interpretation of these measurements assumes that they represent a well-mixed, homogeneous seawater sulfate reservoir whose composition is set by global processes. Although the results in Figure 19 have their basis in the assumption that the sulfate entering the model is unfractionated relative to bulk Earth estimates, the relative positions of the SRB and SRB-SDB fields are not affected by variations in the isotopic composition of the sulfate entering the model. Specific inferences about

Geologic Formation	age	$\delta^{33}S$	$\delta^{34}S$	$\delta^{36}S$	$\Delta^{33}S$	$\Delta^{36}S$
Uygurian Fm., Siberian Platform, Russia	510.7	18.25	35.69	69.01	0.025	0.12
Orakta Fm., Siberian Platform, Russia	517.1	20.61	40.46	78.35	-0.024	0.09
Zhivalovo Fm., Irkutsk Basin, Russia	530	17.10	33.46	64.56	0.004	0.03
Zhivalovo Fm., Irkutsk Basin, Russia	530	16.23	31.76	61.25	0.004	0.06
Zhivalovo Fm., Irkutsk Basin, Russia	530	16.52	32.34	62.37	-0.002	0.03
Kuanchanpu Mbr., Yangtze Platform, China	537	22.77	44.74	87.66	-0.030	0.94
Shelogontsi Markha Fm., Irkutsk Basin, Russia	540	17.15	33.53	64.42	0.021	-0.25
Krasnoporog Fm., Siberian Platform, Russia	556.5	17.94	35.14	68.27	-0.007	0.45
Krasnoporog Fm., Siberian Platform, Russia	559.8	19.96	39.10	75.58	0.010	-0.02
Subkharikhan Fm., Siberian Platform, Russia	561.2	17.67	34.60	67.13	0.001	0.37
Hanseran Evap. Fm., Rajasthan, India	571	16.97	33.25	64.47	-0.020	0.34
Hanseran Evap. Fm., Rajasthan, India	571	16.13	31.56	61.19	0.004	0.37
Hanseran Evap. Fm., Rajasthan, India	571	16.60	32.47	62.62	0.004	0.03
Doushantuo Fm., Yangtze Platform, China	571	17.00	33.57	64.97	-0.156	0.22
Dengying Fm., Yangtze Platform, China	571	15.91	31.10	60.15	0.011	0.24
Redstone River Fm., MacKenzie Fold Belt, CA	750	8.51	16.60	31.69	-0.007	-0.09
Redstone River Fm., MacKenzie Fold Belt, CA	750	9.03	17.62	33.74	-0.004	NA
Redstone River Fm., MacKenzie Fold Belt, CA	750	8.82	17.22	32.96	-0.011	-0.01
Bitter Springs Fm., Amadeus Basin, Australia	850	10.88	21.23	40.56	-0.001	-0.17
Bitter Springs Fm., Amadeus Basin, Australia	850	9.96	19.38	36.98	0.026	-0.16
Bitter Springs Fm., Amadeus Basin, Australia	850	11.12	21.67	41.54	0.019	-0.03
Bitter Springs Fm., Amadeus Basin, Australia	850	10.36	20.19	38.60	0.019	-0.10
Walcott Mbr., Colorado Plateau Province, USA	850	12.00	23.42	44.81	0.006	-0.15
Jupiter Mbr., Colorado Plateau Province, USA	930	6.25	12.23	0.00	-0.028	NA
Katav Fm., Bashkirian Anticlinorium, Russia	940	16.17	31.69	61.83	-0.025	0.77
Society Cliffs Fm., Bylot S. Gp., Canada	1200	16.87	32.96	63.63	0.034	0.08
Society Cliffs Fm., Bylot S. Gp., Canada	1200	15.30	29.79	57.46	0.060	0.09
Society Cliffs Fm., Bylot S. Gp., Canada	1200	17.79	34.75	66.96	0.045	-0.08
Society Cliffs Fm., Bylot S. Gp., Canada	1200	17.87	34.85	68.11	0.067	0.85
Society Cliffs Fm., Bylot S. Gp., Canada	1200	13.72	26.72	51.16	0.046	-0.22
Society Cliffs Fm., Bylot S. Gp., Canada	1200	14.69	28.65	54.87	0.038	-0.26
Society Cliffs Fm., Bylot S. Gp., Canada	1200	16.66	32.56	62.59	0.023	-0.19
Duguan Fm., N. China Platform, China	1200	11.43	22.36	43.24	-0.020	0.34
Longjiayuan Fm., N. China Platform, China	1300	8.31	16.28	0.00	-0.043	NA
Dismal Lakes Gp., Canada	1300	15.88	31.05	60.42	0.006	0.59
Dismal Lakes Gp., Canada	1300	11.12	21.68	0.00	0.015	NA
Dismal Lakes Gp., Canada	1300	14.77	28.90	56.48	-0.012	0.85
Dismal Lakes Gp., Canada	1300	12.53	24.47	47.35	-0.001	0.34
Helena Fm., Belt S.Gp., USA	1450	8.90	17.48	33.71	-0.065	0.25
Helena Fm., Belt S.Gp., USA	1450	4.99	9.75	19.00	-0.016	0.40
Helena Fm., Belt S.Gp., USA	1450	9.58	18.78	36.29	-0.043	0.31
Helena Fm., Belt S.Gp., USA	1450	6.74	13.19	25.30	-0.030	0.10

continued...

Geologic Formation	age	$\delta^{33}S$	$\delta^{34}S$	$\delta^{36}S$	$\Delta^{33}S$	$\Delta^{36}S$
Bungle Bungle Dolomite, Birrindudu Basin, Australia	1600	17.20	33.84	65.69	-0.088	0.40
McNamara Gp., Australia	1680	16.12	31.61	61.61	-0.036	0.69
McNamara Gp., Australia	1700	17.08	33.41	64.91	0.010	0.48
McNamara Gp., Australia	1700	19.99	39.16	76.08	0.014	0.36
McNamara Gp., Australia	1700	16.90	33.05	64.43	0.011	0.70
McArthur Gp., McArthur Basin, Australia	1700	8.92	17.39	33.32	0.003	0.02
Kona Dolomite, Marquette Range, USA	2000	7.01	13.72	0.00	-0.031	NA

Table 6: Sulfur isotopic measurements of seawater sulfate proxies. I focus on established proxies for seawater sulfate (i.e., evaporites; Claypool et al. 1980; Strauss, 1997; and CAS; Kampschulte et al., 2001; Hurtgen et al., 2002, 2005; Kah et al., 2004; Lyons et al., 2005). Ages listed are from Claypool *et al*. (1980), Schopf (1983), Strauss (1993), Kampschulte et al. (2001), Kah et al. (2004), Condon et al. (2005), and Gellatly and Lyons (2005). While I recognize that there are uncertainties associated with these radiometric constraints, they are not large enough to change the interpretation of temporal ^{33}S variations.

the exact values of f_{py} and $f_{r\text{-}o}$ that are implied by $\Delta^{33}S$ and $\delta^{34}S$ measurements of

seawater sulfate proxies depend on the assumed isotopic composition of the sulfate

entering the model. Because of this, for the time being I focus the interpretation of the

new measurements on their general placement within the SRB and SRB-SDB fields.

These conclusions are valid with reasonable isotopic variations of the incoming

sulfate ($\delta^{34}S \pm 5$‰ (Holser et al., 1988); $\Delta^{33}S \pm 0.03$‰). The majority of the

Neoproterozoic/Cambrian data in Figure 19a occupy the modeled SRB-SDB field.

This $\Delta^{33}S$ and $\delta^{34}S$ evidence for active microbial sulfur disproportionation is

consistent with phylogenetic studies and previous interpretations of the $\delta^{34}S$ record

(Canfield and Teske, 1996). This approach, however, also yields evidence for an

active SRB-SDB system in the Mesoproterozoic (Figure 19b), leading to the

suggestion that microbial sulfur disproportionation was not initiated in the

Neoproterozoic but, instead, operated for at least part of the Mesoproterozoic

(Hurtgen et al., 2005).
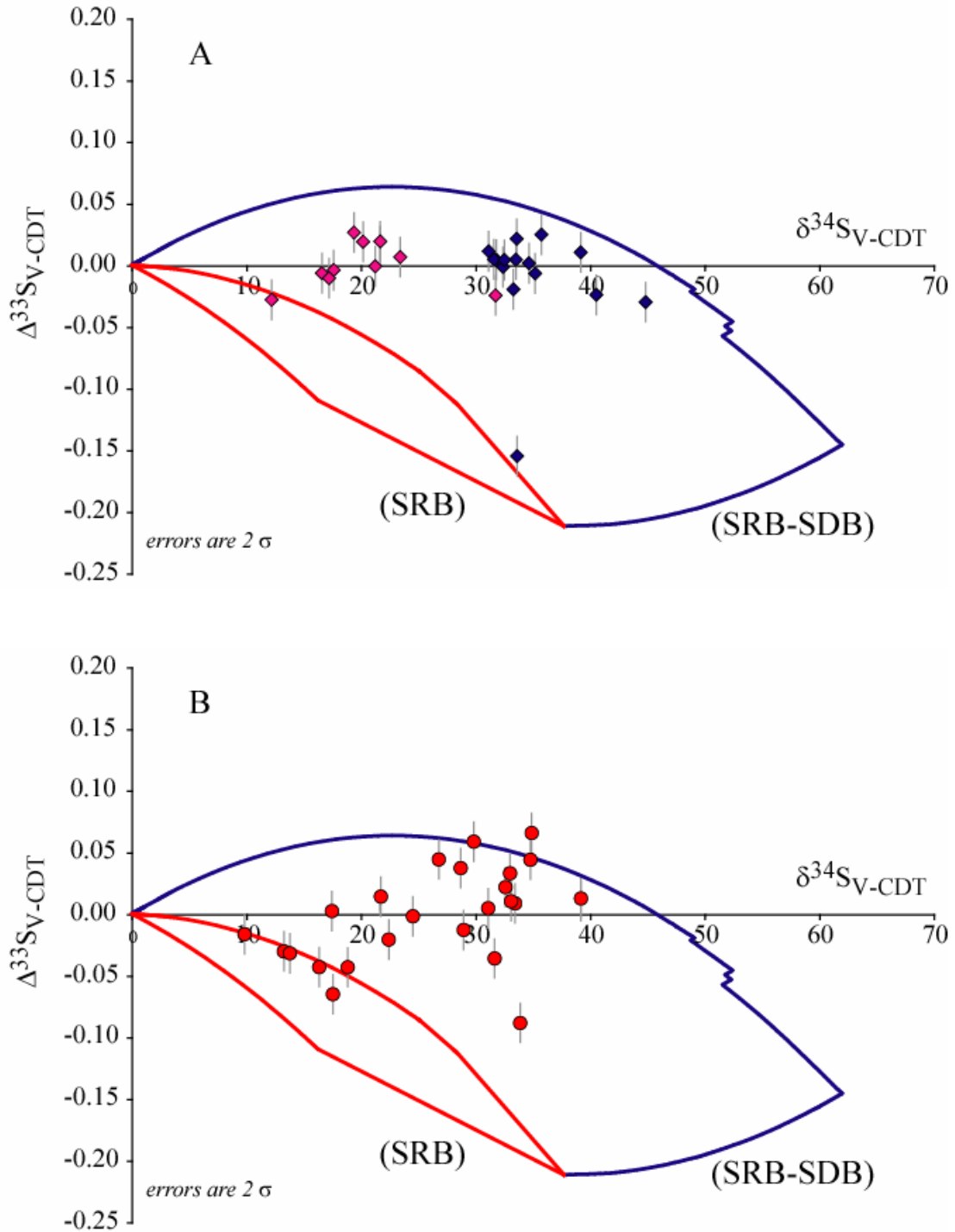
Figure 19: Measured $\Delta^{33}S$ vs. $\delta^{34}S$ values for Proterozoic/Cambrian seawater sulfate proxies combined with model predictions (Figure 18). Errors are 2 σ. **(A)** Neoproterozoic-Cambrian data (1000 – 500 Ma) divided into older (1000 – 750 Ma; pink diamonds) and younger (571 – 500 Ma; blue diamonds) groups. Variation between the two groups likely reflects differences in f_{py} in a system with both SRB and SDB. **(B)** Paleo- to Mesoproterozoic data (2000 – 1000 Ma; red circles). The Paleo- Mesoproterozoic data extend across a range that is defined by the SRB system and the SRB-SDB system.

The isotopic composition of seawater sulfate from the Mesoproterozoic Society Cliffs Formation (~1200 Ma) and the Dismal Lakes Group (~1300 Ma) show clear evidence for active microbial sulfur disproportionation (Figure 20a). The Society Cliffs data contain a strong SDB signature, and the relationship between this data and the model indicates extensive sulfur processing through disproportionation reactions. The $\Delta^{33}S$ - $\delta^{34}S$ data for Dismal Lakes samples also contain a clear SDB signature and are consistent with lower proportions of sulfide re-oxidation and pyrite burial. In contrast, the isotopic compositions of CAS in the ~1450 Ma Helena Formation are consistent with a strict SRB system (Figure 20a) and do not require the influence of SDB. The data indicate that SDB became progressively more important in the global sulfur cycle over the ~250 million year time interval from 1450 to 1200 Ma. While these conclusions should be confirmed with additional data from other Mesoproterozoic basins, most pre-1300 Ma samples in the current dataset exhibit $\Delta^{33}S$ - $\delta^{34}S$ values that unambiguously reflect an SRB-only system (Table 6, Figure 20b).

Thus far, samples from only one pre-1300 Ma sedimentary basin (McNamara Gp., ~1660 Ma; Figure 20b) appear to be inconsistent with the conclusions drawn above. These data, however, display some unusual isotopic characteristics. The $\delta^{34}S$ values of these samples span a wide range (~17 to 39‰), covering a significant portion of the entire dataset (~9 to 44‰). In addition, McNamara $\Delta^{33}S$ values vary in a near-
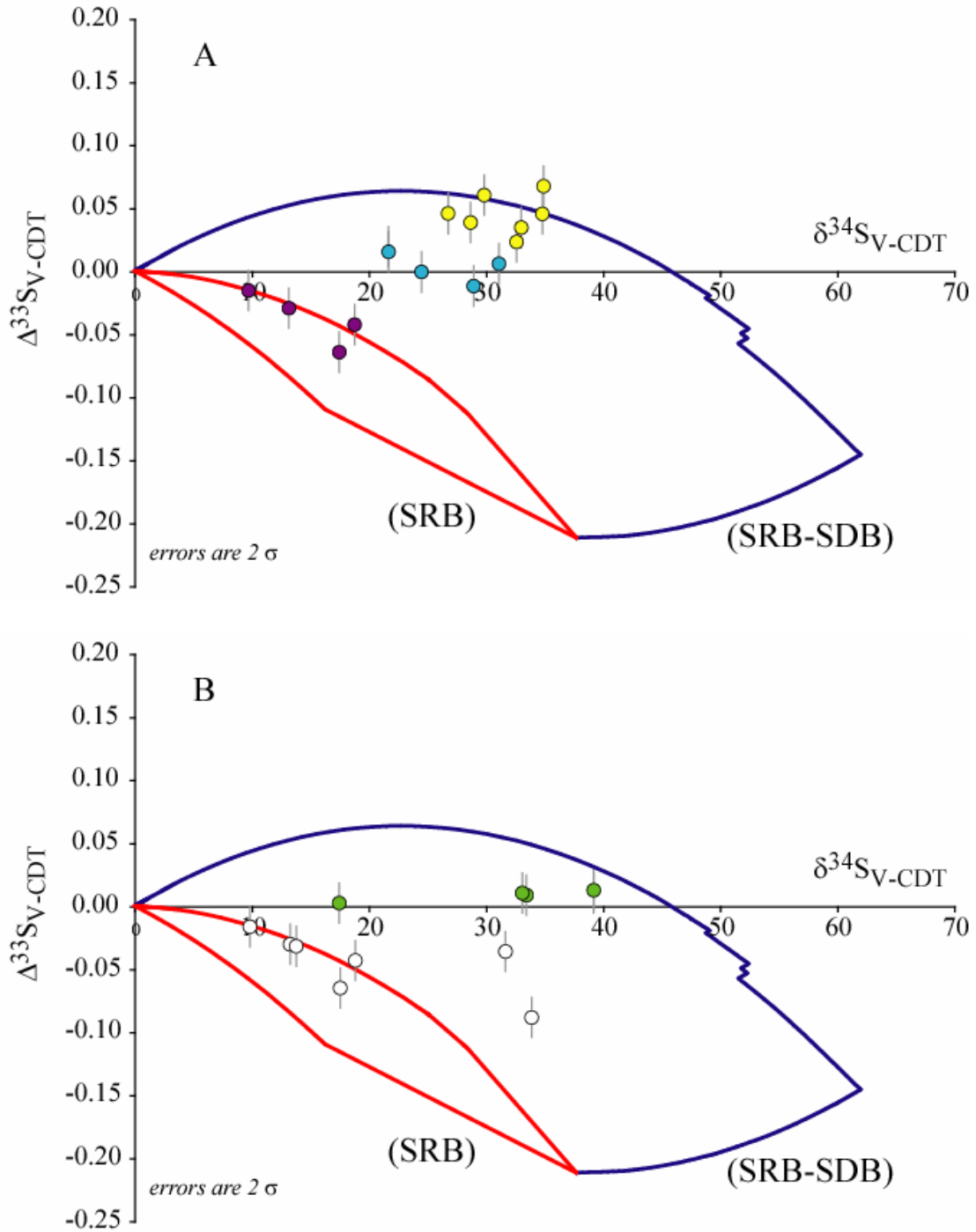
Figure 20: Measured $\Delta^{33}S$ vs. $\delta^{34}S$ values for seawater sulfate proxies from Mesoproterozoic basins and model predictions (Figure 18). (A) The ~1200 Ma Society Cliffs Formation (yellow circles) and the ~1300 Ma Dismal Lakes Group (blue circles) require active SDB at the time of their deposition. Samples from the ~1450 Ma Helena Fm. (purple circles) fit within the bounds of a strict SRB system, and do not require the presence of SDB. (B) Measured $\Delta^{33}S$ vs. $\delta^{34}S$ values from pre 1300 Ma basins (circles) plot for the most part in the SRB system field. Green circles are for the ~1660 Ma McNamara Gp. span almost the complete range of values observed for Proterozoic sulfate, and exhibit a linear correlation with $\Delta^{33}S$ measurements. These isotopic systematics are consistent with the exclusive operation of SRB on a limited sulfate pool.

linear fashion with δ^{34}S. Both of these characteristics are indicative of Rayleigh fractionation, and I can reproduce the McNamara data with such a model involving only SRB. Although I cannot rule out the possibility that the McNamara samples retain isotopic evidence of the effects of disproportionation, I hypothesize that this formation records a sulfur cycle dominated by SRB operating on a limited sulfate pool. This hypothesis is consistent with recent discussions of low sulfate levels during the deposition of the McNamara Basin sediments (Kah et al., 2004; Gellatly and Lyons, 2005), and it is testable by sulfur isotope analysis of sedimentary sulfides that formed contemporaneous with carbonates of the McNamara Group. These types of systematics are further discussed in Chapter 5.

Conclusions

Taken together, the results bracket the appearance of a globally significant disproportionation pathway between 1450 and 1300 Ma. This predates prior estimates by several hundred million years (Canfield and Teske, 1996) and exposes an inherent limitation of using δ^{34}S to explore biogeochemical aspects of the sulfur cycle. Positive δ^{34}S evidence for SDB requires that the fractionations expressed in the isotope record must exceed the extreme fractionations observed for SRB (Canfield and Teske, 1996). By contrast, ^{33}S traces the contribution of microbial disproportionation at smaller ^{34}S/^{32}S fractionations that would seem to be completely consistent with sulfate reduction from δ^{34}S alone.

While the new ^{33}S measurements suggest a major change in the microbial regimes that controlled the isotopic composition of Proterozoic seawater sulfate, the environmental impetus for this change is less clear. The intermediate sulfur compounds required for SDB are generated by chemical oxidation of sulfide by O_2 and metal oxides (Thamdrup and Finster, 1993; Canfield and Teske, 1996), by photosynthetic sulfide oxidizers (Canfield and Teske, 1996), and by O_2 or nitrate-respiring anaerobic non-photosynthetic sulfide oxidizers (Thamdrup and Finster, 1993; Canfield and Teske, 1996). On modern Earth, the compounds produced by these processes occur in a variety of chemical transition zones, such as at oxic/anoxic interfaces in marine sediments and stratified water columns, and within the layers of microbial mat communities (Troelsen and Jorgensen, 1982). This suggests that sulfur disproportionation dominantly occupied surface ocean and/or shelf environments where local oxidative processes were responsible for the production of sulfur intermediates.

Other indicators of an oxidative surface environment, such as $\delta^{13}C$ variations (Frank et al., 2003; Kah et al., 2004), evolutionary arguments (Knoll, 1994; Canfield, 1998), and sulfate concentration estimates (Kah et al., 2004; Gellatly and Lyons, 2004), are temporally consistent with a Mesoproterozoic onset of disproportionation. A high-resolution ^{33}S record from the critical interval between 1450 and 1300 Ma may capture this onset in action, revealing whether the rise of SDB lagged or accompanied the progressive oxygenation of Earth's surface.

Chapter 5: Evolution of the Oceanic Sulfur Cycle at the End of the Paleoproterozoic

Introduction

Here I present new measurements of ^{32}S, ^{33}S, ^{34}S, and ^{36}S in sedimentary sulfides and couple these measurements with modeling treatments to study the sulfur cycle of a late Paleoproterozoic marine basin. I target the transition in ocean chemistry from the deposition of Paleoproterozoic iron formations (Gunflint, Biwabik, Trommald, and Mahnomen iron formations) to the inferred sulfidic ocean conditions recorded by overlying shale (Rove Formation). The data suggest that certain features of the global sulfur cycle, such as a control by sulfate reducing microorganisms, and low (mM) concentrations of oceanic sulfate, were maintained across this transition. This transition was associated with changes in the structure of the basin-scale sulfur cycle during deposition of these sediments. Sulfide data from the iron formations are interpreted to reflect sedimentary sulfides formed from microbial reduction of pore-water sulfate that was supplied through steady-state exchange with an overlying oceanic sulfate reservoir. The sulfide data for the euxinic Rove Formation shales reflect the operation of a sulfur cycle that included the loss of sulfide by a Rayleigh-like process. I suggest that the prevalence of large and variable heavy isotope enrichments observed in Rove Formation sulfide minerals reflect a sustained and significant net loss of sulfide from the euxinic water column, either as a result of a

90

shallow chemocline and degassing to the atmosphere or as a result of a water column

pyrite sink. The inclusion of ^{36}S measurements (in addition to ^{32}S, ^{33}S and ^{34}S)

illustrates the mass-dependent character of these sedimentary environments, ruling

out contributions from the weathering of Archean sulfides and pointing to at least

modest levels of sustained atmospheric oxygen (> 10^{-5} present atmospheric levels of

O_2).

Background

Recent studies of redox sensitive elements, mineral speciation, and isotopic systems

have indicated a transition from ferruginous (Fe^{2+}-rich) to widespread euxinic (S^{2-}-

rich) water-column conditions coincident with the cessation of iron formation (IF)

deposition in the late Paleoproterozoic (Poulton et al., 2004). Sulfidic conditions are

thought to have become widespread at the time of this transition, persisted into the

middle Proterozoic, and may have had profound effects on the isotopic composition

and size of the seawater sulfate reservoir (Canfield, 1998; Shen et al., 2002; 2003;

Arnold et al., 2004; Canfield, 2004; Rouxel et al., 2005). The lithologic progression

from iron formation (Gunflint Formation, Biwabik Formation, Trommald Formation,

and the Mahnomen Formation) to shale (Rove Formation) in the Animike Basin,

North America, has been interpreted as capturing the transition from ferruginous to

sulfidic conditions (Poulton et al., 2004). The observation of a high proportion of

highly reactive iron (Fe_{HR}) to total iron (Fe_{Total})(Fe_{HR} / Fe_{Total} >0.38) points to

persistent anoxic bottom water conditions throughout this succession, and the ratio of

pyrite iron (Fe_{Py}) to highly reactive iron indicates a change from ferruginous

conditions during deposition of the Gunflint Formation ($Fe_{Py} / Fe_{HR} = 0.001 \pm 0.001$)

to sulfidic conditions in the upper Rove Formation ($Fe_{Py} / Fe_{HR} = 0.87 \pm 0.04$). In this

study I evaluate 38 new measurements of the four stable sulfur isotopes (^{32}S, ^{33}S, ^{34}S

and ^{36}S) for Cr-reducible sulfur (herein referred to as sulfide) from samples of the

laterally equivalent Gunflint Iron Formation (n=10), Biwabik Iron Formation (n= 3),

Trommald Iron Formation (n=5), and Mahnomen Formation (n=3), with additional

samples from the overlying Rove Formation (n=17) (Table 7). This approach

expands on that used in prior studies of sulfur isotopes because it includes new

modeling and evaluates the significance of $\delta^{33}S$ and $\delta^{36}S$ in addition to the more

commonly reported $\delta^{34}S$.

Setting, Systems and Methods

Geologic setting

At approximately 2450 Ma, a rift to passive margin developed along the southern

edge of Superior Province when a land-mass to the south separated (Fralick and

Miall, 1989). Later closure of the resultant ocean led to the deposition of the

Animikie and North Range Groups as a backarc basin developed (Pufahl and Fralick,

1995; 2004; Hemming et al., 1995; Van Wyck and Johnson, 1997; Pufahl et al.,

2000), which, with a collision, was later transformed into a foreland setting

(Hoffman, 1987; Southwick and Morey, 1991; Hemming et al., 1995; Ojakangas et

al., 2001; Maric and Fralick, 2005). Initial south to north flooding of the backarc led

to deposition of siliciclastic tidal deposits (Ojakangas, 1983) forming the Mahnomen,

Pokegama and Kakabeka Formations (Figure 21). These are thickest in the south, forming only a sporadically developed basal conglomerate in the northernmost area. The chemical sediment dominated Trommald, Biwabik and Gunflint formations overlie the basal siliciclastics (Figure 21). Chemical sediments are also prominent within parts of the Mahnomen Formation. These units are primarily composed of both granular and fine-grained iron oxides, carbonates and chert. The sedimentary strata are organized into fining- and coarsening-upward successions reflecting transgressive-regressive cycles (Fralick and Barett, 1995) on an open, wave and tide dominated shelf (Ojakangas, 1983; Fralick, 1988; Pufahl and Fralick, 1995; 2004; Pufahl et al., 2000). Water depths during the deposition of these chemical sediments, even on the mid-shelf, probably did not exceed 10's of meters (Pufahl and Fralick, 2004). U-Pb age determinations of zircons from a reworked tuff in the Gunflint Formation yielded an age of 1878 ± 1 Ma (Fralick et al., 2002).

Deposition of the iron formations probably ended in the northern area, and possibly to the south, as closure with a land-mass to the south caused upwarping and withdrawal of the sea (Addison et al., 2005) during the 1860-1835 Ma (Sims et al., 1989) Penokean Orogeny. During this interval, at approximately 1850 Ma (Krough et al., 1984), a large hypervelocity impact occurred 700 km to the east, near Sudbury, and the ejecta is present very near the top of the Gunflint and Biwabik Formations (Addison et al., 2005). This uppermost portion of the Gunflint is highly altered with intense silicification and the development of agate and pyrite veins and vugs. The alteration may be the result of subareal exposure during a hiatus inferred from a U-Pb
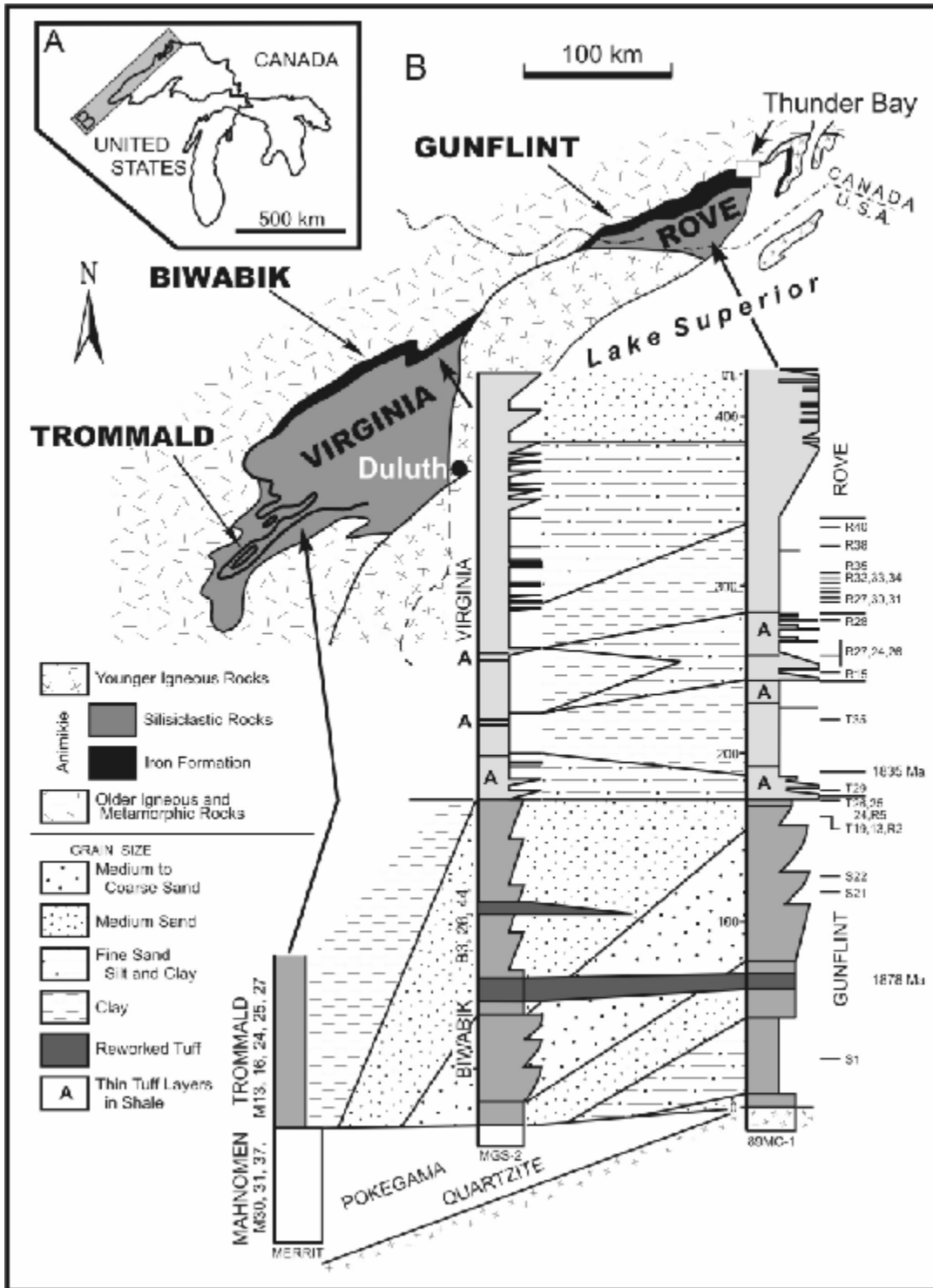
Figure 21: Geology and location of the Animikie Basin a.) **Location map.** b.) **Animikie sedimentary rocks generally dip gently to the southeast with their lower unconformable contact with Neoarchean rocks exposed to the northwest. The southernmost portion of the basin is more intensely deformed, and there structural contacts are probably present. Mesoproterozoic intrusive rocks related to the Mid-Continental Rift divide the basin and Rift basalts overlie the basin. The stratigraphic sections depict the rocks present in three continuously cored drill-holes. Shales to sandstones of the Mahnomen Formation and Pokegama Quartzite underlie the Trommald, Biwabik and Gunflint iron formations. The Trommald is dominated by fine-grained iron and manganese oxides deposited in the outer shelf to slope environment (ocean to the south, shoreline to the north) (Pufahl et al., 2000). Cycles containing fine-grained chemical sedimentary rocks overlain by coarsening-upwards grainstone assemblages, composed of chert, iron oxide and iron carbonate sand, dominate these shallow shelf deposits. Two tuff layers provide chronostratigraphic markers and show that the lithofacies boundaries are diachronous and reflect south to north transgression-regression-transgression (Fralick and Barrett, 1995; Pufahl et al., 2000). A hiatus appears to occur between the iron formation and the overlying siliciclastic rocks of the Virginia and Rove Formations (Addison et al., 2005). See the text for a more detailed discussion. Figure from data in Pufahl (1996) and Maric and Fralick (2005). Sample positions are indicated to the right of the stratigrpahic column, with width of the column indicating grain size.**

age on zircons of approximately 1835 Ma from tuffs immediately above the Gunflint and Biwabik formations (Addison et al., 2005). These tuffs are contained in the Virginia and Rove formations (Figure 21). The lower 100 to 150 m of these units consists of alternating shale-siltstone and black, pyritiferous shale successions, probably reflecting fluctuations in sea level (Maric and Fralick, 2005). These successions, and especially the upper black shale, likely represent a major condensed interval deposited in water ~100 to 200 m deep. Lucente and Morey (1983) ascribed sedimentation of this interval to pelagic rainout of fine-grained sediment from dilute suspension or hemipelagic processes involving diffuse turbidity currents. The presence of abundant, sub-millimeter rip-up intraclasts also denotes the operation of sporadic bottom currents (Maric and Fralick, 2005). Tidal deposits present in correlative rocks to the south of Lake Superior (Ojakangas et al., 2001) confirm open connection to the ocean. Above the upper, pure black shale interval, graded fine-grained sandstones are organized into a coarsening-upward succession approximately 100 m thick that is transitional into 400 m of medium-grained, sandstone-dominated,

stacked parasequences (Maric and Fralick, 2005). This is overlain by lenticular to wavy bedded sandstones and shales with both wave and current ripples. The coarsening-upward to sandstone-dominated portion of the Virginia and Rove formations has been interpreted as a submarine fan (Lucente and Morey, 1983; Maric and Fralick, 2005) with the uppermost ripple laminated succession representing progradation of distal distributary mouth bars of a delta (Maric and Fralick, 2005). A sandstone sample from the submarine fan portion of the succession yielded a youngest U-Pb detrital zircon age of approximately 1780 Ma (Heaman et al., 2005). The predominantly Paleoproterozoic zircon population (Heaman et al., 2005), and paleocurrents indicating sediment derivation from the north (Morey, 1973), strongly suggest the Trans-Hudson Orogen was the source of the detritus. The northern sedimentary rocks of the Animikie Basin are essentially undeformed and unmetamorphosed, making them ideal targets for the study of low temperature biogeochemical cycling.

Analytical methods

The majority of the samples examined here were previously studied by Poulton et al. (2004) using methods described in Poulton and Canfield (2005). All additional samples were chemically prepared in the same manner as those previously studied (Poulton et al., 2004). In addition to the samples prepared for this study, splits of the Ag_2S extracted as Cr-reducible sulfur (considered to be pyrite; Canfield et al., 1986) by Poulton et al. (2004) were analyzed. General wet chemical and fluorination

methods are presented in Appendix 3, with details of V-CDT normalization described in Appendix 1.

Modeling treatment

I use a box model of the surface sulfur cycle (c.f., Garrels and Lerman, 1981) to evaluate how sulfur moves between different terrestrial sulfur reservoirs and to make
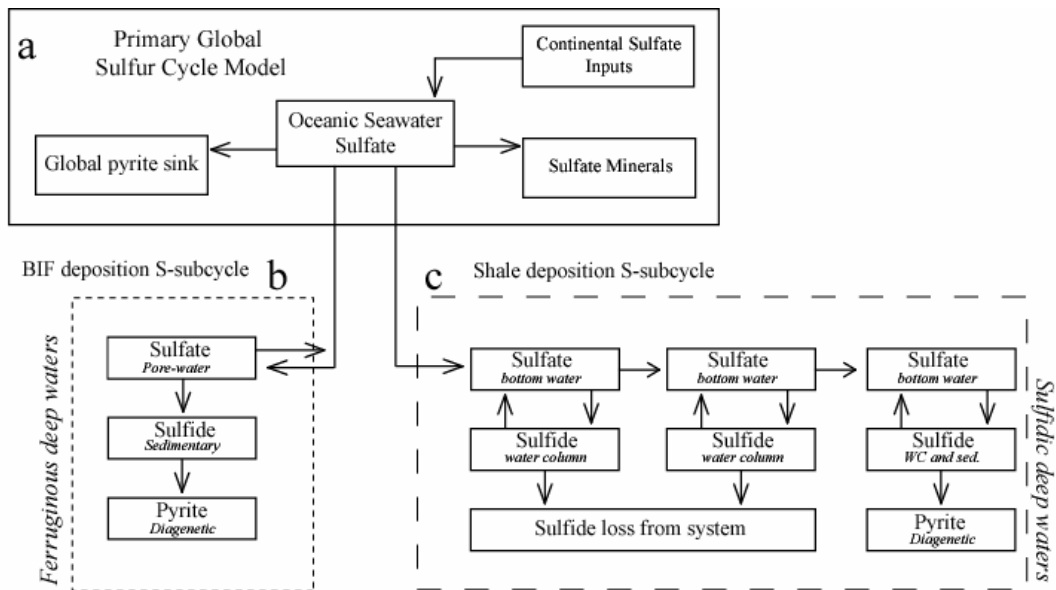
Figure 22: A box model representation of the global steady-state sulfur cycle. Arrows represent fluxes between reservoirs (boxes). The relative placement of the boxes in the figure is independent of the actual environmental location of the pool. a.) **I model a global sulfur cycle with one source (continental/riverine) and two global sinks (sulfide and sulfate minerals). The recycling of the oceanic sulfur pools (global sulfide and global sulfate minerals) is not incorporated here due to the relatively short depositional period represented by these sediments.** b.) **The modeled sub cycle used to describe the BIF depositional environment. Here, the global seawater sulfate reservoir feeds to a ferruginous deeper water reservoir.** c.) **The modeled sub cycle used to describe the shale depositional environment. In order to satisfy the data using a steady state model, multiple sulfide reservoirs were included in the sub cycle.**

predictions about the $\delta^{33}S$, $\delta^{34}S$, and $\delta^{36}S$ of Proterozoic seawater sulfate. A previous study used a similar approach and considered the isotopic fractionations associated with sulfate reduction and re-oxidative processes such as disproportionation (see Johnston et al., 2005a for a more detailed description). The form of the model in this

97

study is presented in Figure 22, and is modified from Chapter 4 (Johnston et al.

2005a) in order to account for some new features of the data (sulfides enriched in

^{34}S).

Results

The data are presented in Table 7. The ranges of δ^{34}S, Δ^{33}S, and Δ^{36}S are -0.96 to

32.92 ‰, -0.073 to 0.078 ‰, and -0.35 to 1.03 ‰ respectively. The δ^{34}S data parallel

those presented in Poulton et al. (2004) with the IF (lower Gunflint, Biwabik

Trommald, and the underlying siliciclastic Mahnomen Formations) yielding an

average δ^{34}S of 8.4 ± 4.6‰ (1 σ), the lower ~100 m of the Rove Formation (assigned

to a transitional environment between ferruginous and persistent euxinia; Poulton et

al., 2004) yielding an average δ^{34}S of 13.2 ± 11.0 ‰ (1 σ), and the data for the upper

'sulfidic' Rove Formation yielding an average δ^{34}S of 16.6 ± 6.8 ‰ (1 σ).

Comparison of new SF_6 analyses with earlier SO_2-based analyses (see Poulton et al.,

2004; Johnston et al., 2006) of the same Ag_2S precipitates suggests a correlation of

$\delta^{34}S_{SF6}$ = 1.009 (± 0.051; 1σ) $\delta^{34}S_{SO2}$ -0.066 (± 0.711; 1σ). However, when three

significant outliers (> 3 σ; R30, R28, and R5) are removed from the comparison, the

same linear regression technique suggests a correlation of $\delta^{34}S_{SF6}$ = 1.055 (± 0.016;

1σ) $\delta^{34}S_{SO2}$ -0.166 (± 0.210; 1σ). Both predicted correlations are within 2σ of

comparisons of these two methods ($\delta^{34}S_{SF6}$ = 1.035 $\delta^{34}S_{SO2}$ -0.135; Rees, 1978), in

which the differences are interpreted to reflect scale compression on the SO_2

measurements as a result of memory effects.

Geologic Formation	lithology	age	$\delta^{33}S$	$\delta^{34}S$	$\delta^{36}S$	$\Delta^{33}S$	$\Delta^{36}S$
Rove Fm.	black shale	1840	9.11	17.84	34.60	-0.037	0.44
Rove Fm.	black shale	1840	12.89	25.18	48.60	-0.004	0.21
Rove Fm.	black shale	1840	11.75	23.02	44.48	-0.040	0.29
Rove Fm.	black shale	1840	9.26	17.97	34.65	0.044	0.23
Rove Fm.	black shale	1840	6.02	11.66	22.25	0.032	-0.02
Rove Fm.	black shale	1840	8.88	17.42	33.95	-0.057	0.59
Rove Fm.	black shale	1840	11.46	22.42	43.46	-0.028	0.42
Rove Fm.	black shale	1840	2.57	4.95	9.40	0.028	-0.02
Rove Fm.	black shale	1840	4.83	9.27	17.37	0.068	-0.33
Rove Fm.	black shale	1840	9.25	18.06	34.93	-0.008	0.34
Rove Fm.	black shale	1840	6.14	11.99	23.00	-0.018	0.09
Rove Fm.	black shale	1840	5.11	9.99	19.60	-0.025	0.54
Rove Fm.	black shale	1840	2.11	4.14	8.11	-0.023	0.22
Rove Fm.	black shale	1840	16.84	32.91	63.63	0.021	0.17
Rove Fm.	black shale	1840	11.77	22.92	44.29	0.027	0.29
Rove Fm.	black shale	1840	3.15	6.17	12.27	-0.025	0.51
Rove Fm.	black shale	1840	-0.49	-0.97	-1.77	0.008	0.07
Gunflint Fm.	*iron Fm.*	*1880*	*1.95*	*3.81*	*7.29*	*-0.007*	*0.03*
Gunflint Fm.	*iron Fm.*	*1880*	*0.79*	*1.46*	*2.39*	*0.040*	*-0.39*
Gunflint Fm.	*iron Fm.*	*1880*	*7.05*	*13.75*	*26.42*	*-0.006*	*0.13*
Gunflint Fm.	*iron Fm.*	*1880*	*11.25*	*21.95*	*42.32*	*0.003*	*0.20*
Gunflint Fm.	iron Fm.	1880	5.20	10.20	19.94	-0.044	0.47
Gunflint Fm.	iron Fm.	1880	5.23	10.21	20.02	-0.019	0.53
Gunflint Fm.	iron Fm.	1880	6.79	13.33	26.19	-0.056	0.71
Gunflint Fm.	iron Fm.	1880	-0.30	-0.51	-0.55	-0.038	0.41
Gunflint Fm.	iron Fm.	1880	-0.23	-0.43	-0.60	-0.013	0.22
Gunflint Fm.	iron Fm.	1880	2.07	4.06	8.02	-0.018	0.28
Biwabik Fm.	iron Fm.	1880	3.54	6.97	13.43	-0.041	0.15
Biwabik Fm.	iron Fm.	1880	4.99	9.83	19.16	-0.065	0.40
Biwabik Fm.	iron Fm.	1880	1.67	3.26	6.43	-0.007	0.22
Trommald Fm.	iron Fm.	1880	6.22	12.23	23.82	-0.061	0.44
Trommald Fm.	iron Fm.	1880	7.88	15.53	30.36	-0.083	0.66
Trommald Fm.	iron Fm.	1880	3.92	7.73	15.24	-0.058	0.50
Trommald Fm.	iron Fm.	1880	4.10	8.05	16.03	-0.037	0.69
Trommald Fm.	iron Fm.	1880	4.38	8.64	17.14	-0.061	0.65
Mahnomen Fm.	iron Fm.	1880	4.92	9.71	19.00	-0.071	0.47
Mahnomen Fm.	iron Fm.	1880	4.87	9.59	19.29	-0.062	0.99
Mahnomen Fm.	iron Fm.	1880	6.91	13.58	26.67	-0.061	0.72

Table 7: All sulfur isotope data grouped by formation. Samples from the Gunflint and Rove fms. are arranged in stratigraphic order. Samples in italics were visually identified as compromised by secondary processes (silicification). These measurements are included in this table and the Results section, but not interpreted as representative of the depositional environments.

Our results for ^{33}S and ^{36}S yield Δ^{33}S and Δ^{36}S of -0.037 ± 0.022 and 0.54 ± 0.22‰

for the IF, -0.004 ± 0.021 and 0.32 ± 0.18‰ for the transitional shales, and $0.010 \pm$

0.044 and 0.24 ± 0.29‰ for the upper euxinic Rove Formation samples. The IF data

cluster towards lower δ^{34}S, negative Δ^{33}S, and positive Δ^{36}S, whereas the shale data

cover almost the entire data set. No strong stratigraphic trends are observed within

the data, although a slight positive trend in δ^{34}S and Δ^{33}S (negative in Δ^{36}S) is

observed moving up-column. The Δ^{36}S and Δ^{33}S values are correlated and form an

array given by Δ^{36}S $= -6.28$ (± 0.78; 1σ) Δ^{33}S $+ 0.300$ (± 0.029; 1σ) (with sub-

trajectories of Δ^{36}S $= -5.58$ (± 2.12; 1σ) Δ^{33}S $+ 0.336$ (± 0.091; 1σ), Δ^{36}S $= -3.76$ ($\pm$

3.08; 1σ) Δ^{33}S $+ 0.338$ (± 0.063; 1σ), Δ^{36}S $= -5.77$ (± 1.116; 1σ) Δ^{33}S $+ 0.301$ ($\pm$

0.048; 1σ), and Δ^{36}S $= -10.31$ (± 2.79; 1σ) Δ^{33}S $+ 0.201$ (± 0.064; 1σ) for the IF,

transitional shale, sulfidic shale, and silicified samples respectively)**.**

Discussion

Previously published treatments of the sulfur cycle suggest that the sulfur isotope

composition of the oceanic sulfate and sedimentary sulfide pools depends on

material-balance constraints given by the fraction of sulfur lost to pyrite burial (f_{py}),

the magnitude of fractionation by sulfate reducing bacteria, and when relevant, the

magnitude of fractionations associated with other reaction and transfer pathways such

as sulfur disproportionation (Jorgensen et al., 1977; Claypool et al., 1980; Garrels

and Lerman, 1981; Berner, 1991; Strauss, 1993; Hurtgen et al., 2002; 2005; Canfield,

2004; Johnston et al., 2005a; Ono et al., 2006). Some of these studies have also

suggested that non steady-state effects can introduce additional isotopic effects associated with material balance (Johnston et al., 2005a; Ono et al., 2006). In the first part of the following discussion I use steady-state sulfur cycle models to make inferences about the composition of seawater sulfate and sedimentary sulfide during IF deposition. The models have a global component with a structure that is similar to that used in Johnston et al. (2005a) (Figure 22a), but also includes local recycling of sulfur (Figure 22b). In the second part of the discussion I make inferences about an expanded steady-state model (Figure 22c) and a basic non steady-state system. Here, I draw on a combination of Rayleigh (e.g., Goldhaber and Kaplan, 1975) and mixing effects to gather information about the behavior of non steady-state systems.

Implications of the steady-state box model approach

The average composition of the source of sulfur for the oceanic sulfur cycle is thought to have an isotopic composition near, or slightly more enriched (< 5 ‰ in $\delta^{34}S$) than that of CDT ($\delta^{33}S \approx 0$, $\delta^{34}S \approx 0$, and $\delta^{36}S \approx 0$) (Farquhar et al., 2002). When combined with constraints imposed by conservation of mass, the dominant fractionations in the surface sulfur cycle produce ^{34}S-depleted reservoirs of reduced sulfur (ie. pyrite) and ^{34}S-enriched reservoirs of oxidized sulfur (ie. sulfate). The observation that a majority of the sulfide data (35 of 38) from the successions examined here has positive delta values (are ^{34}S-enriched) indicates that the global sulfur sink (Figure 22a) is not represented by this sample set. Observations of ^{34}S-enriched sulfide minerals have also been described in other Proterozoic shales (e.g., Walker and Brimblecombe, 1985; Hayes et al., 1992; 1993; Shen et al., 2002; 2003;

Canfield, 2004). Hayes et al. (1992) suggested that the lack of [34]S-depleted sulfides

at this time reflects poor preservation of deep-water settings, where isotopic

fractionation associated with sulfate reduction would have been large. Those authors

suggest that lower rates of sulfate reduction in deep water settings would facilitate

larger isotopic fractionations and the production of [34]S-depleted sulfide. These

sulfides would likely be subducted and lost from the surface record (Canfield, 2004).

Conversely, continental shelf and inta-cratonic basin settings, which represent much

of the sampled record during these time intervals, and where organic carbon is readily

available, are locations where sulfate reduction rates are assumed high and where

near quantitative reduction of available sulfate is feasible. This would result in

sedimentary sulfides with isotopic compositions near that of seawater sulfate, or in

the case of the Proterozoic, between 0 and 20 ‰ in δ^{34}S. I suggest that the data

reflect the operation of a (basin-scale) sub-cycle similar to that presented in Figure

22B. In this model, and consistent with the Hayes (1992) model, the global cycle

produces an oceanic sulfate reservoir with positive δ^{34}S ([34]S-enriched) that serves as

the source pool for the basin-scale sub-cycle, thus allowing for the production of

positive δ^{34}S sulfides on the shelves or shallower water settings.

The oceanic sulfate reservoir: The isotopic composition of the global oceanic sulfate

reservoir during the late Paleoproterozoic remains poorly constrained. Traditional

approaches to assess the isotopic composition of the past oceanic sulfate reservoir

have been through direct analyses of proxies for oceanic sulfate (e.g., evaporite

sulfate, carbonate associated sulfate, marine barite; Holser et al., 1979; Claypool et al. 1980; Burdett et al., 1989; Strauss, 1993, 2004; Paytan et al., 1998; 2004; Turchyn and Schrag, 2004; Lyons et al., 2004) and models of the sulfur cycle, which often rely on sulfide data (Canfield and Teske, 1996; Canfield, 2001). In recent studies by Johnston et al. (2005a) and Ono et al. (2006), the composition of the oceanic sulfate reservoir has also been evaluated using oceanic box models. These authors argue that the composition of oceanic sulfate will occupy an isotopic field that extends from the composition of the sulfate source to the oceans (roughly zero) to more positive $\delta^{34}S$ and variable but small positive and negative $\Delta^{33}S$ and $\Delta^{36}S$ values. The generation of non zero ^{33}S and $\Delta^{36}S$ values is due to the continued removal of isotopically fractionated sulfide and mixing.

An expanded version of model predictions from Johnston et al. (2005a) is presented in Figure 23. Whereas earlier treatment focused on predicting the isotopic composition of seawater sulfate, the current treatment has been expanded to include predictions for the isotopic composition of sulfides. An assumption built into the model results is that the isotopic composition of the sulfur entering the system is roughly zero, and use microbial fractionation factors from Johnston et al. (2005b). Model interpretations do not change with small variations (up to ~ 5 ‰ in $\delta^{34}S$) in the composition of the sulfur source to the oceans. The model results define an "SRB field" representing a sulfur cycle with only active sulfate reduction and a "SRB-SDB field" representing the predictions for a sulfur cycle with contributions from both sulfate reducers and sulfur disproportionators. The isotopic field defined by a sulfur
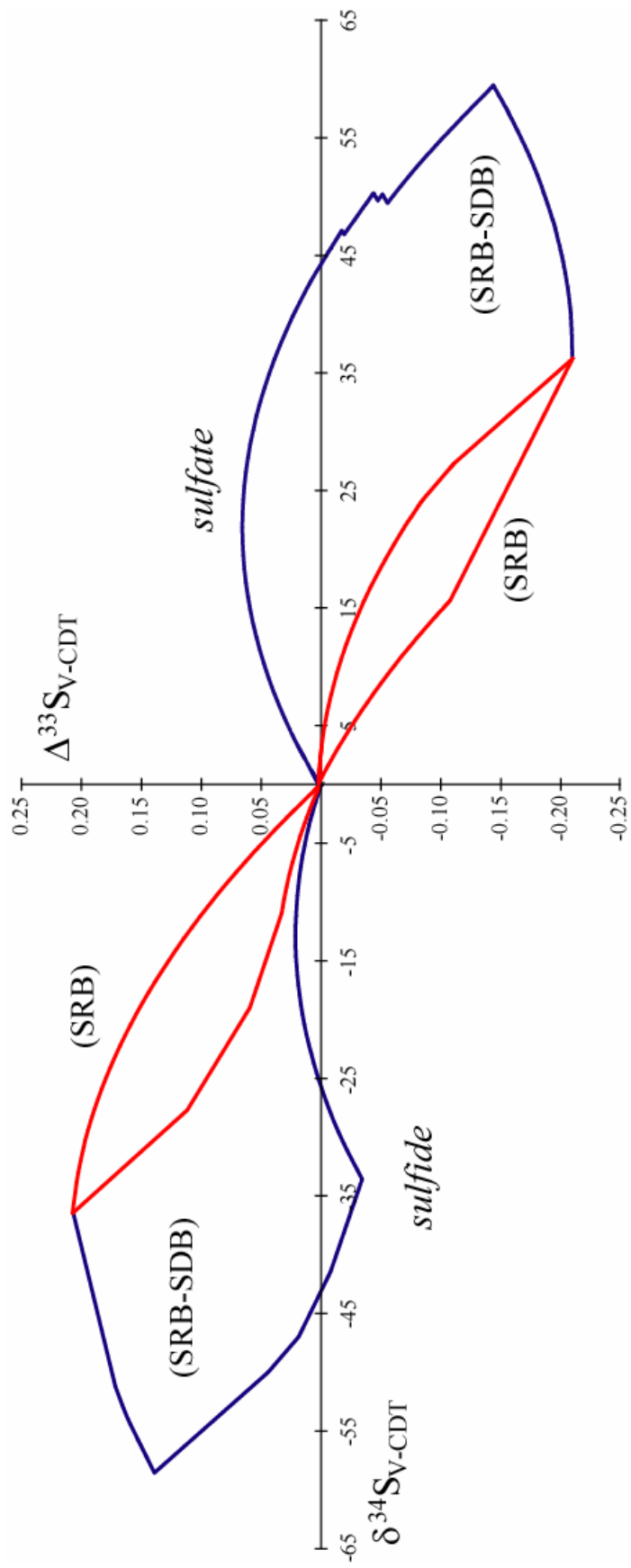
Figure 23: Triple isotope plot (Δ^{33}S versus δ^{34}S) illustrating the steady–state sulfur cycle modeling solutions for the isotopic composition of sulfate and sulfide. Fractionation factors are derived from experiments with SRP conducted by Johnston et al. (2005b) (Chapters 2-3). The fields outlined in red represent a sulfur cycle with only SRB active, whereas fields outlined in blue have both SRB and SDB present. This model is an extended version of those presented in Johnston et al. (2005a). The position along each respective curve represents the fraction of pyrite being buried (f_{py} in Johnston et al., 2005a). In the case of the sulfate curve, the intercept represents no pyrite burial with pyrite burial increasing to 100% as you move away from the origin to the right. Due to mass balance, the pyrite curve is demarcated in a similar manner with no pyrite burial at the left most point on the curve, and increasing towards 100% pyrite burial as you approach the origin. In all cases, sulfate and sulfide predictions evolve away from the origin since I assume a continental/riverine flux that is isotopically similar to bulk Earth (δ^{3i}S ~ 0 ‰). All modeling represents steady-state box modeling of the global sulfur cycle. The same treatment applies for Δ^{36}S.

cycle with only sulfate-reducing microorganisms occupies a smaller region of predicted isotopic compositions than if other microbial processes, such as sulfur disproportionation, are active as well (see Johnston et al., 2005a). Previous studies suggest that only sulfate reducers operated within the sulfur cycle during the late Paleoproterozoic (Canfield and Teske, 1996; Canfield, 1998; Johnston et al., 2005a), suggesting that the smaller SRB field defines the range of compositions for oceanic sulfate at that time.

This model is used to provide a context for interpreting isotopic data for sulfides from the Gunflint, Biwabik, Trommald and Mahnomen Formations. The steady-state box model would reproduce the IF sulfide data using fractionations associated with only sulfate reducing microorganisms and a fitted composition for oceanic sulfate of δ^{34}S ~ 17 ‰, Δ^{33}S ~ -0.085 ‰ and Δ^{36}S ~ 0.60 ‰ (Figure 24), which is the minimum estimate (in δ^{34}S and Δ^{36}S, maximum in Δ^{33}S) to satisfy the data. This prediction also supports the lack of a prominent isotopic contribution from SDB at this time. The validity of the estimate for the isotopic composition of the seawater sulfate reservoir

hinges on the appropriateness of the model approach, but it also illustrates a new type

of constraint for seawater sulfate compositions. This treatment provides a seawater

sulfate composition that is not only consistent with earlier predictions of the $\delta^{34}S$ of
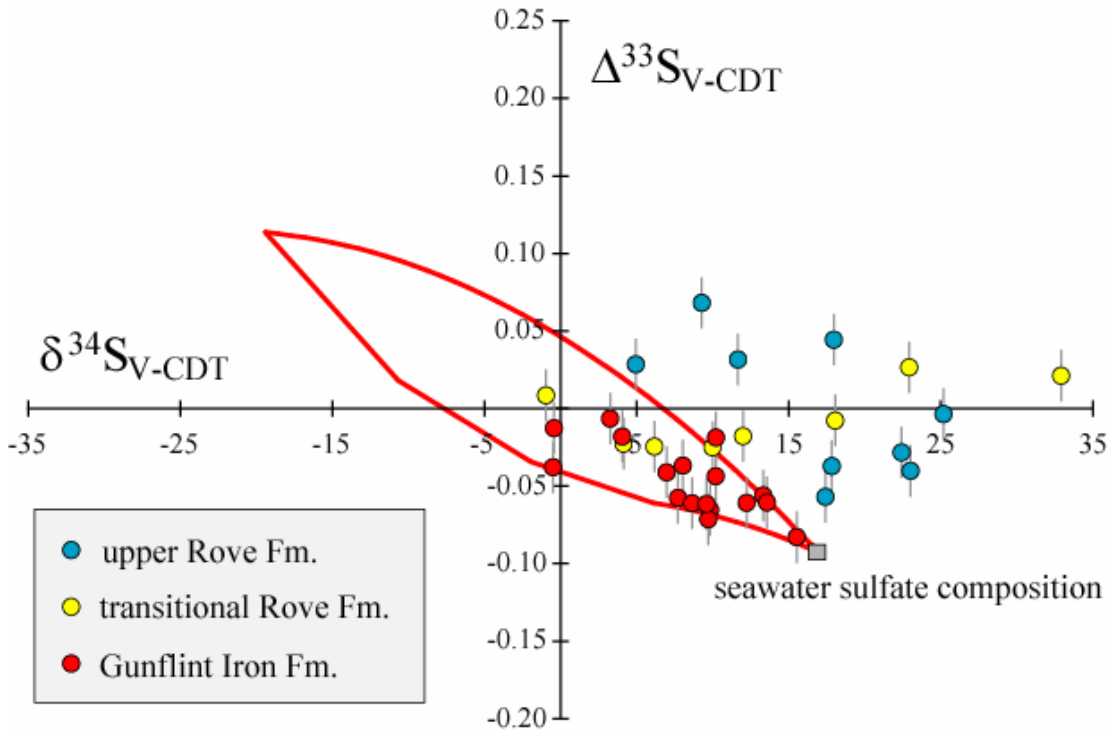
Figure 24: All the data along with a steady-state modeling result for a sulfur cycle with only active sulfate reducers. The inclusion of a sub-cycle, as presented in Figure 22b, can shift the isotopic predictions, such that the sulfide and sulfate fields would not evolve away from a continental composition (original source pool; seen in Fig. 24), but would be rooted from a composition within the original seawater sulfate field (new source pool). In this case, global processes would be controlling the isotopic composition of the overlying seawater, but local effects are controlling the isotopic composition of the sedimentary sulfides in the sediment column. Red circles represent IF sulfide data (with 2 σ errors), while transitional data (defined by iron speciation, depths C to V) are in yellow and sulfidic Rove data is in blue. The red lines represent the global predictions for a sulfur cycle with only SRB active and are rooted at the predicted seawater sulfate composition (gray square). This seawater sulfate prediction is non-unique and falls within the range predicted by Figure 23 (an experimentally constrained field). Since the model adequately encompasses the IF data, I suggest that these sulfides are derived from the microbially (SRB) reduction of pore-water sulfate within a sediment column under steady state conditions.

Paleoproterozoic seawater sulfate (Strauss, 2004; Gellatly and Lyons, 2005), but

consistent in ^{33}S and ^{36}S with the predictions from steady-state global box models

(see position of sulfate field Figure 23A versus the composition suggested for the

period of BIF deposition: Figure 24). Similar steady-state modeling cannot explain

the significant scatter of the Rove Fm. sulfide data, thus a prediction of the associated

seawater sulfate composition is not appropriate.

Iron formation environments: I interpret the IF data to reflect operation of a localized

sulfur sub-cycle linked to the IF depositional environment (ie. pore-water sulfate and

local sedimentary sulfide) (Figure 25). I envision the overlying seawater sulfate

infiltrating the sediment column where microbial reduction of pore-water sulfate

would generate sulfide that was captured as pyrite. In this environment, the small

($\sim$10 ‰) δ^{34}S fractionations between the model prediction for seawater sulfate and

the measured sedimentary sulfide indicate either a high fraction of pore-water sulfate

sulfur was reduced and captured as pyrite (local $f_{py} \rightarrow 1$, where local f_{py} is the ratio of

pyrite sulfur to sulfur infiltrating as pore-water sulfate), or low pore-water sulfate

concentrations. The high Fe-content of the sediments, coupled with low organic

matter contents, suggest that lowered pore-water sulfate concentrations was most

likely the limiting constituent in this environment (Habicht et al., 2002). The

requisite source of Fe for pyrite formation is taken to be similar to other Superior-type

IFs, which are thought to sample water derived from a deep ferruginous ocean, and

where a majority of the ferrous iron would be chemically or microbially oxidized on

the shelf (e.g. Derry et al., 1992).

Transitional environments: The suite of samples that lie between the underlying IF

and the overlying euxinic shales of the upper Rove Formation were grouped by

Poulton et al. (2004) on the basis of evidence from Fe-speciation work and designated as "transitional." The transitional nature of the depositional environment from which these samples were derived is further supported by the sulfur isotope data for this horizon, which straddles both the field defined by the Gunflint IF and the field defined by the overlying euxinic Rove Formation shale. The two lowermost samples in the transitional Rove Formation shales fall within the steady-state IF field, suggesting an initial consistency with the underlying IF data (ie. deposition under ferruginous water column conditions). Data for immediately overlying samples
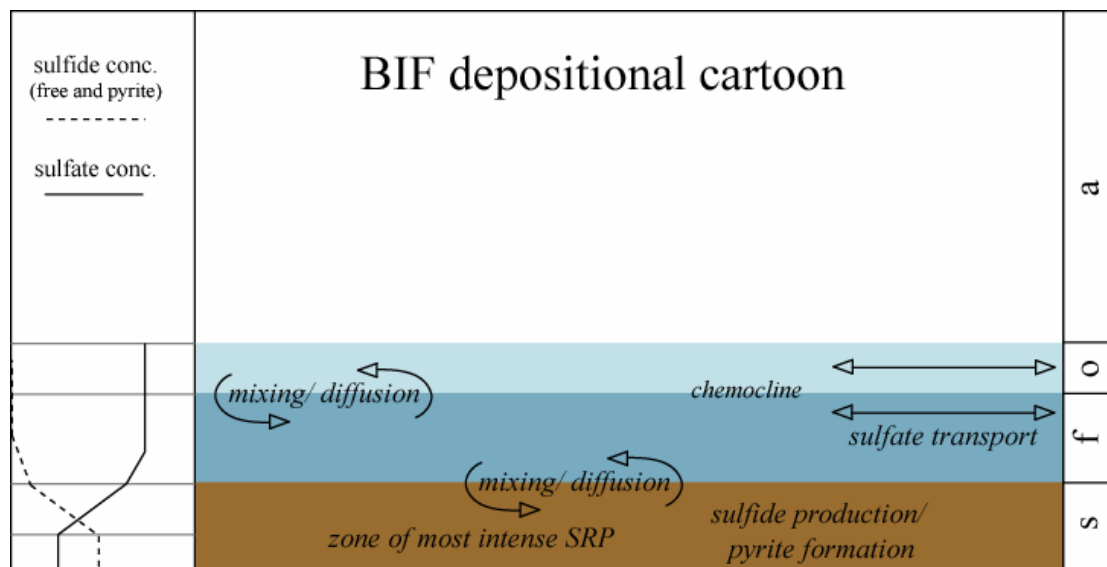
Figure 25: A cartoon representing the envisioned IF depositional environment. The focus of this graphic is to constrain the cycling of sulfur through the system, and in doing so, other important elements and cycles may be underappreciated. In the right-most column, a = atmosphere, o = oxic ocean, f = ferruginous ocean, and s = sediments. This environment is interpreted to have a shallow, stratified water column with a component of horizontal (possibly wind/upwelling driven) transport. There would likely be significant oxic/anoxic interaction at the chemocline, with the zone of most intense SRB activity and pyrite production in the upper portions of the sediments, where organic material would most readily accumulate. The lifetime of sulfide in this system would be very short, as the available iron would quickly scavenge the free sulfide for Fe-S formation (and later pyrite). The profiles at left represent speculative ion profiles for two different sulfur species (sulfate and sulfide). The sulfate concentration would remain relatively constant until entering the lower portion of the water column, where the compositional gradients extending from the sediment system could draw down sulfate. This is a function of the most prominent sulfate sink being in the sediments. In the sediments, sulfate would be expected to decrease through the zone of active sulfate reduction and level off as methanogensis begins to dominate. The sulfide profile is a reflection of the sulfate prediction.

diverge from the IF field and fall within the field for the euxinic Rove Formation shales. Further up-column, there is a brief return to coincidence with the IF field before the data terminally diverge to occupy the euxinic shale field. Noteworthy is that the 'transitional' samples overly the Gunflint/Rove disconformity, suggesting that the change in ocean chemistry or the establishment of a different basin scale sulfur cycle (discussed below) captured by these samples, post-dated the refilling of the Animike Basin, roughly 40 Ma after the deposition of the underlying iron formations.

Insight into the euxinic shale environment

The large amount of isotopic variability for the euxinic Rove Formation sulfides appears to be independent of stratigraphic position, cannot be explained by the inclusion of active SDB, and is inconsistent with the box model approach described in Figure 22B. Similarly, the isotopic data for euxinic Rove sulfide occupy an area to the right of the sulfide field presented in Figure 24. This observation leads us to consider the possible role of other effects within the euxinic Rove Fm. sulfur cycle. Two recent studies have described how removal of sulfide by Rayleigh fractionation processes can produce sulfur isotope compositions for sulfate and sulfide that migrate to positive $\delta^{34}S$ with only small changes of $\Delta^{33}S$ (Johnston et al., 2005a; Ono et al., 2006). Similar effects may be produced in systems at steady-state with continuous sulfide loss, or in systems where changes in the source or sink terms have resulted in a non steady-state condition. I will discuss both the possibility for a non steady-state

explanation for the euxinic Rove Fm. data, as well as the possibility that the data may

be explained by a steady-state sulfur cycle with continuous loss of sulfide.

Possibility of a non steady-state sulfur cycle: Non steady-state conditions, of which

Rayleigh effects are a limit, arise when variability in either the source or the sink

reactions leads to a significant fluctuation in the size of one or more of the sulfur

pools. I consider the temporal variability in seawater sulfate concentration as a
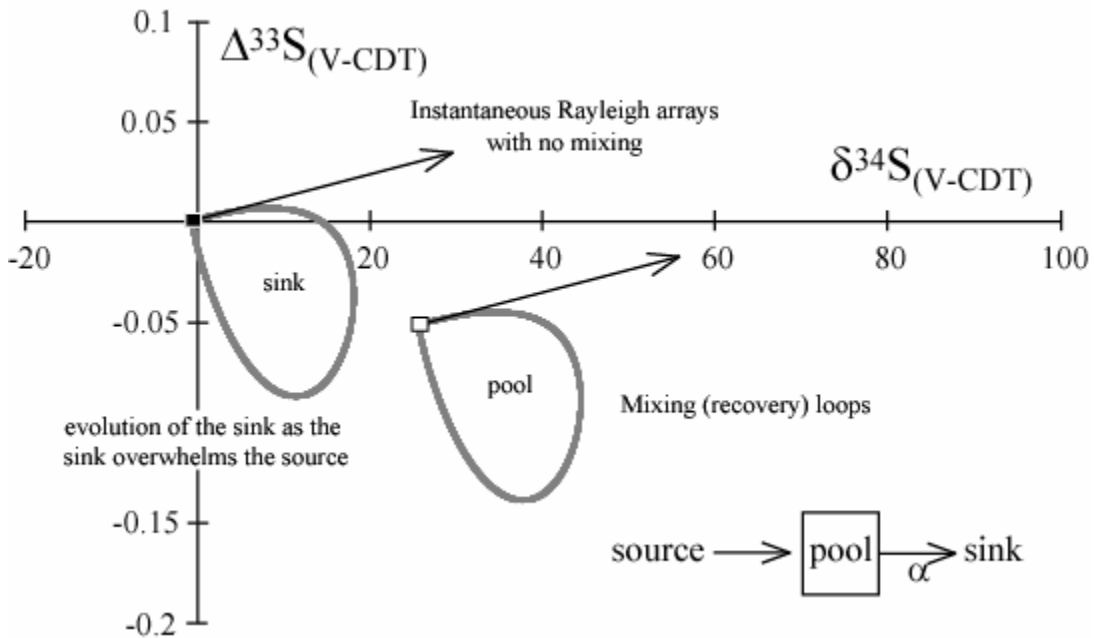
Figure 26: A triple isotope plot describing the consequences of Rayleigh fractionation and mixing for the simple one box model presented in the lower corner of the figure. The black and white boxes are the steady state predictions for the compositions of the sink and pool respectively. The Rayleigh fractionation trajectories (straight arrows) constrain the initial direction that the loops (which include mass balance considerations) proceed in. The right most loop represents the evolving composition of the "pool," whereas the left most loop represents the evolving composition of the "sink", and is offset by a fractionation factor (α). Plotted is the scenario where the sink overwhelms the source.

function of the sum of fluxes in and fluxes out. The isotopic ratio of these fluxes

results in the definition of a fractionation factor for the process. Thus, the isotopic

consequence of a non steady-state depends on the fractionation between reservoirs

and the magnitude of the change in reservoir size. These can be described by a combination of Rayleigh effects and mixing. In Figure 26 I illustrate the way that a one-box system responds when the source flux decreases relative to the sink flux. In this system, the initial isotopic evolution follows a trajectory defined by conventional Rayleigh fractionation ($R_f = R_0 f^{(\alpha-1)}$, where f is the fraction of Rayleigh distillation, and R_f and R_0 are the isotopic ratios for the instantaneous composition at fraction f and for $f=0$)(Figure 26). As the size of the pool continues to change, the predicted isotopic evolution begins to loop back around towards the starting composition as a function of mass balance (noted as 'mixing (recovery) loops'). This treatment predicts a drastic initial isotopic evolution as a response to non steady-state conditions, but a slow and less isotopically drastic response as the system reaches a new steady state.

In order for a non steady-state interpretation of the euxinic Rove Fm. sulfide data to be valid, it must explain the general geological and geochemical features of the euxinic Rove shale. Those features include the interpretation that deposition occurred in a marine setting, and that large (tens of ‰) [34]S enrichments occur throughout about ~40 meters of stratigraphic section. Given the measured fractionations (>20 ‰ in $\delta^{34}S$ and highly variable $\Delta^{33}S$ and $\Delta^{36}S$), the magnitude of the non-steady state effects for the Rove Fm. would require a process capable of generating significant changes in the size of the sulfate pool. This is because in order for a Rayleigh-like process to produce the observed effects, a significant fraction of the local sulfate reservoir (either bottom water sulfate or pore-water sulfate) must have been removed. This

estimate may represent a lower limit, since this isotopic variation is captured in the sulfide, rather than sulfate, pool. A standing pool of sulfide in a sulfidic water column has the potential to damp the magnitude of isotopic signals that are transferred to it from the sulfate pool. For example, if 10's of μM sulfide are produced and assimilated into a standing sulfide pool of 100's of μM sulfide, the isotopic contribution of that most recent addition will not be fully expressed, whereas if there was no standing sulfide reservoir, the composition of the recently produced sulfide would be representative of the standing pool and could then be captured as pyrite.

Prior studies have suggested that some non steady-state effects may accompany the geographic restriction of a basin, with episodic re-supply from a sulfate source (e.g., Johnston et al. 2005a). I do not favor this for the Rove Formation because it has been interpreted to have been deposited in a marine environment, and thus communicating with the open ocean. As an alternative, I explore the possibility that the euxinic Rove Formation data reflect the normal operation of a low sulfate marine environment. I focus on two parts of this system, (1) the water column and (2) the underlying sediments.

High rates of sulfate reduction are common for organic rich sedimentary environments. Thus, it may be possible, given increased organic material, for euxinic water column sulfate reduction rates to consume a significant proportion of water column sulfate and induce a non steady-state behavior within the system. This type

of situation can be described using a simple expression and observed rates for modern

water column processes. I calculate steady-state, 1-D penetration depths to gain an

'order of magnitude' estimate of how sulfate concentrations might vary as a function

of overlying water column depths. I begin with a simple diffusion length-scale

expression, where $L \sim \sqrt{Dt}$ (or length is related to the square root of diffusion

multiplied by time). However, if I make the assumption that the characteristic

timescales of the system are set by sulfate reduction rates (SRR), which is reasonable,

I can substitute time (t) with the expression: [boundary concentration/sulfate

reduction rate]. This is easier to understand when considering units, where boundary

concentrations are reported in moles per liter (M), and sulfate reduction rates are

reported in moles per liter per unit time (time = M/[M/time]). I run this calculation

using low sulfate concentrations (1-4 mM), Black Sea water column mixing rates

from Neretin et al. (2001)(0.5 to 3 cm^2/sec) as a proxy for effective diffusivity, and

for sulfate reduction rates of 1μM/day which are at the high end of those reported for

euxinic water columns (e.g., 0.0035 to 1.569 μM/day; Jørgensen et al., 1991;

Il'chenko and Sorokin, 1991; Albert et al., 1995; Neretin et al. 2001; Sørensen and

Canfield, 2004). These results indicate that sulfate concentrations will approach zero

at depths between ~ 50 and 350 meters below the chemocline, which spans the

inferred water column depths overlying the Rove Fm. As sulfate reduction rates

increase, the water column depth required to remove significant amounts of sulfate

decreases. Sørensen and Canfield (2004) observed a rate enhancement when water

column samples were augmented with acetate and lactate. It has also been argued

(Logan et al., 1996) that concentrations of suspended organic carbon (dissolved and

particulate) were higher in the Proterozoic, which they argue would have fostered increased rates of water column sulfate reduction during that period. Both suggestions indicate that significant water column sulfate removal is likely under supposed Proterozoic shelf conditions (euxinic with high organic carbon). These predictions assume that there is not significant lateral transport of sulfate-rich water onto the shelf, but acknowledging that lateral homogeneity is more likely in closed basins or where continental shelves are extensive.

The development of a sulfate-limited system, which is modeled as a non steady-state response in the euxinic Rove Formation sulfur cycle, may also have been initiated as a result of changes in the rates of sulfate uptake by sediments. Considerations of the contribution of active sulfate reduction in the underlying sediments, and the role that this sulfate sink can play in water column chemistry, must also be considered. In low sulfate concentration water column-sediment systems, variations in sulfate reduction may influence the size of the water column sulfate pool. The depths inferred for the Rove Formation depositional environments (~100-200 m) are on the same order as the characteristic diffusion length-scales described using the same equation described above ($\sqrt{Dt}$) and using the above listed mixing rates. Given typical rates for uptake of sulfate measured in modern sedimentary systems (~0.2 to 50 mol/m^{2}yr) (e.g., Jorgensen, 1977), it is predicted that there will be a significant extension of the sedimentary/ water column boundary layer that would result in sulfate draw down in the water column. For example, a 100 meter by 1m^2 water column with 1mM of sulfate contains only 100 moles of total sulfate, and variability within the range of

observed rates of sedimentary sulfate uptake will have a significant impact on the size (2-50 % change) and isotopic composition of the sulfate pool in this system. This interpretation assumes lateral homogeneity aided by bottom water currents, and the presence of rip-up interclasts suggests that bottom water currents were, at the very least, sporadic. However, this also depends on the lateral extent (scale) of the system and whether these water currents introduced sulfate-rich water from other deep-water sources. Since active communities of sedimentary sulfate reducers (or the physical process producing water column drawdown of sulfate concentrations) are largely independent of small variances in bottom water currents, the general treatment presented above should apply. In essence, a low sulfate water column can easily become sulfate limited when sedimentary SRB communities are present, and especially where the water column is shallower and organic inputs high, such as in the Rove Fm.

For variations in the intensity of water column sulfate reduction rates, or variations in the intensity of the sedimentary sulfate drawdown mechanism to be feasible explanations, these rates must vary on timescales that are comparable to the response time of the Rove Formation sulfur cycle. This will depend, in part, on water column mixing rates, but will also be influenced by changes in controls on sulfate reduction rates, such as ambient water temperatures and nutrient availability. I infer that the Rove Formation water column had a short response time (months to years), which I estimated using the length-scale expression presented above. Another issue that must be considered in evaluating the plausibility of a sulfate-limited explanation for the

Rove Formation data is related to the size of the standing pool of water column sulfide. A large standing sulfide pool would have the potential to damp the isotopic signal of the sulfide reservoir. This leads us to suggest that although these scenarios have the potential to produce variations in the water column sulfate concentration profiles, they would not be sufficient to produce the sustained and significant Rayleigh isotopic signal observed for the sulfides. For these reasons, I do not favor this interpretation.

Possibility of a sulfur cycle with continuous sulfide loss: An alternative model I propose for the euxinic Rove Formation sulfide data is a steady-state sulfur cycle that includes a significant and continuous loss of sulfide. A box model with this structure is presented in Figure 22c. The field of sulfide compositions that can be produced by this box model using experimentally determined sulfur isotope fractionations (e.g., Johnston et al., 2005b; Farquhar et al., 2003) is plotted in Figure 27. In general, as more sulfate and sulfide boxes are added to the model, mass-balance requires that the composition of sulfate moves to the lower right of Figure 27, due to the removal of isotopically depleted sulfides. Sulfide removal can occur through a number of processes, such as oxidation, burial, and various transports pathways out of the system.

Figure 27a presents all the data with the steady-state predictions for the isotopic composition of seawater sulfate (right field) and global sedimentary sulfide, assuming only one sulfide sink (left field). Figure 27b show the evolution of predicted sulfide

compositions as additional sulfide sinks are added, with Figure 27b representing a

scenario with four sulfide sinks (global pyrite plus all sulfide sinks presented in

Figure 22c). Strictly speaking, the model is an incremental batch loss process rather

than a Rayleigh process, but the expansion of the sulfide field reflects the loss of ^{32}S-

enriched sulfur from the system, as it does in Rayleigh systems. More complex

models such as those with additional steps for sulfide loss (Figure 27b) are capable of

producing an even larger field for sulfide isotopic compositions and
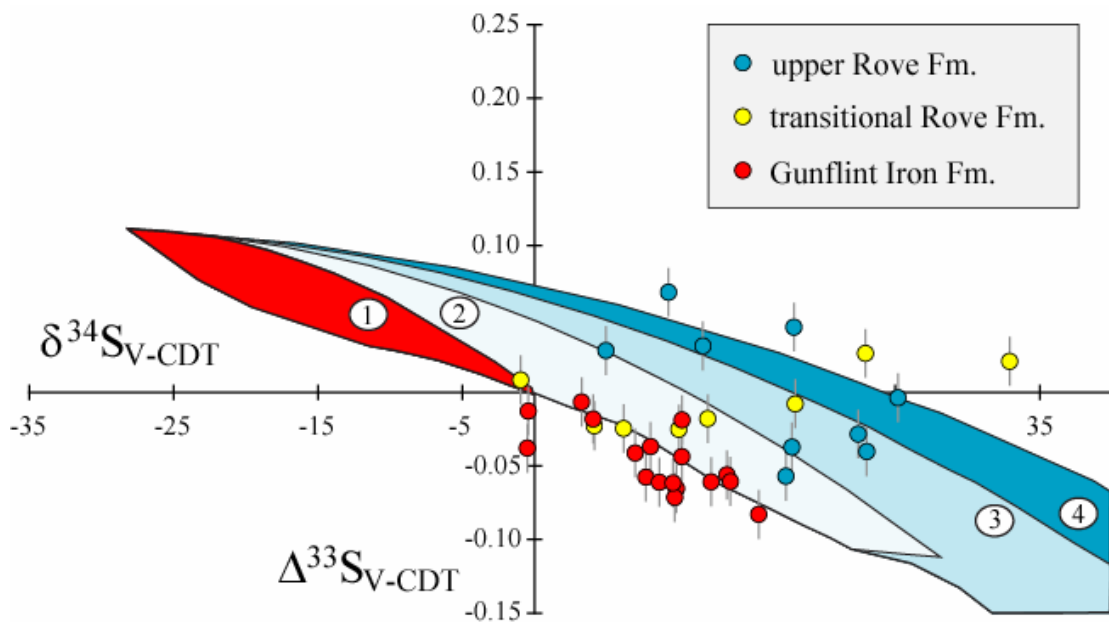
**Figure 27: A triple isotope plot of the sulfide data, with a focus on understanding the period of
shale deposition. Iron formation data are represented by red circles, the transitional shale with
yellow ciclres and the euxinic shale with blue circles. All errors are 2 σ. A scenario with four
sulfide sinks, labeled 1-4 (the global sulfide, with all three additional sulfide sinks in Fig. 22c).
The model is calibrated with sulfate reduction fractionations from Farquhar et al. (2003). It can
be seen from the figure that as the number of sulfide sinks increases, steady state models can
produce more enriched sulfide compositions.**

predict isotopic compositions that more closely match that of the Rove Fm. data.

This style of explanation would not require the extreme situation required for

Rayleigh effects, but only multiple sulfide sinks for the system. This explanation

becomes even more achievable (i.e. less sinks required) if the fractionation associated

with SRB increases (due to limited experimental data, the upper fractionation used in the modeling is $\sim 27‰$ in $\delta^{34}S$). For the model represented in Figure 27 to work, it must allow a significant loss of sulfide from the system (>50%), a fraction that is significantly higher than the fraction of sulfide lost to pyrite formation in the Black Sea (e.g., Neriten et al. 2001).

Recently, Kump et al. (2005) suggested that upward excursions of the chemocline in the Proterozoic oceans may have ventilated sulfidic waters in upwelling zones, releasing hydrogen sulfide into the atmosphere. Evidence for a shallow chemocline in some Paleoproterozoic environments is given by recent biomarker evidence that placed the sulfidic/oxic chemocline within the photic zone of the McArthur basin (Brocks et al., 2005). Such a loss process may apply to the Rove Formation sulfur cycle, but would further require that sulfide delivered to the atmosphere be laterally transported away from the basin before returning to the oceanic sulfur cycle (as either sulfide, or more likely as sulfate). Transport implied by the Kump et al. (2005) model provides a way to remove this sulfur from the Rove Formation sulfur cycle; however the possibility also exists that the loss may be associated with lateral heterogeneity, where a gradual isotopic enrichment of seawater sulfate (due to the progressive removal of isotopically depleted sulfide) accompanies the transport of sulfate through the system.
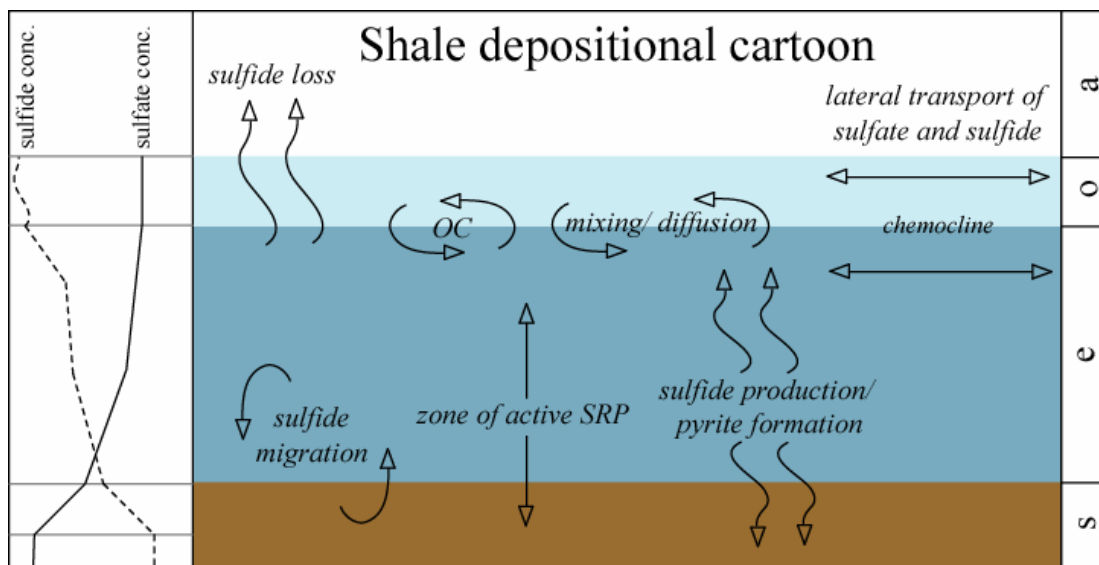
Figure 28: A cartoon representing the envisioned shale depositional environment. The focus of this graphic is to constrain the cycling of sulfur through the system, and in doing so, other important elements and cycles may be underappreciated. In the right-most column, a = atmosphere, o = oxic ocean, e = sulfidic (or euxinic) ocean, and s = sediments. This environment is interpreted to have been deep waters than the IF environment, with a larger anoxic portion of the overall water column. In this scenario, lateral transport could move both sulfate and sulfide (sulfide in sulfidic waters). Sulfate reduction would be active in the water column of this environment, which makes this system inherently more dynamic (a sulfur sink in the water column with the capability of migrating). With this in mind, the recycling of organic carbon (OC) and the mixing/diffusion across the oxic/anoxic interface are of vital importance. Recent propositions even suggest that the chemocline could reach the surface of the ocean, venting sulfide directly to the atmosphere (Kump et al., 2005). The outgassing mechanism is a viable solution for satisfying the sulfide data (see text for more detail). The zone of most intense SRB activity and pyrite production would still remain in the upper portions of the sediments, but sulfate reduction would inhabit the water column. The lifetime of sulfide in this system would be much longer than in the IF setting, as the available sulfide would overwhelm the available iron. The profiles at left represent speculative ion profiles for two different sulfur species (sulfate and sulfide). The sulfate concentration would begin to decrease in the euxinic portion of the water column as a function of low, but present rates of microbial sulfate reduction. A similar extension of the compositional gradient would draw down sulfate more quickly as the sediment/water interface is approached. In the sediments, sulfate would be expected to decrease through the zone of active sulfate reduction and level off as methanogensis begins to dominate. The sulfide profile is similar, but not a direct reflection. Potential outgassing to the atmosphere requires a variable amount of sulfide in the surface ocean, which is represented by the wavy line atop the sulfide concentration profile. Sulfide would increase quickly below the chemocline as a function of the diffusive boundary layer with the overlying oxic waters, and due to more labile organics near the surface, followed by slow accumulation through mid-depths. The compositional gradient produced in the sediment system would still intrude into the water column, causing an increase in sulfide near this interface. Below this, sulfide concentrations stabilize and are largely represented by pyrite.

Further, reports of sulfide samples with strongly positive δ^{34}S from other middle Proterozoic sequences such as the Reward Formation, Wollogorang Formation, and Roper Group (e.g., Hayes et al., 1992,1993; Shen et al., 2002; 2003), may provide a link between the data and global mid-Proterozoic sulfur cycle that had a component of continuous sulfide loss. Tests for this hypothesis would include studies that include δ^{33}S and δ^{36}S in addition to δ^{34}S for these and other localities, where I would predict isotopic compositions similar to those seen in the Rove Formation.

A cartoon describing the interpretation of the Rove Fm sub-cycle is presented in Figure 28. This suggests that the local sulfate reservoir is a combination of euxinic water column sulfate and pore-water sulfate. The sulfate source to this system is seen to be the overlying oxic surface ocean seawater sulfate pool and sulfate from this overlying reservoir would vertically mix into the sulfidic portions of the water column and diffuse into underlying sediments. Sulfate reducing microorganisms populating both the euxinic portions of the water column and the underlying sediments would contribute to the variability observed in the Rove, where fluctuations in the biological controls (temperature, nutrient fluxes and organic rain from surface environments) and sulfate delivery to the sulfidic parts of the sulfur cycle would have lead to development of non steady-state concentration effects, but only minor isotopic variations if the standing pool of water column sulfide was significant. Transport of sulfide out of the system, either as a result of horizontal transfer within the ocean, or as a result of ocean - atmosphere transfer of hydrogen sulfide, would leave the residual reservoir ^{34}S enriched and contribute to the positive

$\delta^{34}S$ observed in the shale sulfide reservoir. As suggested above, the Rove Formation may not be unique, as similar processes may have operated in other middle Proterozoic settings.

Dispelling non mass-dependent contributions and calibrating a new relationship

The question of whether a sulfur isotopic composition is entirely the result of mass-dependent processes, or also possesses a component attributable to non mass-dependent chemistry, is not a trivial one when interpreting the Precambrian geologic record. Large (‰ scale) non mass-dependent isotopic signals have been observed in sulfur samples older than 2.45 billion years old. These observed effects have thus far been attributed to gas-phase photochemical reactions in a low O_2 atmosphere (e.g., Farquhar et al., 2000; 2001; Farquhar and Wing, 2003; 2005; Ono et al., 2003; Hu et al., 2003; Pavlov and Kasting; 2002; Mojzsis et al., 2003; Bekker et al., 2004; Papineau et al., 2005). Some workers have further argued for the persistence of small non mass-dependent signals into the Paleoproterozoic, where a resolvable, but much smaller signature remains (for samples with ages between 2.4 and 2.0 billion years old; Stage II of Farquhar et al., 2000; Farquhar and Wing, 2003; 2005). The samples studied here are slightly younger than those defining Stage II, but can serve to test the proposed lack of non mass-dependent signatures and presence of a mass-dependent surface sulfur cycle at the time of deposition.

Previous research has suggested that the relationships between $\delta^{33}S$ and $\delta^{34}S$ ($\delta^{33}S$ / $\delta^{34}S$) and $\Delta^{36}S$ and $\Delta^{33}S$ ($\Delta^{36}S$ / $\Delta^{33}S$) can be used to distinguish between

fractionations produced by mass-dependent and non mass-dependent processes

(Farquhar and Wing, 2003; 2005; Wing et al., 2004; Ono et al., 2006). Ono et al.

(2006) recently argued that isotope effects associated with mass-dependent (MD)
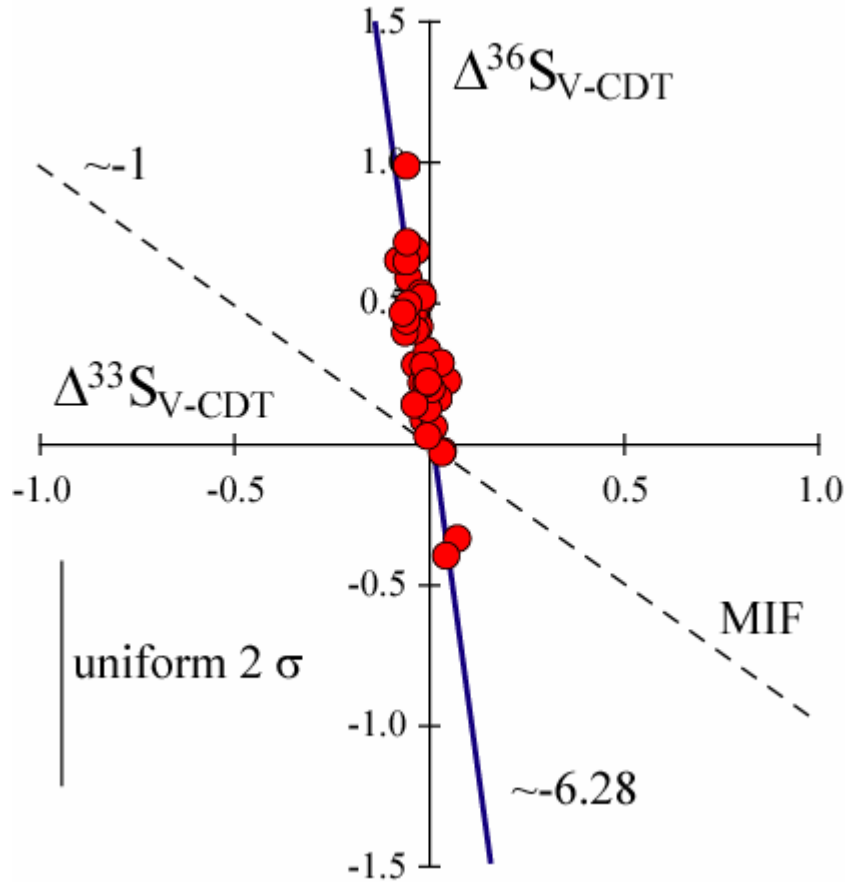
Figure 29: The data plotted in terms of $\Delta^{36}S$ and $\Delta^{33}S$ plot (in ‰). A representative error bar is reported in the bottom left. The short dashed line is an observational trend noted in Archean sediments (see text for details and citations) and plots with a slope of ~ -1 and is further labeled as 'MIF' for mass-independent fractionation. Also plotted is a regression through the data, which produces a trend of slope -6.28. The observed slope for the data is within 1 σ of predictions from Ono et al. (2006), who predicted a slope of -6.85. The observed consistency between mass-dependent predictions and the data, reinforced by the gross deviation from the observed Archean line, suggests that these samples were produced by only mass-dependent fractionation processes. I postulate that the observed small-scale variations are the result of a slight decoupling of ^{33}S and ^{36}S fractionations related to both the geochemical redistribution of material (accounted for both in this treatment and in Ono et al., 2006) and a biologically produced effect (modeled here). The later will be addressed in a subsequent study.

geochemical systems would yield a $\delta^{33}S / \delta^{34}S$ ~ 0.512-0.515 and a $\Delta^{36}S / \Delta^{33}S$

relationship that would converge on a value of ~ -7. Non mass-dependent evidence

suggests a much more variable $\Delta^{36}S / \Delta^{33}S$ (ranging from $\Delta^{36}S / \Delta^{33}S$ of -10.36 [Zmolek et al., 1999] to 1.8 [Farquhar et al., 2001]), however observation of Archean samples suggests a terrestrial record of ~ -1. These data are consistent with the mass-dependent criteria (e.g., Figure 29), and suggest that non mass-dependent isotopic fractionation effects, and non mass-dependent detrital contributions, can be ruled out at the time that this succession was deposited. The nonzero intercept for the $\Delta^{36}S / \Delta^{33}S$ of ~0.3 suggests a consistent sulfur source to the system with a composition different from the normalization (V-CDT). While the observations are consistent with prevailing hypotheses about modest levels of oxygen in the early to middle Proterozoic, they provide a constraint on the extent of the hypothesized Stage II, which marks the transition period between the non mass-dependent world and one more like the modern. Important to understanding element cycles at this time is accepting the difference between what is implied by Stage II in the sulfur and iron isotope records (Farquhar et al., 2000; Rouxel et al., 2005), as the S-record is based on contributions from low O_2 settings and the associated processes whereas the Fe-record is based on oceanic redox conditions.

Conclusions

I have argued that the transition from ferruginous to sulfidic ocean conditions circa 1840 My ago is coincident with significant changes in the sulfur cycle. Despite these changes, the data do not require a significant change in seawater sulfate concentration at this transition. The data and models suggest that during the period of IF deposition, the sulfur cycle fell under local diagenetic control and that seawater and

pore-water sulfate reached an isotopic steady-state. Isotopic variability within this setting is interpreted as the result of changes in local pyrite burial associated with fluctuations in iron inputs and sulfate reducer activity. These modeling treatments also provide a new means of estimating the isotopic composition of seawater sulfate. This estimate is also consistent with a lack of prominent isotopic contributions from SDB at this time. The data suggest that low seawater sulfate concentrations, coupled with active microbial sulfate reduction and a euxinic water column, destabilized the sulfur cycle that dominated during IF deposition and ushered in a sulfur cycle during deposition of the Rove Formation that included loss of ^{34}S-depleted sulfide. The occurrence of positive δ^{34}S sulfides throughout the entire Rove Formation with Δ^{33}S that are consistent with a local loss process, and ^{34}S-enriched sulfides in other late Paleoproterozoic sequences leads to the suggestion the sustained loss process for ^{34}S-depleted sulfur was widespread. This may reflect outgassing of water column hydrogen sulfide to the atmosphere (Kump et al., 2005). Further studies of all four sulfur isotopes from other Proterozoic, sulfide-bearing sulfidic successions should provide a test for this hypothesis. The data suggest that the oscillations between different modes of the sulfur cycle from the steady-state regime associated with the Gunflint Formation, Biwibik Formation, Trommald Formation, and Mahnomen Formation, to the continuous loss regime associated with the Rove Formation was not immediate and that at least one reversal preceded the permanent establishment of sulfidic conditions. I recognize that the connections between biology, ocean mixing, ocean-atmosphere exchange, and basin-scale cycling of sulfur during the Proterozoic remain to be better explored. However, the possibility of continuous loss of hydrogen

sulfide to the atmosphere, coupled with the potential for a pervasive shallow

chemocline, would have undoubtedly influenced myriad elemental cycles and

hindered the advancement /evolution of life through this time.

Chapter 6: Evidence for a mid-Proterozoic oxygenation

Introduction

Detailed carbon and sulfur isotopic and biological studies of Proterozoic surface

environments provide a growing picture of an Earth in transition between an anoxic

Archean world and that of the more oxic Phanerozoic (Canfield, 2005; Holland,

2006). The character of this transition includes a proposal that the surface ocean

during most of the Proterozoic was oxygen-rich due to active oxygenic

photosynthesis, whereas the deep ocean remained anoxic, and likely sulfidic because

of the activity of sulfate reducing microorganisms (Canfield, 1998; Shen et al., 2002;

Poulton et al., 2004; Arnold et al., 2004; Holland, 2006). The stratification of the

ocean may have also played a role in biological evolution as the upwelling of

anoxic/sulfidic waters would serve as a means of extinguishing aerobic life on the

continental shelves. Here, sulfur isotope measurements are used to track the interplay

and relative oxygenation of the deep and shallow oceans as a way to better understand

both the long-term evolution and oxidation state of the Earth's surface and, in turn,

the character and diversity of the biosphere.

Sulfur isotope studies (Canfield, 1998; Canfield and Teske, 1996) provide insight into

the geochemistry of the Proterozoic oceans, as information regarding biological

activity and ocean chemistry is believed to be recorded in these chemical records.

Traditional studies of $^{34}S/^{32}S$ use the range of observed sedimentary sulfide isotopic

compositions to infer the composition and relative concentration of seawater sulfate

126

(cf. Canfield, 1998), as sulfate is conventionally perceived as the most faithful recorder of global processes (cf. Claypool et al., 1980). Recent studies (Burdett et al., 1989; Kah et al., 2004; Gellatly and Lyons, 2005) have made strides towards developing new proxies to directly access the composition of seawater, which has reinforced the understanding of sulfate as the 'target' sulfur reservoir for understanding global processes. New developments from measurements of ^{33}S and ^{36}S in pyrites have broadened the use of pyrites as paleo-environmental indicators. This is especially important since the analysis of sedimentary sulfides (pyrite and acid volatile sulfur) remains more straightforward, both from the perspective of analytical ease and geologic distribution. In this study, I present 42 sulfur isotope (^{32}S, ^{33}S, ^{34}S, and ^{36}S) measurements of Proterozoic sedimentary sulfides and couple them with a revised model of sedimentary cycling in order 1) to place constraints on the isotopic composition of Proterozoic seawater sulfate, 2) to investigate temporal changes in the activity of the sulfur related biosphere, and 3) to develop a tool for tracking periods of progressive Earth surface oxygenation.

Geologic Setting

The sulfide samples presented here are from the McArthur Basin, Northern Australia, which represents a thick and laterally extensive package of relatively un-metamorphosed and un-deformed Proterozoic sedimentary rocks (Scott et al 2000; Abbott and Sweet, 2003). The ~1637 Mya Reward Formation, McArthur Gp. (Page and Sweet, 1998), consists primarily of laminated siltstones and mudstones (Figure 30). The ~ 1431 Mya Velkerri Formation and overlying McMinn Formation

(age is on McMinn Fm.: Jackson et al., 1987), both part of the marine Roper Gp., are comprised of mudstones and siltstones deposited in a low energy deep marine environment (Figure 30). These formations are thought to have been deposited in an intracratonic or epicontinental sea containing sulfide-rich bottom waters (Jackson, 1987; Abbott and Sweet, 2003; Shen et al., 2002, 2003).
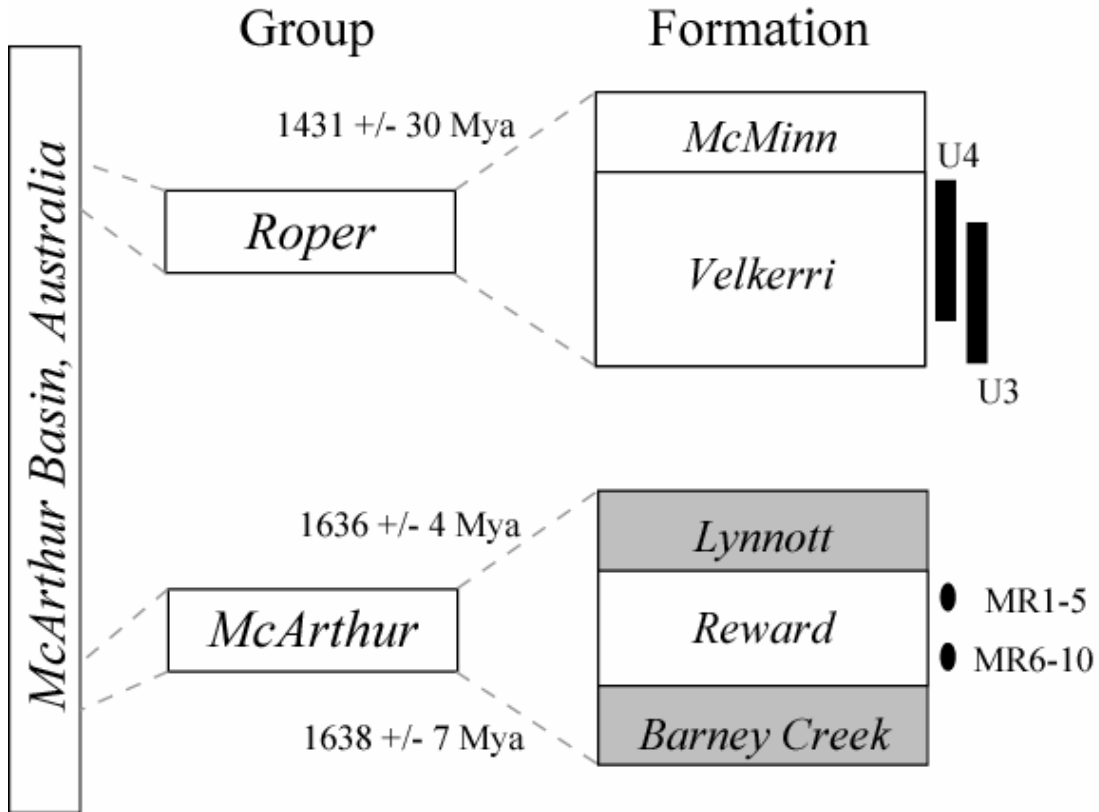
Figure 30: A schematic representation of the stratigraphic relationship between the McArthur Group and Roper Group, both of which are within the McArthur Basin in present day Northern Australia. Age constraints are from the McMinn Formation, Lynnott Formation and Barney Creek Formation. Shales are in white with more carbonate rich sediments in gray. Samples were taken from two drill cores through the Velkerri Formation (U3 and U4), the top and bottom of the Reward Formation and hand samples from the McMinn Formation.

Results

The isotopic compositions of samples from the Reward Formation (n = 10) have a total range from 26.98 to 18.75‰, -0.025 to -0.056‰, and -0.25 to -0.59‰ in $\delta^{34}S$,

128

$\Delta^{33}S$ and $\Delta^{36}S$ respectively (Table 8). The array extending through the Reward data

suggest a $\Delta^{33}S$ versus $\Delta^{36}S$ slope of: $\Delta^{36}S = -6.0 \ (\pm 3.1) \ \Delta^{33}S \ -0.66 \ (\pm 0.13)$. The

isotopic composition of sulfide samples from the Roper Gp. vary from 24.72 to -

23.44‰, 0.125 to -0.053‰, and 0.58 to -2.17‰ in $\delta^{34}S$, $\Delta^{33}S$ and $\Delta^{36}S$ respectively

(Table 8). The sulfur isotopic compositions for shale samples (n = 18) from

Urapunga 3 (U3) cover a range from 24.72 to -19.95‰, 0.083 to -0.053‰, and 0.58

to -1.99‰ in $\delta^{34}S$, $\Delta^{33}S$ and $\Delta^{36}S$ respectively. Similarly, the range for the Urapunga

4 (U4) shales (n = 10) is 22.35 to -23.44‰, 0.125 to -0.037‰, and 0.46 to -2.17‰ in

$\delta^{34}S$, $\Delta^{33}S$ and $\Delta^{36}S$ respectively. Finally, hand samples from the overlying McMinn

Formation (n = 4) range from 13.30 to -8.92‰, 0.103 to 0.040‰, and -0.91 to -

2.07‰ in $\delta^{34}S$, $\Delta^{33}S$ and $\Delta^{36}S$ respectively. The slope of the array extending through

Roper Gp. data ($\Delta^{33}S$ versus $\Delta^{36}S$) is: $\Delta^{36}S = -11.1 \ (\pm 1.4) \ \Delta^{33}S \ -0.62 \ (\pm 0.07)$. The

carbon isotopic composition of the Roper Gp. samples was relatively constant,

varying from -32.11 to -34.56‰.

Formation	Sample (ID)	$\delta^{34}S$ (‰)	$\Delta^{33}S$ (‰)	$\Delta^{36}S$ (‰)
Reward Fm.	MR-1	26.98	-0.048	-0.50
Reward Fm.	MR-2	24.63	-0.037	-0.48
Reward Fm.	MR-3	22.34	-0.025	-0.59
Reward Fm.	MR-4	18.75	-0.028	-0.53
Reward Fm.	MR-5	21.01	-0.036	-0.42
Reward Fm.	MR-6	25.49	-0.037	-0.31
Reward Fm.	MR-7	25.38	-0.056	-0.41
Reward Fm.	MR-8	25.71	-0.040	-0.39
Reward Fm.	MR-9	26.66	-0.045	-0.37
Reward Fm.	MR-10	26.98	-0.048	-0.25

| Formation	depth (meters)	$\delta^{13}C$ (‰)	$\delta^{34}S$ (‰)	$\Delta^{33}S$ (‰)	$\Delta^{36}S$ (‰)
McMinn Fm.	NA	-33.38	0.44	0.058	-1.54
McMinn Fm.	NA	-33.94	1.75	0.040	-1.34
McMinn Fm.	NA	-33.89	-8.92	0.103	-2.07
McMinn Fm.	NA	-33.42	13.30	0.04	-0.91
Urapunga 3					
Velkerri Fm.	26.6	-33.33	-19.95	0.083	-1.99
Velkerri Fm.	31.3	-33.65	6.89	-0.037	-0.69
Velkerri Fm.	41.82	-34.09	3.95	0.07	-0.96
Velkerri Fm.	46.86	-33.43	18.04	-0.016	-0.69
Velkerri Fm.	50.1	-33.11	14.80	0.041	-0.57
Velkerri Fm.	54.95	-33.42	16.47	0.012	-0.48
Velkerri Fm.	61.15	-33.19	15.07	0.04	-0.80
Velkerri Fm.	65.9	-33.96	20.71	-0.03	-0.09
Velkerri Fm.	71.55	-34.17	16.43	-0.044	-0.80
Velkerri Fm.	76.98	-34.21	8.83	-0.026	-0.62
Velkerri Fm.	79.95	-34.33	16.02	-0.054	0.11
Velkerri Fm.	82.38	-33.47	16.92	-0.041	-0.27
Velkerri Fm.	91.41	-33.04	20.80	-0.046	0.18
Velkerri Fm.	95.84	-33.01	17.93	-0.034	0.18
Velkerri Fm.	99.57	-33.00	13.57	-0.046	-0.34
Velkerri Fm.	105.6	-34.23	24.72	-0.053	0.58
Velkerri Fm.	110	-34.30	1.42	0.048	-1.50
Velkerri Fm.	121	-33.48	17.35	-0.037	-0.13
Urapunga 4					
Velkerri Fm.	90.93	-33.16	-23.44	0.125	-2.17
Velkerri Fm.	97.97	-32.11	-6.73	0.05	-1.02
Velkerri Fm.	122.8	-33.36	-11.67	0.021	-1.68
Velkerri Fm.	137.76	-33.12	6.31	0.01	-0.61
Velkerri Fm.	145	-33.31	7.97	0.10	-0.93
Velkerri Fm.	158.17	-33.12	22.35	-0.037	0.46
Velkerri Fm.	166.9	-33.43	8.42	0.01	-0.26
Velkerri Fm.	181.3	-34.56	8.29	-0.012	-0.73
Velkerri Fm.	187.7	-34.16	10.53	-0.019	-0.63
Velkerri Fm.	197.8	-34.07	15.21	-0.03	-0.70

Table 8: Isotopic and depth data for the Reward Formation, McArthur Group and Velkerri and McMinn Fms, Roper Gp. Reward Fm. samples were previously described in Shen et al., (2002) and Roper Gp. samples were previously studied in Shen et al. (2003).

Discussion

Chemostratigraphic record

I begin by interpreting the new sulfide data in a stratigraphic context. The Reward Fm. is not subjected to this analysis, since the variability recorded in that formation was small. Figure 31 presents the isotopic data ($\delta^{13}C$, $\delta^{34}S$, $\Delta^{33}S$, and $\Delta^{36}S$) for the U3 and U4 drill cores. The chemostratigraphic records from U3 and U4 were matched, in terms of depth, based on $\delta^{34}S$ records of the two cores (with the assumption of similar rates of deposition). Previous interpretations (Logan et al., 1995; Shen et al., 2003) of $\delta^{34}S$ data from U4 and other cores through the Roper Gp. suggested that more isotopically depleted samples ($\delta^{34}S < 0$) reflect basinal settings with limited reduction of seawater sulfate (upper portion of the core), whereas heavy $\delta^{34}S$ sulfides reflect the quantitative reduction of seawater sulfate (in pore waters), likely in a shallower water environment ($\delta^{34}S > 10$) (seen lower in the core). As presented in Figure 31, I observe a monotonic rise in $\Delta^{33}S$ and an inversely correlated decrease in $\Delta^{36}S$. These two isotopic relationships are correlated because they reflect the process imparting the fractionations, which in the case of the Velkerri Fm., is likely heavily controlled by microbial sulfate reduction. The organic carbon isotopic composition remains relatively constant throughout the cores. Even though a co-variation between $\Delta^{33}S$ and $\Delta^{36}S$ is expected, the coupling of these two records and, their relationship to $\delta^{13}C$, should receive more attention as our understanding of these systems improves.

Figure 31: Chemostratigraphic record through the Velkerri Formation, Roper Group. The entire interval reported is sulfidic mudstone. Errors are 2 σ. Data is presented in Table 8. See text for discussion.

131
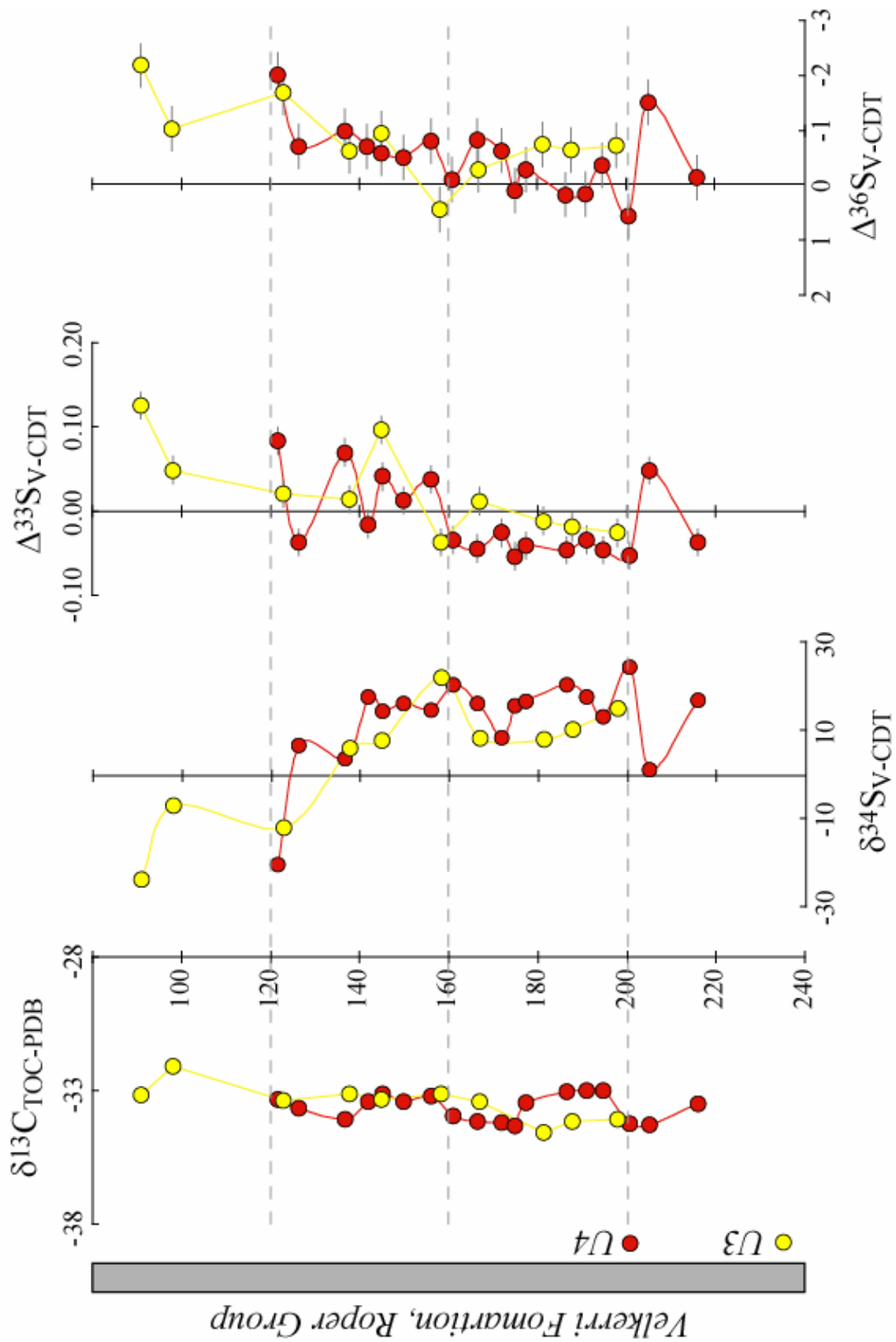
Constraints on seawater sulfate

The Reward Formation: A previous $\delta^{34}S$ study of the Reward Fm. (Shen et al., 2002) suggested that the tight grouping of isotopically enriched sulfides pointed to the quantitative reduction of pore-water sulfate, which would have had the same composition as that measured in the sulfides ($\delta^{34}S \approx 27$ ‰). The new ^{33}S and ^{36}S analyses are consistent with this hypothesis, as the Reward Fm. sulfides cluster tightly in all four isotopes and suggest a seawater sulfate composition of $\delta^{34}S \approx 27$ ‰, $\Delta^{33}S \approx$ -0.05 ‰ and $\Delta^{36}S \approx$ -0.25 ‰ (gray ellipse in Figure 32). The relative isotopic homogeneity within the Reward Fm. data suggests that sulfate concentrations in this basin were high enough to not be drastically affected by any basin-scale chemical closure or active sulfate sinks, such as microbial sulfate reduction. Although this study is fully consistent with previous $\delta^{34}S$ predictions, additional information is gained through interpreting the consequences of the minor isotope prediction, as the predicted isotopic composition of seawater suggests the presence of active sulfur disproportionating microorganisms when the Reward Fm. was deposited. The environmental requirement for active disproportionation is the presence of sulfur intermediate species (S^0, SO_3, S_2O_3). These intermediates are generally understood to be the product of microbial sulfide oxidation (either phototropic or non-phototropic utilizing O_2 or NO_3). With biomarker evidence for active purple and green sulfur bacteria in younger portions of the McArthur Basin (Brocks et al., 2006), it is likely that the necessary sulfur intermediate species were present when the Reward Fm. was deposited.
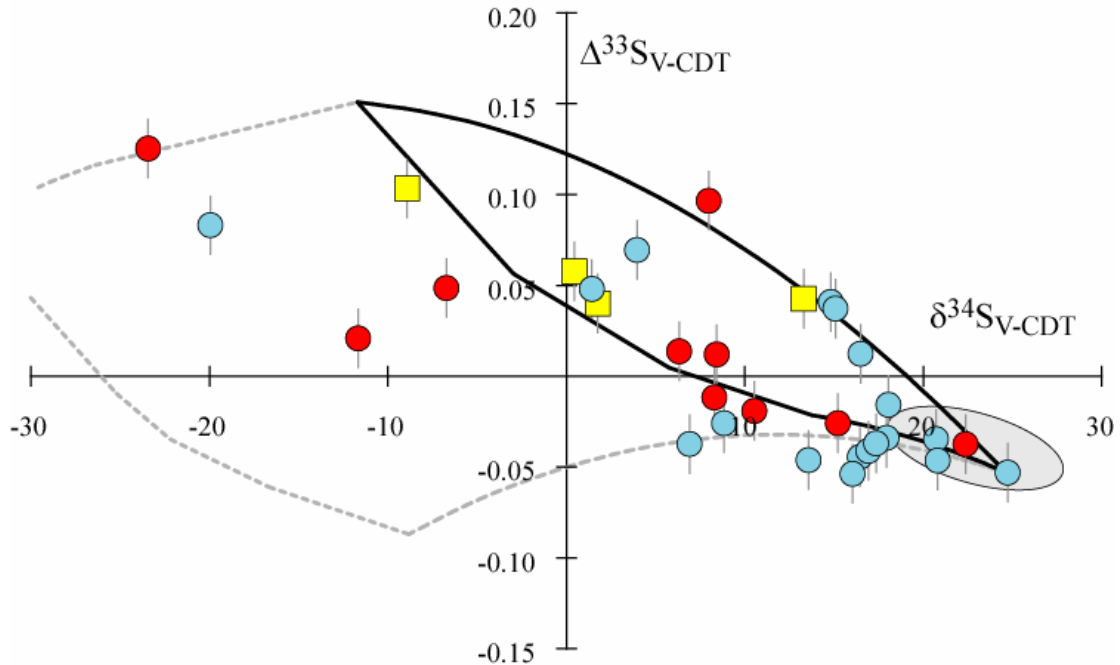
Figure 32: A plot of δ³⁴S versus Δ³³S with a model sulfide field for the Reward Fm. (gray ellipse in lower right) and Roper Gp. (symbols). Reward Fm. was previously studied in Shen et al. (2002). Roper Gp. samples are from drill cores Urapunga 3 (blue circles) and 4 (red circles), with hand samples from the McMinn Fm. (yellow squares). These sediments were previously interpreted as typical of Proterozoic shelf environments. Errors are 2 σ. Modeling is derived from Chapter 5. The small field (outlined in black) represents a sulfur cycle with only sulfate reduction active, whereas the larger field (dashed lines) represents a sulfur cycle with both sulfate reduction and sulfur disproportionation active.

The Roper Group: The greater δ³⁴S variability observed in the Roper Gp. samples

(Velkerri and McMinn Fms.) was previously described as reflecting basinal, distal

shelf, and inner shelf facies following traditional models of Proterozoic

biogeochemistry (Logan et al., 1995; Shen et al., 2003). The manner in which the

data cluster in δ³⁴S and Δ³³S allows for a direct assessment of the isotopic

composition of contemporaneous seawater sulfate ($\delta^{34}S \approx 25$ ‰, $\Delta^{33}S \approx -0.05$ ‰,

$\Delta^{36}S \approx 0.60$ ‰). As seen in Figure 32, the isotopic scatter in the Roper Gp. data

collapses toward a single δ³⁴S - Δ³³S composition as δ³⁴S increase and Δ³³S decreases

(lower right of figure). First, since one isotopic composition of seawater can explain

the range of observed sulfide data, the concentration of basin-scale sulfate must have been stable, despite constant drawdown from sulfate reduction. This is similar to the interpretation of the Reward Fm. and the treatment of the Gunflint IF data presented in Chapter 5. Interestingly, even though both the McArthur and Roper Gps. are understood as being deposited in an intracratonic/epicontinental environment, they do not record any indications of closed system effects.

Proterozoic seawater sulfate

The δ^{34}S record of seawater sulfate through the Proterozoic suggests an overall isotopic stability or slight enrichment (Canfield, 2001; Strauss, 2004). The possible enrichment is thought to reflect the integrated burial of sulfide-rich marine sediments underlying and associated with a long-lived sulfidic ocean (Canfield, 2004). However, a new ^{33}S (and ^{36}S) record provides further insight into the evolutionary track of seawater sulfate, and more importantly, provides information about the processes contributing to that isotopic evolution. Namely, the inclusion of ^{33}S and ^{36}S allows for changes in the biosphere, as well as in the bulk isotopic composition of the surface sulfur cycle (as is called on in the δ^{34}S record) to be assessed. When the seawater sulfate predictions generated in this chapter are coupled with other recent estimates (Chapters 4-5; Johnston 2005a, 2006), a more dynamic story for the evolution of seawater sulfate evolution appears (Figure 33a), with a general progression from the ~ 1880 Mya Gunflint Iron Formation to the ~ 1200 Mya Society Cliffs Fm. (and potentially even until ~ 940 Mya Katav Fm.: see Chapter 4). This

observed isotopic progression through the mid-Proterozoic can be interpreted in a number of manners, two of which I address below.

Our understanding of microbial fractionations suggests that disproportionation is required to produce the seawater sulfate isotopic compositions measured and inferred for the mid-Proterozoic. This is based on model predictions presented in Chapter 4 and the distinction between a sulfur cycle with active sulfate reduction (SRB) and one with additional fractionations from microbial disproportionation (SRB-SDB). Variability within the SRB-SDB model field was originally interpreted (see Chapter 4) as reflecting changes in either relative pyrite burial (f_{py}) or the activity of sulfur disproportionation (f_{r-o}). Though I feel this interpretation remains valid (and further apply it below), variability within the SRB-SDB model field could also reflect changes in the expression of microbial fractionations. Thus, the first possible explanation is that the variability within the Proterozoic record reflects changes in the isotopic fractionation produced by sulfate reducers and sulfur disproportionators and not the presence or absence of these metabolic processes. Experimental evidence presented in Chapter 2 highlights the range of disproportionation related fractionations, any of which could be representative of the Proterozoic biosphere. The variability in Proterozoic seawater sulfate may be related to the activity or expression of different types of microbial sulfur disproportionation (sulfite, thiosulfate, or elemental sulfur), as well as possibly indicating the presence of other metabolic process, such as sulfide oxidation.

The second possible description of the evolution in Proterozoic seawater sulfate

returns to the original model interpretation, where changes in isotopic composition

within the SRB-SDB model field are interpreted in terms of f_{py} and f_{r-o} (also see

Chapter 4). In this model, seawater sulfate becomes more isotopically enriched from

1880 – 1667 Mya, suggesting an increase in the activity of the oxidative sulfur cycle

(increasing f_{r-o}). The period from 1667 to 1460 Mya[3] is characterized by a decrease in

relative pyrite burial (f_{py}) and is followed by a brief interval (1460-1449 Mya) where

f_{py} held constant but where the activity of the oxidative sulfur cycle decreased (f_{r-o}

decreased). During the remainder of the Mesoproterozoic (1429 -1200 Mya), the

Formation/time interval	age	1 σ	n	f_{py}	f_{r-o}
Paleozoic (*)	282	26	2	0.3	0.5
late NeoP / Cambrian (4)	547	21	14	0.6	0.8
early Neoproterozoic (4)	826	62	9	0.4	0.5
Society Cliffs Fm. (4)	1200	-	7	0.5	1.0
Roper Gp. (6)	*1431*	*-*	*-*	*0.6*	*0.3*
Helena Fm. (4)	1450	-	4	0.4	0.0
Dismal Lakes Gp. (4)	1460	-	5	0.5	0.5
Reward Fm.(6)	*1667*	*-*	*-*	*0.6*	*0.3*
Gunflint IF (5)	*1880*	*-*	*-*	*0.6*	*0.0*

Table 9: Here I present minimum estimates for flux values at the formation/time interval level. Numbers in parentheses represent the chapter in which the data was originally presented, with a '*' referring to Goldman et al. (in review). Uncertainties are given on the ages where 'n' samples were averaged over a time domain. Otherwise, 'n' refers to the number of samples measured in a given formation. Uncertainties on formation and group ages can be found in the text. Rows in regular font are direct measurements of sulfates, whereas rows in italics represent estimates of seawater sulfate from sulfide data.

oxidative sulfur cycle becomes more active, as indicated by increasing f_{r-o}. If I take

the maximum possible microbial fractionations, values for f_{py} and f_{r-o} can be uniquely

estimated (presented in Table 9) and the <u>relative</u> changes over geologic time directly

---

[3] The age of the Dismal Lakes Group was recently revisited by Evans (2006) and determined to be 1460 Mya, as opposed to previously reported estimates (Kah et al., 2004; Chapter 4) of 1300 Mya.

assessed. Note that these values represent minimums. Although no strong temporal trend is recognized, estimates for environments > 1200 Mya are more so characterized by wide ranges in f_{r-o} (as may be expected) and less variable in f_{py}. Conversely, changes in f_{py} and f_{r-o} in younger environments (Neoproterozoic forward) are loosely correlated along a ~ slope 1 line. This observation stands contrary to the expectation that as more sulfide is oxidized (greater f_{r-o}) less pyrite would be available to be buried (lower f_{py}), suggesting an inverse correlation (slope closer to -1).

The transitional period, where the depositional ages are statistically equivalent (1460-1429 Mya), may reflect either a true and interpretable 'loop' in the composition of sulfate (as seen in Figure 33a) or simply show the variability within a less stable sulfur cycle that is progressively becoming more oxidizing with time. If the later is the case, then these samples represent a general intermediate state between the reduced Gunflint I.F. sulfur cycle and that of the more oxidizing environment recorded in the Society Cliffs Fm. The data does not require that the gradual mid-Proterozoic oxygenation reflect changes in pyrite burial alone, nor does it require the change in the composition of the surface sulfur cycle (Canfield, 2004). The inclusion of ^{33}S and ^{36}S points to a complex and coupled interplay between pyrite burial, the activity of the oxidative sulfur cycle, and possibly tectonics.

The Neoproterozoic

Sulfur isotope data for the Neoproterozoic also suggests variability in the oxidation state of the Earth's surface (Figure 33b). Rather than the transience observed for the
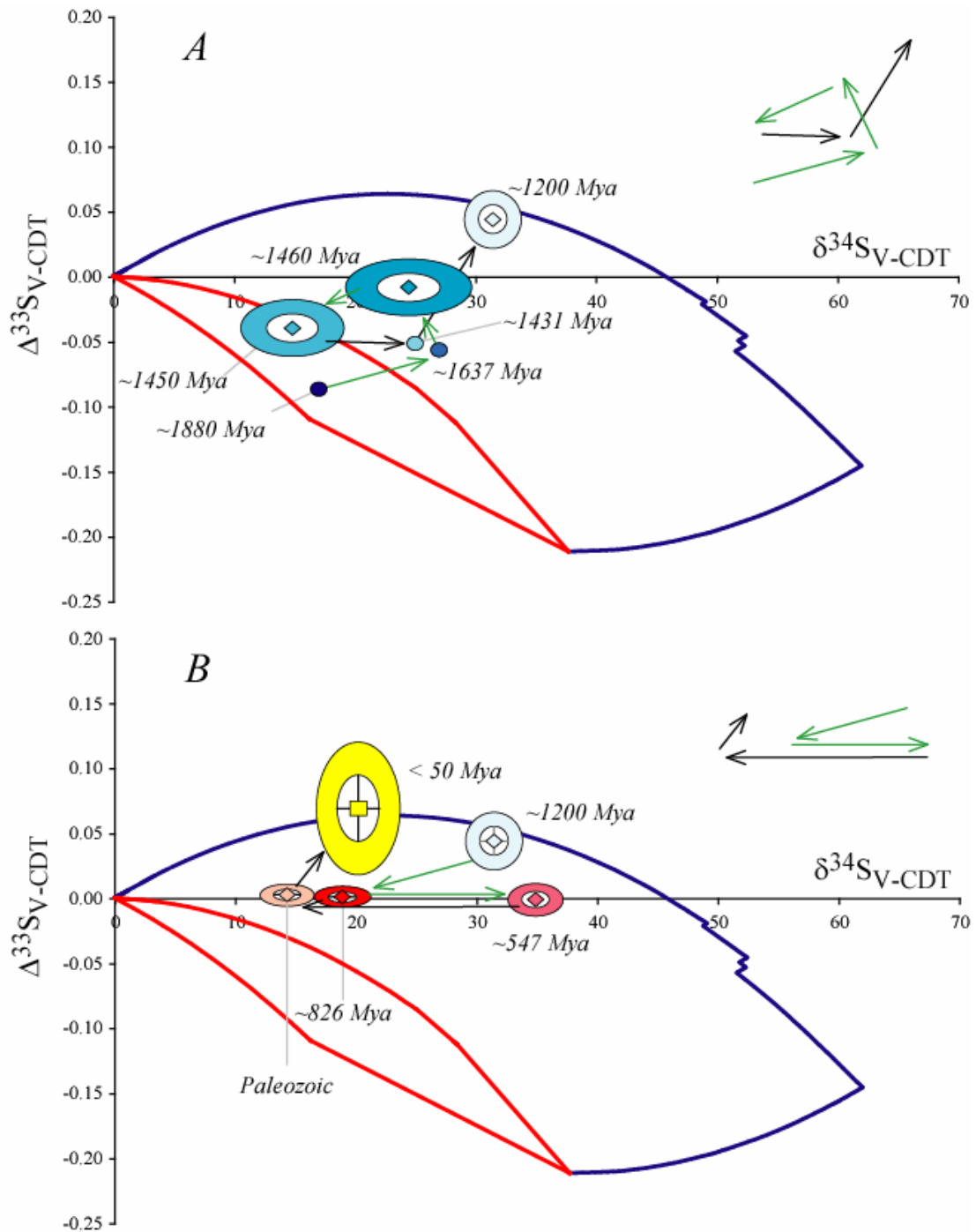
Figure 33: A predictive model for $\delta^{34}S$ versus $\Delta^{33}S$ of seawater sulfate. The red lines enclose a sulfate reduction sulfur cycle whereas the blue lines include sulfur disproportionation. Samples are discussed in text, and ages/labels are taken from Table 9. Ellipses represent 1 and 1 s standard errors on a given population. Modern data (< 50 Mya) is vetted from Farquhar et al. (2002). Insets represent a more lucid picture of the evolutionary track of seawater sulfate. A) The evolution of seawater sulfate in the mid-Proterozoic. B) The evolution of seawater in the Neoproterozoic through today.

mid-Proterozoic, 23 measurements of Neoproterozoic seawater sulfate suggest two well defined populations, one representing the pre-Sturtian (earliest) Neoproterozoic and the second recording the post-Marinoan Neoproterozoic/Cambrian world (Kaufman and Knoll, 1995; Kaufman et al., 1997; Hoffman et al., 1998). The relative global consistency within each group of samples (defined temporally) suggests that sulfate concentrations were high enough for sulfate to be globally conservative. In terms of sulfate evolution, the transition from the Meso- into Neoproterozoic is marked by a strong decrease in relative pyrite burial (f_{py}), possibly associated with a step-wise oxygenation of the atmosphere (Derry et al., 1992; Kaufman et al., 1993; DesMarais et al., 1994). Limited estimates for modern seawater sulfate (Farquhar et al., 2002) suggest a similar composition to that which I observe for the early Neoproterozoic, perhaps indicating either a similarity between these two environments or pointing to an especially stable state of the surface sulfur cycle. The isotopic composition of seawater sulfate at the end of the Neoproterozoic and into the Cambrian reflects a return to a 1200 Mya-like sulfur cycle (see Figure 33b). This would require that the relative fraction of pyrite burial (f_{py}) increased between the early and late Neoproterozoic. Though the Phanerozoic seawater sulfate record is limited, data suggests that the isotopic composition of seawater sulfate returned to a more modern-like value in the Paleozoic, where it may have remained until today.

The role of tectonics

The observed trend of increasing oxygenation in the mid-Proterozoic is occurring over tectonic timescales. For this reason, I investigate the potential link between the

biosphere and the assembly and break-up of a pre-Rodinia supercontinent, Columbia

(aka. Nuna). Although not well understood, Columbia was thought to have been

initially assembled by 1800 Mya, experienced long-lived subduction related accretion

(until ~ 1500 Mya), and have finally broke up in the mid-Proterozoic (1500 Mya until

at least 1300 Mya, possibly 1200 Mya: see Lupke and Lyons, 2001 and Zhao et al.,

2004 for a review). I consider, as a thought experiment, the potential link between

tectonics and the biogeochemical evolution of the sulfur cycle (discussed above). To

do so, I adopt a BLAG-like model (Berner et al., 1983), which would suggest that

increased spreading rates would result in greater quantities of CO_2 released at

spreading centers and warmer oceanic crust, which would cause an overall shallowing

of oceanic basins. As a consequence, the deep ocean would become shallower and

the continental shelves would record marine transgression and actual become

generally deeper. The coupled CO_2 flux and increase in submerged continental shelf

would boost primary productivity and stimulate the biosphere, since a vast majority

of marine biological activity occurs in shelf environments (Jorgensen, 2006).

Enhanced organic carbon production would fuel sulfate reduction and foster the

production of biogenic pyrite. With larger reservoirs of both biogenic pyrite and

organic carbon, the amount of available free oxygen would be expected to increase

(associated with the removal of these reduced pools). Such an environmental scenario

would be one way to account the inferred mid-Proterozoic oxygenation.

Following the evolution of Δ^{33}S versus Δ^{33}S

In addition to evaluating the relationship between Δ^{33}S and δ^{34}S, added information is

captured in Δ^{36}S / Δ^{33}S relationships (Johnston et al., 2006; Ono et al., 2006) (Figure

34). Recently, studies of < 2000 Mya mass-dependent environments (Chapter 4-5;

Johnston et al., 2005a, 2006; Ono et al., 2006, 2007), geochemical box models

(Chapter 5; Johnston et al., 2006), and independent experimental studies (Chapter 3)

help to constrain and illustrate the types of isotopic variability possible within a

purely mass-dependent record (Figure 34a). The apparent variability is related to

both the biological pathways that are present at that time and the changes in mass-

balance associated with the sulfur cycle itself (model in Figure 34b). Figures 34b and

34c track the evolution the isotopic composition of seawater sulfate (in Δ^{36}S versus

Δ^{33}S) relative to model predictions for that reservoir (Figure 34b). These data

illustrate a wide range of compositions, all of which are 100% mass-dependent (see

Figure 6.5a) and can be described within error by the global sulfur cycle model. The

consistency of the sulfate values and the model prediction demonstrates a simple

understanding of the generation of these compositions; however the scatter within the

sulfide data (Figure 34a) points a record potentially rich with information.
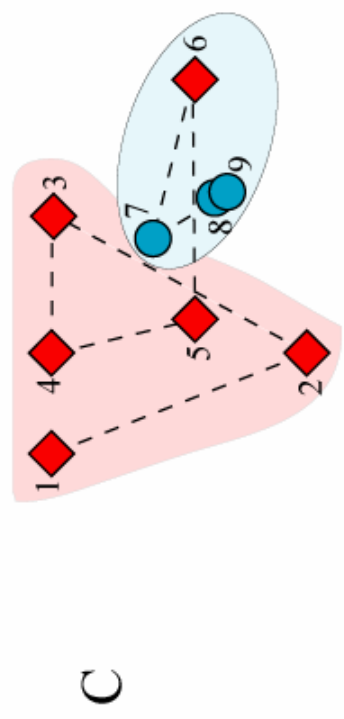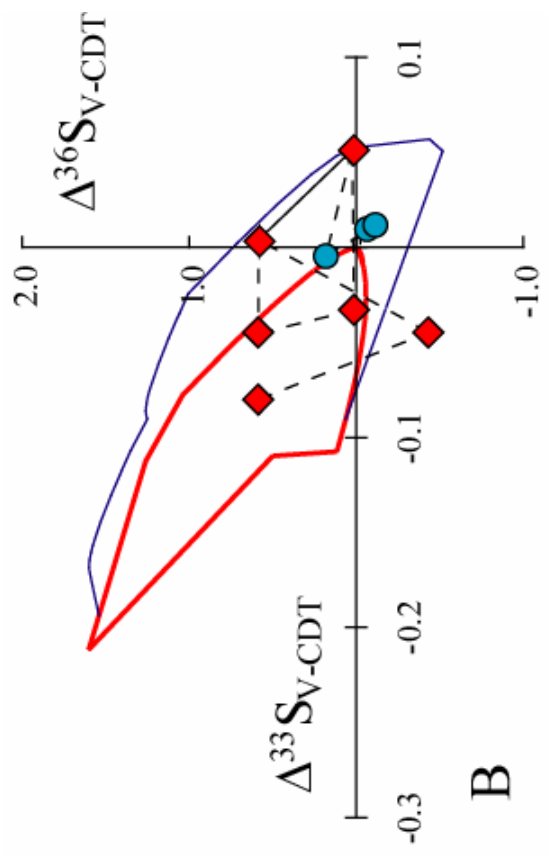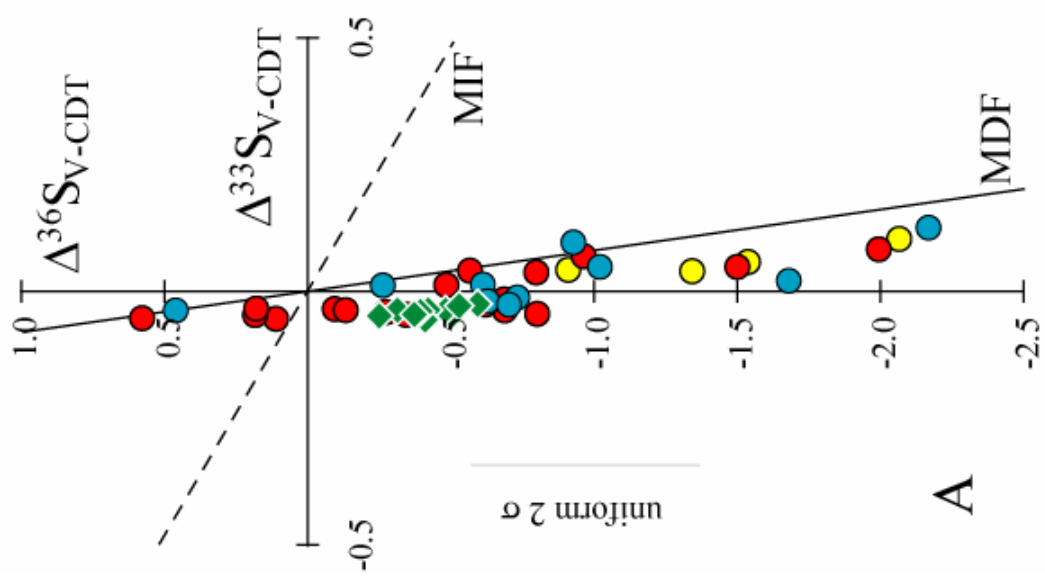
143

Figure 34: A plot of Δ^{33}S versus Δ^{36}S for the Reward Fm and Roper Gp. A) The traditional 1-1 aspect ratio (scale) with the data and lines representing mass-dependent fractionations (MDF) and mass-independent fractionations (MIF). The Roper Gp. samples plot with a slope of: Δ^{36}S = 11.1 (±1.7) Δ^{33}S + 0.20 (±0.09), whereas the Reward Fm. samples plot in a tight cluster with a slope of: Δ^{36}S = -6.0 (±3.1) Δ^{33}S – 0.66 (±0.13). B) A model field prediction for the composition of seawater sulfate, where the red line envelopes the sulfate reduction field and the blue line outlines the combined sulfate reduction-sulfur disproportionation field. Also included is a predicted evolutionary track for the composition of seawater sulfate. C) The temporal evolution of seawater, where 1 = Gunflint Fm. (1880), 2 = Reward Fm. (~ 1667 Mya; see text), 3 = Dismal Lakes Gp. (1460 Mya: Evans, 2006), 4 = Helena Fm. (1449 ± 10 Mya: Aleinikoff et al., 1996), 5 = Roper Gp. (1429 ± 30 Mya), 6 = Society Cliffs Fm. (1199 ± 24 Mya: Kah et al., 2001), 7 = early Neoproterozoic, 8 = late Neoproterozoic, 9 = Paleozoic. Estimates of modern seawater from Farquhar et al. (2002) did not include ^{36}S data.

In addition, the temporal evolution observed in Figure 34c is interesting and suggestive. First, the isotopic variability in seawater sulfate in the post-1200 Mya world is significantly less than is observed in the pre-1200 Mya world. This may reflect an increase in the concentration of seawater sulfate and as a result, the relative stabilization of the marine sulfur reservoir[4]. Second, the locus of the two distinct populations shifts from the upper left to the lower right of Figure 34c, suggesting one of two possible scenarios (or a combination of both). First, if the mid-Proterozoic oxygenation was significant enough to usher in a modern-like sulfur cycle, where sulfate concentrations where in fact relatively high (as suggested above), then the shift in values may reflect the unidirectional (terminal) activation of the fully active (both reduced and oxidative) sulfur cycle. An alternative hypothesis is that the isotopic difference between the two suites records a change in the overall composition of the Earth's surface sulfur budget (as was proposed for δ^{34}S: Canfield, 2004). If the Gunflint Formation pyrites are characteristic of sulfides from the first half of the Proterozoic, then long-term burial of such a pool would drive the overall composition

---

[4] Higher seawater sulfate concentrations would buffer against significant isotopic variability. However, higher relative seawater sulfate levels does not require the 29 mM indicative of a truly modern sulfur cycle, but perhaps between 1 and 10 mM.

of the bulk surface sulfur reservoir (and in turn seawater sulfate) in the same direction as suggested by Figure 34c.

Conclusions

Phanerozoic atmospheric oxygen levels are most commonly inferred from the coupled change in the carbon and sulfur isotope records (cf. Berner, 1991). In the Proterozoic, however, reservoir effects (ie. stability and size) have limited the application of this approach and such a proxy for changes in atmospheric oxygen did not appear possible. This new multiple isotope approach, however, holds promise to open the environmental window into Precambrian atmospheric oxygen levels. The data illustrate the sensitivity of this tool and point to a progressive change oxidation state of the mid to late Proterozoic biosphere. Detailed stratigraphic studies of correlative successions from throughout the Proterozoic will answer questions about the timing and causes of the apparent change. I look optimistically to similar studies in the Phanerozoic, and in addition to tracking oxygen levels, these studies will provide a more detailed understanding of processes active in Phanerozoic diagenesis, such as bioturbation.

Chapter 7: Conclusions, directions, and closing thoughts

General conclusions

The primary goal of this study was to characterize biological sulfur isotope effects and apply this understanding to Proterozoic biosphere reconstructions. Detailed experimental work has determined that sulfate reducing microorganisms and sulfur disproportionating microorganisms, the two metabolic processes thought to be responsible for a majority of the observed $\delta^{34}S$ fractionation recorded throughout Earth history, produce $^{33}S/^{32}S$ and $^{36}S/^{32}S$ fractionations that are resolvable from one another. These experimental fractionations were used as input parameters for a global box model in order to make predictions for the isotopic composition of different surface sulfur reservoirs, when one or both metabolisms are active. Using this approach, the onset of active microbial sulfur disproportionation was pushed back from ~ 800 Mya well into the mid-Proterozoic. Studies of two marine basins adapted this approach and developed a novel means of using sulfide minerals, rather than sulfates (which underpin the study noted above), to determine the character of the basin-scale sulfur cycle and composition of contemporaneous seawater sulfate. These latter studies will allow for a more pervasive application of this tool, as sulfide minerals are more abundant than sulfates.

Lessons learned at the cellular level

The results of experimental studies with both microbial sulfate reducers and microbial

sulfur disproportionators are compiled in Table 10. The primary conclusion suggests

that there is a metabolism-specificity to the ^{33}S and ^{36}S fractionations, as is best

represented by the various λ values (see below). I take the range that these data cover

as generally representative of what will be observed in future experiments with these

metabolisms. This is more appropriate for sulfate reduction, where the present data

set is quite large. What remains to be further understood are the specific controls and

mechanisms that govern the production of these signatures. The trend established by

this data loosely suggests that $\lambda_{SRB} < \lambda_{EP}$ (EP: equilibrium prediction) for ^{33}S and

$\lambda_{SRB} > \lambda_{EP}$ for ^{36}S. The opposite is generally true for disproportionation. I speculate

that this difference is largely dependent on the direction of the redox reaction, with

$\lambda_{RP} < \lambda_{EP}$ (RP: reductive processes) and $\lambda_{OP} > \lambda_{EP}$ (OP: oxidative processes).

Metabolism	$^{33}\lambda$	$^{36}\lambda$	n
Dissimilatory sulfate reduction	0.5077 - 0.5125	1.905 - 1.974	51
Sulfur disproportionation	0.5145 - 0.5187	1.889 - 1.902	6

Table 10: A compilation of experimental fractionation factors (in ^{33}S and ^{36}S) from Chapters 2-3.
Both the maximum and minimum values are presented, as well as the number of experiments (n)
for each metabolic process.

A new picture of the Proterozoic biosphere

The primary environmental target for applying mass-dependent sulfur isotope

fractionations has thus far been the Proterozoic. The overall contributions of this

work to the Proterozoic record are seen in Figures 35-37. It can be seen that the δ^{34}S

record provided by this study is consistent with the range of observations previously

reported (Canfield, 2001) whereas the minor isotope record is novel. Also included is
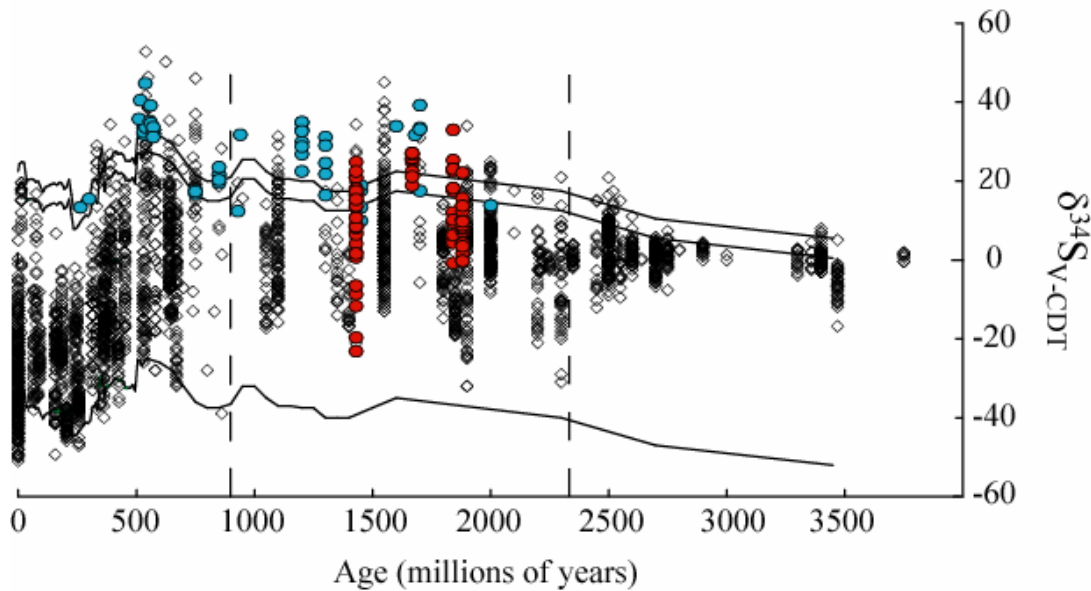
Figure 35: Here I represent a compilation originally presented in Canfield (2001) and redrafted in Figure 1. The data collected throughout this study are plotted in color over the top of the original figure. Measurements of sulfates (seen in blue) correspond well with the predictions of the upper black lines in the Canfield compilation. Plotted in red are measurements of sedimentary sulfides, which nicely correspond with the black diamonds in the original plot. Errors are smaller than the points.

an updated version of Figure 3 (Figure 36), which in addition to highlighting the

contribution of this study, illustrates the work done by the community. A new look of

the sulfur isotope record of the Proterozoic is presented in Figure 37. In addition to

the data, I include an inferred seawater sulfate curve. Excluding one outlier from the

Neoproterozoic Doushantou Fm., I observe a temporal decrease in the Δ^{33}S of

seawater sulfate, with greater structure in the Neoproterozoic record. Values of Δ^{36}S

remain relatively stable throughout the Paleo-Mesoproterozoic and fluctuate (in

concert with Δ^{33}S) in the Neoproterozoic. Interestingly, the Δ^{36}S prediction for the

Reward Fm. falls well below the overall temporal trend. The Neoproterozoic

structure seen in both ^{33}S and ^{36}S may reflect a response to global, low latitude
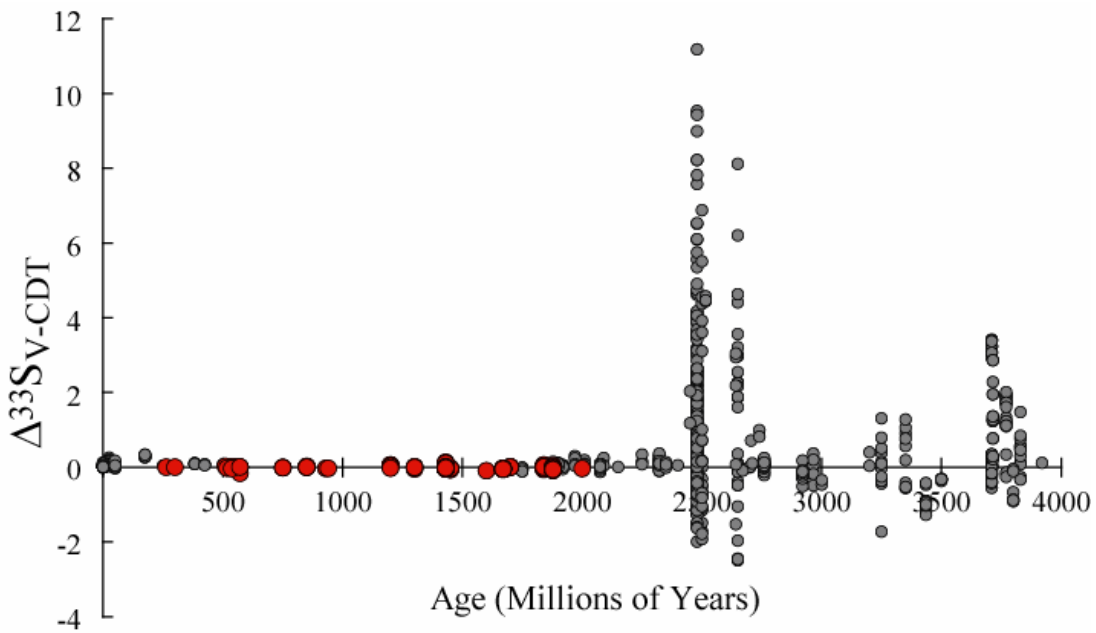
Figure 36: Compilation of ^{33}S isotope data, updated from Figure 3. Red circles represent measurements included in this study, whereas gray circles represent published contributions from the community. Errors are smaller than the symbols. Data is from Farquhar et al., 2000, 2002; Hu et al., 2003; Mojzsis et al., 2003; Hu et al., 2003; Ono et al., 2003, 2006a, b, 2007; Bekker et al., 2004; Whitehouse et al., 2005; Johnston et al., 2005a, 2006; Papineau et al., 2005, 2006: Ohmoto et al., 2006; Cates and Mojzsis, 2006.

glaciation events or a change in deep ocean chemistry. In either case, the coincident

excursion is provocative. Perhaps even more intriguing is periods where the records

may not faithfully follow one another, such as may be the case ~ 1650 Mya. Little is

known about the Cambrian/Phanerozoic and the first half of the Paleoproterozoic, as

indicated in Figure 37.

The first of the Proterozoic studies focused on testing hypotheses about the timing of

microbial innovation: namely the activation of sulfur disproportionation reactions in

tandem with the onset of non-photosynthetic sulfide oxidizers. To address this

question, numerous proxies for seawater sulfate were measured and used to construct
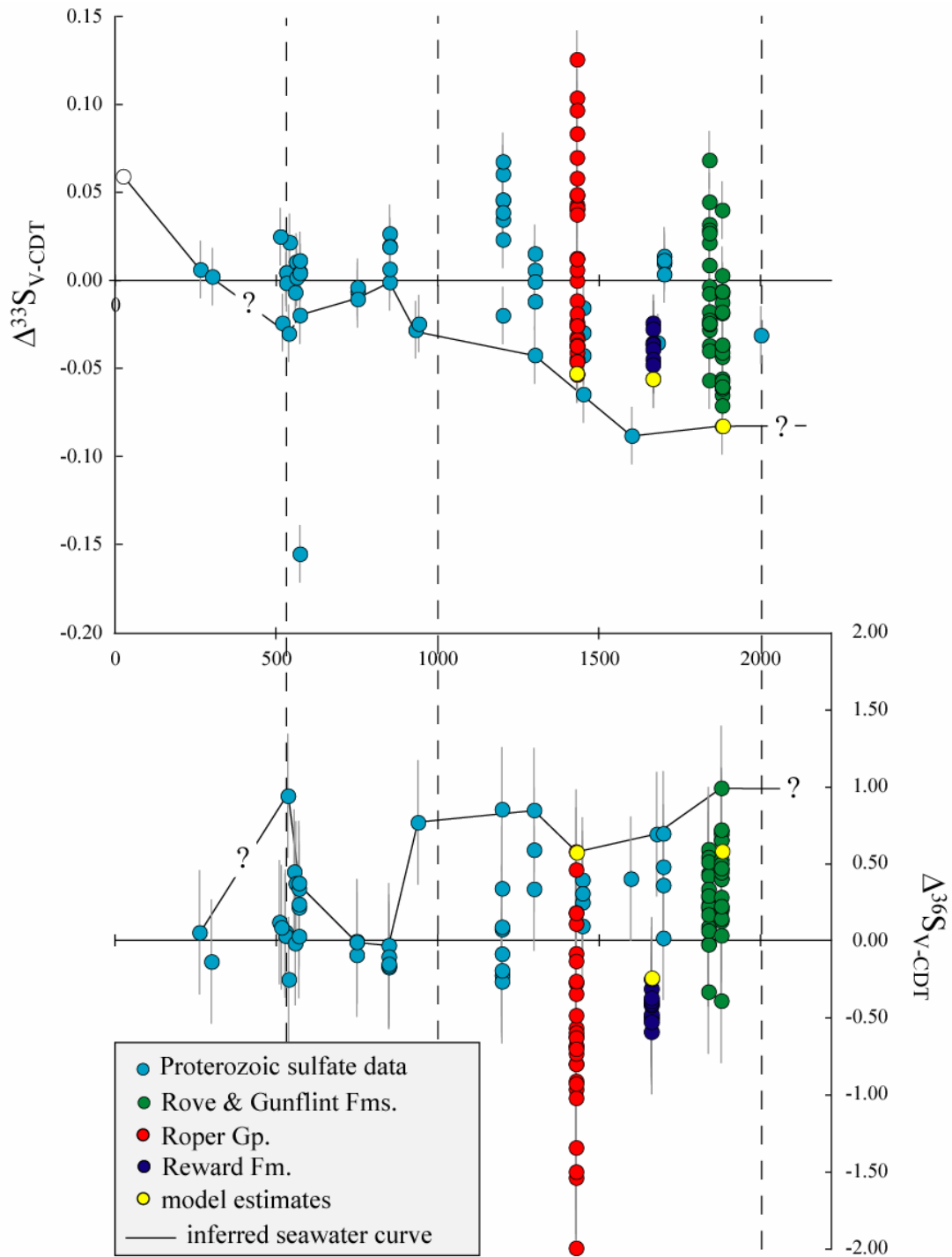
Figure 37: Here I present temporal records for both $\Delta^{33}S$ (A) and $\Delta^{36}S$ (B). All errors are 2 σ. The legend on the figure describes the details of the points. The only additional point is an estimate of modern seawater (50 Mya average) From Farquhar et al. (2002) noted in A. The solid black bounding line is a qualitative prediction for the isotopic composition for seawater sulfate. These trends are discussed further in the text.

a temporal record of $\delta^{34}S$ and $\Delta^{33}S$ change from 2000 Mya to 500 Mya. When

coupled with an experimentally constrained global box model, these data point to

active sulfur disproportionation reactions extending into the middle Proterozoic. This

contrasts with earlier work which had suggested a ~ 800 Mya arrival for this

metabolism. The requirement of non-photosynthetic sulfide oxidation could not be

specifically addressed in this study, as numerous oxidation pathways are

environmentally relevant and possible.

Direct proxies for seawater sulfate, as used in this study (Chapter 4), are not as

abundant in geologic record as the reduced component of the sulfur cycle,

sedimentary sulfides. With this in mind, the two follow-up chapters (Chapters 5-6)

developed a framework for using sulfide measurements to unveil information about

more local, basin-scale sulfur cycling and the contributions from microbial processes.

The first study targeted the transition from ferruginous to sulfidic deep-water

conditions, which is captured in the 1900-1800 Mya Animike Basin. The sulfur

isotope record in the Gunflint Iron Formation and overlying sulfidic black shale of the

Rove Formation (within the Animike Basin) suggests a period of stability during the

deposition of the Gunflint Fm., but a destabilization of the sulfur cycle during the

period of Rove deposition. It is proposed that the destabilization may be related to

the combination of low seawater sulfate concentrations and outgassing of a sulfidic

water column to the atmosphere; the latter has also been suggested as a mechanism

for the Permian-Triassic extinction (Kump et al., 2005). In addition to providing

insight into the Paleoproterozoic sulfur cycle, these data and the modeling used to

explain them provides a constraint on the isotopic composition of seawater sulfate. A similar approach was applied to the younger sulfidic black shales of the mid-Proterozoic marine Reward Fm. and Roper Gp. These data suggest that sulfur disproportionation reactions were active in these basins, and provides a prediction for the composition of seawater sulfate.

Prior to this work, the changes in the surface biosphere during the second half of the Proterozoic were not well understood. The strongest lines of evidence and associated arguments for describing the evolution of the biosphere during this period was reported in a series of studies by Canfield and friends (Canfield and Teske, 1996; Canfield 1998), which coupled biospheric change to deep-ocean conditions. This dissertation has revisited these earlier works, and expanded on previous conclusions. Taken together, this study provides a detailed picture of progressive biospheric oxidation during the second half of the Proterozoic. This style of oxygenation (progressive, as opposed to step-wise) is further supported by carbon isotope studies, which suggest a similar change (cf. Frank et al., 2003). I note that these conclusions do not negate earlier hypotheses, but begin to provide a more detailed understanding of a complex period of Earth surface evolution. It is intriguing that oxidative microbial cycling developed while deep-waters retained toxic, sulfidic conditions. I also note that the changes outlined here are subtle, and that large-scale environmental swings in climate and deep-ocean chemistry still characterize much of the terminal Proterozoic. These changes undoubtedly influenced the biosphere, but rather than influencing microbial regimes, they likely drove innovation in the Eukaryotic

Domain, giving way to the rise of large animals (cf. Fike et al., 2006; Canfield et al., 2006). Applying the sulfur isotopes to assess material flow through eukaryotic systems remains completely unexplored.

Looking forward...

Part I

This study has only begun to cover the diversity of sulfur metabolisms that are active in nature and likely contribute to the isotope record. Most notably missing are the various sulfur oxidizing microorganisms, which are understood from the perspective of $\delta^{34}S$, but remain to be explored in ^{33}S and ^{36}S. This includes the phototrophic and non-phototrophic microorganisms. This overall effort will benefit from ongoing work to understand the enzymatic activity within studied and unstudied microorganisms, as well as an experimental effort to extract internal chemical species for direct study. In addition to using the sulfur isotopes to better understand specific metabolisms, two other broad targets are identified. First is the measurement of compound-specific multiple sulfur isotope signatures, such as amino acids and sugars. This type of work has been pioneered in other light stable isotope systems (H, C, and O), with modern and paleo-environmental applications. Second is the development of a framework for understanding the relationship between sulfur-bearing isotopomers, such as sulfate. Groundbreaking work on the coupled carbon-oxygen isotopomers, primarily CO_2, has highlighted the information that can be derived from the careful study of isotopomer systems.

Part II

As is noted in the closing remark of the preceding section, much remains to be

discovered and explored using the sulfur isotope tool developed, in part, by this study.

I focused on dissimilatory systems, but realize that applications exist at many

different levels. These include, but are not limited to the study of assimilatory

processes and eukaryotic cycling. In addition, there exists a group of geologically

relevant inorganic process for which we do not understand isotope fractionations. I

point primarily to the process of pyrite formation, but do not exclude the

incorporation of sulfate into carbonates (CAS), since this proxy is proving to be

valuable in reconstructing ancient environments.

Three big questions remain to be studied; one is quite specific while the other two are

broad: 1) From the days of the original temporal records of $\Delta^{33}S$, three periods of

Earth history have been defined (Figure 3; Farquhar et al., 2000). Most researchers

have focused on the transition from Stage I to II, due to the implications for

atmospheric oxygen. However, just as poorly defined, and perhaps even more so, is

the transition from Stage II to III. Chapters 5 placed a younger age limit of 1880 Ma

on this transition, but left open the (likely) possibility that the transition is much

closer to 2400 Mya. This leaves open a period from ~ 2400 – 1870 Ma, when the

contributions to the surface sulfur cycle and the state of the biosphere are not well

understood. Within this task are fundamental questions about the lead and/or lag

between the ocean-atmosphere system, as well as the activity of the different

154

metabolic processes, all of which can be addressed through detailed studies of marine environments during this critical period. The remaining two goals are areas of study rather than specific projects. 2) The Phanerozoic has been almost completely ignored to date, though there are a number of studies in progress that are working in this Eon. I look forward to exploring these environments and reading about works that extend this tool to this period. 3) Though technically within the Phanerozoic, I also explicitly point to the study of modern environments (chemical oceanography and marine ecology) as a lucrative area of future study. Studies in progress suggest that there exists a rich and complicated record that awaits discovery and is deserving of more study.

Part III

Behind the applications of sulfur isotope analyses to different environments is the understanding of isotope systematics. This too remains a target area for future development. I have taken a page from the oxygen isotope literature and used the λ relationship to understand and interpret experimental studies. This tool will certainly prove valuable in natural studies, though the direct application of λ to natural systems has thus far proven a challenge. These applications will certainly benefit from more and more studies, new thinking, and study designs that target the extraction of this type of information (sulfate-sulfide paired measurements). The other isotope relationship that remains in its infancy is $\Delta^{36}S$ versus $\Delta^{33}S$. To date, I have used this tool successfully to distinguish between mass-dependent and non mass-dependent systems. There is detail in these records that has gone largely unexplored thus far.

For instance, I note a variety of empirical trends in environmental data sets as well as process-specific slopes in experimental studies. This type of interpretation can also bee seen when comparing Figures 37a and 37b. These records do not directly track one another, suggesting that there is a layer of interpretability (causes, mechanisms, etc.) that remains largely unexplored.

A few closing thoughts

Many of the statements in these conclusions have looked forward to the potential of future works and areas of research. I would like to end however, with a brief look back. Shortly after my arrival at Maryland, James pulled me aside and made a simple comment that I was not soon to forget, and wonderfully encapsulates the mentality of his group and approach to science. James spoke enthusiastically and with confidence about uncovering bio-signatures in the sulfur isotopes, but noted (and this is the part that really stuck) that I would need to make the mass-spec do things that it was not going to want to do, and achieve precisions that were almost at the level of the machines ability to even report. Although there is always room for improvement, the collective efforts of the Farquhar lab have made these goals a reality, and once again, reflects the ethic by which James does science: never settling and always looking forward. I am forever grateful to have been a part of this process and group. Along the way, we have had a lot of fun and, at least as I optimistically see it, opened up a new field of isotope geochemistry.

Appendices

Appendix 1: Isotope normalization and uncertainties

Uncertainties in isotope measurements are based on the long-term reproducibility of

45 measurements of three international standards (IAEA S1, S2, and S3). These data

are reported fully in Ono et al. (2006). All samples were run following dual-inlet

protocols, and generally balanced to within ~ 30 mV on m/e 127 ($^{32}SF_5^+$). As a

minimum, samples and standards were run for 3 acquisitions, each of which contains

eight sample measurements bracketed by standards, resulting in a minimum of 24

individual isotope ratios. The bellows (standard and reference) were re-balanced

between each acquisition. If the data was deemed poor after the evaluation of the 24

measurements (based on the variability observed in $\Delta^{36}S$, with in-run $\Delta^{36}S$ standard

deviations > 0.25‰ viewed as "poor"), further acquisitions were added (generally up

to ten total aquisitions, or 80 individual isotope ratios). Our analyses were

occasionally subjected to an isobaric interference on the 131 collector, which would

result in an artificially high $\Delta^{36}S$ value. If this was suspected, the sample was frozen

back out of the mass-spectrometer, run through the GC an additional time, and re-

introduced into the mass-spectrometer. On repeated occasions, this technique cleaned

up the interference.

The chosen errors ($\delta^{34}S = 0.14$, $\Delta^{33}S = 0.008$, $\Delta^{36}S = 0.20$: 1 σ) represent the

uncertainty of a single fluorination. This is a conservative estimate of the long-term

reproducibility. Uncertainties for $\Delta^{33}S$ (and $\Delta^{36}S$) are smaller than those for $\delta^{33}S$ (and

$\delta^{36}S$) because variability inherent in the measurement technique leads to correlated

clusters of $\delta^{34}S$ with $\delta^{33}S$ that co-vary by ~ 0.515 (or 1.90 for ^{36}S). For example, as can be seen in Figure A1, the individual measurements are not randomly scattered. The slope of a trend line through the data is consistent with mass-dependent theory and observations. The consistency amongst the data illustrates the correlated errors in $\delta^{33}S$ and $\delta^{34}S$, and further shows how the uncertainty in $\Delta^{33}S$ (which is loosely defined as the deviation from the trend line) is significantly smaller than on $\delta^{33}S$ alone. The literal slope of the trend line (λ) can be calculated, along with uncertainties, using both the methods of Williams (1967) and those described in Appendix 4.
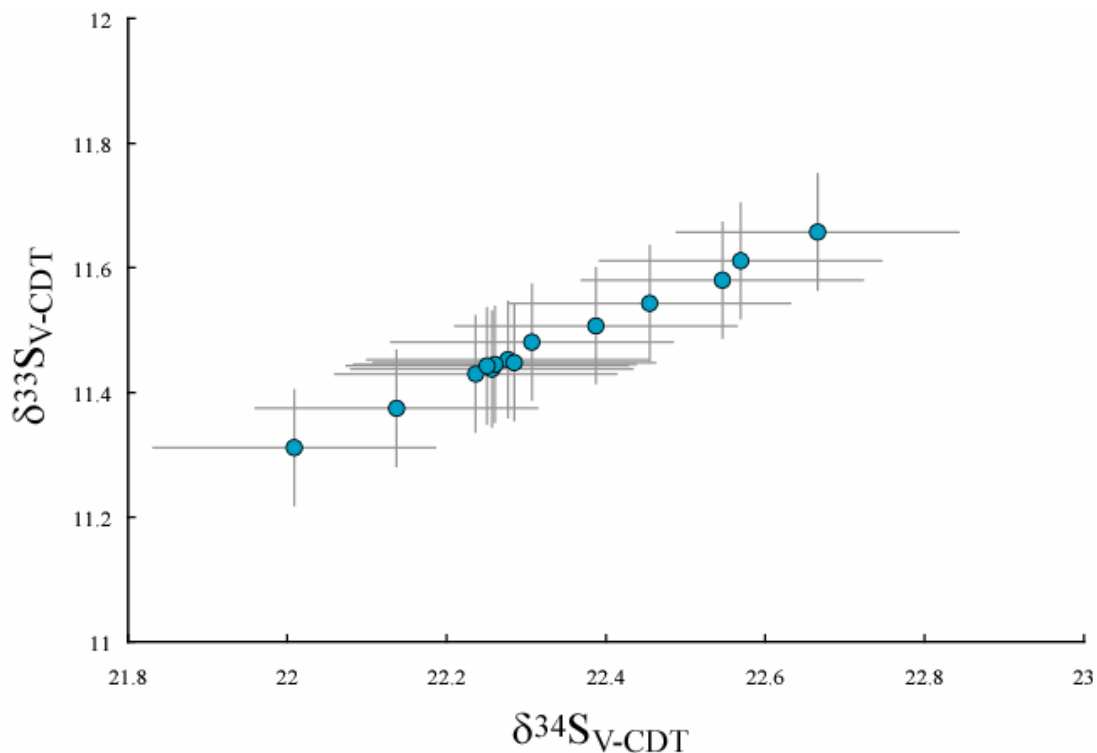
Figure A1: A plot of IAEA S-2 measurements reported in Ono et al. (2006) and normalized according to Table A2. The data are plotted as $\delta^{33}S$ versus $\delta^{34}S$, with errors equivalent to the standard deviation of the population shown. Measurements of other standard materials suggest similar uncertainties. Since the data strongly trend along a line of slope ~ 0.515, the error in $\Delta^{33}S$, which is the deviation from a mass-dependent reference line, is much less than in $\delta^{33}S$.

All standard materials, as well as samples, were fluorinated as clean Ag_2S to limit any sample-dependent variability or matrix effects associated with different mineralogies. However, multiple repeats passed through all wet chemical procedures suggest that the variability associated the wet chemical methods are smaller than those associated with the fluorination (ie. the variability observed on the repeats was within the scatter of the fluorination). Since the uncertainty associated with the wet chemistry cannot be quantified external to the fluorination process, the long-term reproducibility of standard materials is adopted as the best measure of uncertainty. To ensure the accuracy of the measurements, the same standard materials were analyzed throughout the course of this study. In addition, all of the data reported is on samples containing more than 2 μmol S, which equates to ~ 0.5 mg Ag2S and signals on m/e 131 ($^{36}SF_5^+$) over 200 mV (this values will vary depending on the balance, tuning, and how the sample was run).

Accepted value of IAEA S-1 (Wing et al., prep)

$\delta^{33}S$	$\delta^{34}S$	$\delta^{36}S$	$\Delta^{33}S$	$\Delta^{36}S$
-0.060	-0.3	-1.260	0.0944	-0.69

Published values from Ono et al. (2006) for IAEA S-1 at Umd

$\delta^{33}S$	$\delta^{34}S$	$\delta^{36}S$	$\Delta^{33}S$	$\Delta^{36}S$
-2.533	-5.08	-10.310	0.086	-0.68

Composition of Umd Tank SF6 reference gas

$\delta^{33}S$	$\delta^{34}S$	$\delta^{36}S$	$\Delta^{33}S$	$\Delta^{36}S$
-2.47	-4.78	-9.06	-0.0082	0.00

^{33}R	^{34}R	^{36}R
0.99752653	*0.99521857*	*0.99093857*

Table A1: A table explaining the origin of the V-CDT correction. Red values are the literal values that were taken from the publication, whereas the rest of the values are calculated. Values listed from Ono et al. (2006) are normalized to UMd house tank gas. Isotope ratios (in italics) are the correction that is applied to all 'V-CDT' corrected data.

Appendix 2:

The interpretation of all the experimental isotope data begins with the

acknowledgement that these compositions reflect both the fractionation associated

with the sulfate reduction metabolism and two forms of mass balance. First, since

these experiments were run in batch, the experiment itself is subject to closed system,

Rayleigh-like effects. Second, there will be a mass-balance component (mixing)

within the cell as sulfur is back reacted and recycled. Of interest here is the effects

produced by sulfate reduction, thus I recalculate the data as to not consider the mass-

balance effects associated with the batch experimental design, leaving all actual

biological fractionations and cellular mass-balance affects behind for interpretation.

To determine the sulfate reduction component of the observed data I solve:

$$\alpha_{SR} = 1 + \frac{\ln\left|\frac{R_{SO4}}{f_{H2S} * R_{H2S} + [1 - f_{H2S}] * R_{SO4}}\right|}{\ln[1 - f_{H2S}]}, \qquad \text{(A1)}$$

where f_{H2S} (Table A1) is a fraction of sulfide sulfur and R is an isotopic ratio. Also

included in this calculation are the relative concentrations of sulfate and sulfide and

the isotopic composition of the starting sulfide, or effective "blank." I account for the

sulfide blank following: $^{34}\alpha_{\text{reported}} = (^{34}\alpha_{\text{measured}} - ^{34}\alpha_{\text{blank}} f_{\text{blank}})/(1 - f_{\text{blank}})$, where $^{34}\alpha_{\text{blank}}$

is the composition of the inoculum/blank sulfide and f_{blank} is the fraction of total

sulfide contributed by the blank. Although shown in terms of ^{34}S, this form of data

regression is applied to ^{33}S, ^{34}S and ^{36}S. This provides a fractionation factor that is

considered specific to a sulfate reduction experiment (α_{SR}), and does <u>not</u> include the

effects of material balance in the experiment. This fractionation relationship is only

specific to the experiment it describes, and does not represent all sulfate-reducing

microorganisms or even the same strain under different conditions. However, when a suite of unique experiments defines a trend or field, I take that relationship to be representative of the sulfate reduction process. Experiments with sulfur disproportionators do not require this style of data manipulation, because experiments were run until completion, suggesting a quantitative transfer of material.

Raw isotopic measurements for sulfur are reported on a V-CDT scale (see Table A1). Sulfate isotopic compositions range from 2.70 to 32.44‰, -0.150 to 0.033‰ and -0.46 to 1.12‰ in $\delta^{34}S$, $\Delta^{33}S$ and $\Delta^{36}S$ respectively, with an initial starting composition of $\delta^{34}S = 6.18$‰, $\Delta^{33}S = -0.030$‰, and $\Delta^{36}S = 0.16$‰. Sulfide isotopic compositions range from -34.45 to -10.60‰, 0.038 to 0.093‰ and -1.25 to -0.30‰ in $\delta^{34}S$, $\Delta^{33}S$ and $\Delta^{36}S$ respectively, with an initial starting composition, or *blank*, of $\delta^{34}S = -13.12$‰, $\Delta^{33}S = 0.048$‰, and $\Delta^{36}S = -0.87$‰. Contributions from the blank (f_{blank}) can be seen in Table A1. The data can also be presented in terms of the minor isotope relationships, with the observed isotopic compositions defining the line: $\Delta^{36}S = -10.32 (\pm 0.38) \Delta^{33}S -0.200 (\pm 0.024)$, and ranging in $^{33}\lambda_{obs}$ and $^{36}\lambda_{obs}$ from 0.5087-0.5138 and 1.898 – 1.963 respectively.

Table A2: Isotopic compositions and relative concentrations of raw data from experiments described in Chapter 3. All isotopic compositions are corrected to V-CDT, as defined in Appendix 1.

T (°C)	series	$1-f_{H2S}$ (%)	f_{blank} (%)	$\delta^{34}S_{sulfate}$ (‰)	$\Delta^{33}S_{sulfate}$ (‰)	$\Delta^{36}S_{sulfate}$ (‰)	$\delta^{34}S_{sulfide}$ (‰)	$\Delta^{33}S_{sulfide}$ (‰)	$\Delta^{36}S_{sulfide}$ (‰)
2.1	a	0.969	0.588	2.70	-0.032	0.11	-15.99	0.062	-1.09
	b	0.844	0.221	7.53	-0.041	0.11	-17.29	0.071	-0.84
4.2	a	0.955	0.498	6.97	-0.014	-0.25	-17.22	0.067	-1.14
	b	0.956	0.499	8.00	0.033	0.16	-18.12	0.084	-1.25
6.2	a	0.949	0.465	7.89	-0.014	-0.08	-18.34	0.078	-1.14
	b	0.877	0.264	9.15	-0.035	0.03	-17.99	0.081	-0.94
8.3	a	0.954	0.492	7.49	-0.031	0.00	-15.87	0.061	-0.89
	b	0.937	0.411	7.77	0.007	0.22	-17.67	0.065	-1.09
10.3	a	0.737	0.096	10.26	-0.005	0.13	-34.45	0.046	-0.30
	b	0.585	0.144	14.26	-0.031	0.23	-17.60	0.081	-0.93
12.3	a	0.918	0.350	10.12	0.004	0.33	-18.51	0.061	-1.18
	b	0.503	0.082	15.52	-0.003	-0.46	-14.21	0.061	-0.99
14.3	a	0.652	0.113	20.20	-0.064	0.56	-17.54	0.064	-0.81
	b	0.486	0.079	24.00	-0.150	0.78	-15.89	0.080	-1.16
16.3	a	0.877	0.265	9.28	-0.003	-0.06	-16.51	0.079	-0.85
	b	0.776	0.165	11.20	-0.004	0.26	-13.69	0.075	-0.91
18.3	a	0.839	0.216	9.55	-0.022	-0.04	-13.52	0.063	-0.80
	b	0.680	0.121	17.24	-0.085	0.19	-13.95	0.082	-1.21
20.3	a	0.839	0.151	12.33	-0.032	0.178	-13.36	0.077	-0.75
	b	0.751	0.216	12.12	-0.039	0.112	-16.72	0.071	-0.96
21.3	a	0.795	0.178	15.06	-0.012	0.473	-16.78	0.074	-1.11
	b	0.524	0.085	23.05	-0.078	0.534	-13.99	0.078	-0.87
22.3	a	0.616	0.103	14.31	-0.072	0.339	-16.87	0.067	-1.07
	b	0.568	0.093	NA	NA	NA	-12.79	0.084	-0.90
23.2	a	0.754	0.152	13.79	-0.054	0.43	-17.05	0.067	-0.76
	b	0.471	0.077	20.35	-0.049	0.52	-13.26	0.068	-0.87
24.2	a	0.871	0.256	9.12	0.002	-0.06	-15.74	0.062	-0.79
	b	0.596	0.099	13.06	-0.040	-0.01	-17.87	0.075	-0.84
25.2	a	0.658	0.114	16.84	-0.065	0.58	-14.52	0.080	-1.10
	b	0.435	0.073	22.65	-0.063	0.66	-12.23	0.070	-1.03
26.3	a	0.608	0.101	19.05	-0.069	0.53	-14.18	0.070	-0.88
	b	0.357	0.064	NA	NA	NA	-14.94	0.063	-1.05
27.3	a	0.767	0.159	12.02	-0.050	0.53	-14.28	0.069	-1.14
	b	0.308	0.060	24.87	-0.091	0.88	-12.47	0.081	-1.17
28.3	a	0.814	0.192	9.66	-0.041	0.10	-12.23	0.059	-0.96
	b	0.519	0.084	23.89	-0.114	0.74	-12.20	0.072	-1.00
29.3	a	0.663	0.116	16.69	-0.072	0.64	-14.31	0.073	-0.87
	b	0.367	0.065	14.89	-0.056	0.32	-10.85	0.078	-0.95
30.3	a	0.782	0.169	8.07	-0.053	-0.06	-15.50	0.056	-0.98
	b	0.498	0.081	16.78	-0.027	-0.10	-10.78	0.079	-1.01
32.3	a	0.527	0.086	22.03	-0.074	0.67	-11.78	0.054	-1.01
	b	0.252	0.056	32.44	-0.121	1.12	-11.78	0.093	-1.15
34.4	a	0.824	0.201	NA	NA	NA	-10.60	0.058	-0.80
	b	0.818	0.196	10.64	-0.040	0.09	-10.82	0.048	-0.90
36.4	a	0.902	0.306	9.75	-0.006	0.33	-15.34	0.038	-0.84
	b	0.900	0.312	9.06	-0.016	0.04	-14.63	0.047	-0.73
blank				6.18	-0.030	0.16	-13.12	0.048	-0.87

Appendix 3: General chemical methods:

In order to reduce $BaSO_4$ precipitates to Ag_2S for fluorination, I add 25 mL of a

general reduction solution (see recipe below) to a N_2 purged distillation line (N_2 is

also the carrier gas) in order to chemically reduce $BaSO_4$ precipitates to H_2S, which is

captured as ZnS. The reduction solution consists of 125 mL HI, 205 mL HCl, and 61

mL H_2PO_4 (Forrest and Newman, 1977), which is then boiled under a N_2 atmosphere

for 3 hours and filtered (Whatman 1 paper filter) to remove impurities and

precipitates. The product ZnS was converted to Ag_2S through the addition of 2 mL

1M $AgNO_3$, which was later rinsed with 250 mL Milli-Q and 15 mL $NH_4(OH)$.

Chemically reduced sulfates and the original sulfides (all as Ag_2S) were fluorinated

individually with a 10X excess of F_2 to produce SF_6, which was purified

cryogenically (distilled at –110ºC) and chromatograhically (on a 12' molecular sieve

5 Å/Haseq Q column with a TCD).

Gas chromatography analyses were performed using He as a carrier gas, which was

passed through a hydrocarbon trap prior to use. The He flow rate was fixed. The

column oven temperature was run on a 35 minute cycle, with a constant temperature

of 50°C for the first 20 minutes, then ramping at 100°C per minute to 150°C, and held

at that temperature for the remaining 14 minutes. In addition, while at 150°C the

column was back-flushed with He. The detector temperature was held constant at

150°C. The SF_6 peak generally eluted at ~ 11 minutes with a nearly symmetric peak

height of between 2 and 12 mV. The elution time is sample size dependent, with

smaller samples eluting later. The SF_6 peak was physically separated upon elution by

re-directing the GC effluent through a cryogenic trap. The general method calls for one GC pass, however in certain cases, such as when peaks overlapped, strong tailing was observed, or the samples was thought to be heavily contaminated, two passes through the GC were performed.

Clean SF_6 was measured as SF_5^+ (m/e of 127-129, 131) on a Thermofinnigan MAT 253 Gas Source Mass Spectrometer. Samples were originally balanced manually to within 0.1 mbar. Isodat (the software used to run Thermofinnigan instruments) would then balance the sample and standard to (generally) within 20 mV on the 127 cup. Isotopic data are reported relative to either V-CDT (see Appendix 3).

Appendix 4: Calculating errors in λ:

Regardless of the process or magnitude, assessing the uncertainty associated with determinations of mass-dependent slopes (both λ_{obs} and λ_{SR}) is critical. To do so, I use an expression from Bevington and Robinson (2003):

$$\sigma_\lambda = \sqrt{\sigma^2_{\Delta^{33}S} * \left(\frac{\partial\lambda}{\partial\Delta^{33}S}\right)^2 + \sigma^2_{\delta^{34}S} * \left(\frac{\partial\lambda}{\partial\delta^{34}S}\right)^2} ,$$ (A2)

where

$$\frac{\partial\lambda}{\partial\Delta^{33}S} = \left\{ \frac{1}{\ln\left(\frac{\delta^{34}S}{1000}+1\right)} * \frac{1}{\left(\frac{\Delta^{33}S}{1000}+\ln\left(\frac{\delta^{34}S}{1000}+1\right)^{\lambda_{RFL}}\right)} * \frac{1}{1000} \right\}$$ (A3)

and

$$\frac{\partial\lambda}{\partial\delta^{34}S} = \left\{ \frac{1}{\ln\left(\frac{\delta^{34}S}{1000}+1\right)} * \frac{1}{\left(\frac{\Delta^{33}S}{1000}+\ln\left(\frac{\delta^{34}S}{1000}+1\right)^{\lambda_{RFL}}\right)} * \lambda_{RFL}\left(\frac{\delta^{34}S}{1000}+1\right)^{\lambda_{RFL}-1} * \frac{1}{1000} \right\} +$$

$$\left\{ \ln\left(\frac{\Delta^{33}S}{1000}+\ln\left(\frac{\delta^{34}S}{1000}+1\right)^{\lambda_{RFL}}\right) * \frac{-1}{\left(\ln\left[\frac{\delta^{34}S}{1000}+1\right]\right)^2} * \frac{1}{\frac{\delta^{34}S}{1000}+1} * \frac{1}{1000} \right\}$$ (A4)

This formulation does not account for any potential correlated uncertainty between $\delta^{34}S$ and $\Delta^{33}S$, but does incorporate the mass-dependent correlation between the uncertainties of $\delta^{33}S$ and $\delta^{34}S$ (factored into $\sigma_{\Delta33S}$). This expression illustrates the dependence of σ_λ on the magnitude of the $\delta^{34}S$ fractionation. This relationship is generalized in Figure A2, where I plot σ_λ vs. $\delta^{34}S$ for three different sets of

uncertainties ($\sigma_{\delta34S}$- $\sigma_{\Delta33S}$ pairs). Regardless of the analytical errors, as δ^{34}S

approaches zero, σ_λ increases and approaches positive infinity. This exhibits the high

level of confidence that can be placed on slope values that cover large δ^{34}S ranges,

and conversely exposes the large uncertainty in slopes extracted over small δ^{34}S

ranges. This analysis also illustrates the importance of high precision measurements

when making mass-dependent slope arguments over small δ^{34}S ranges.

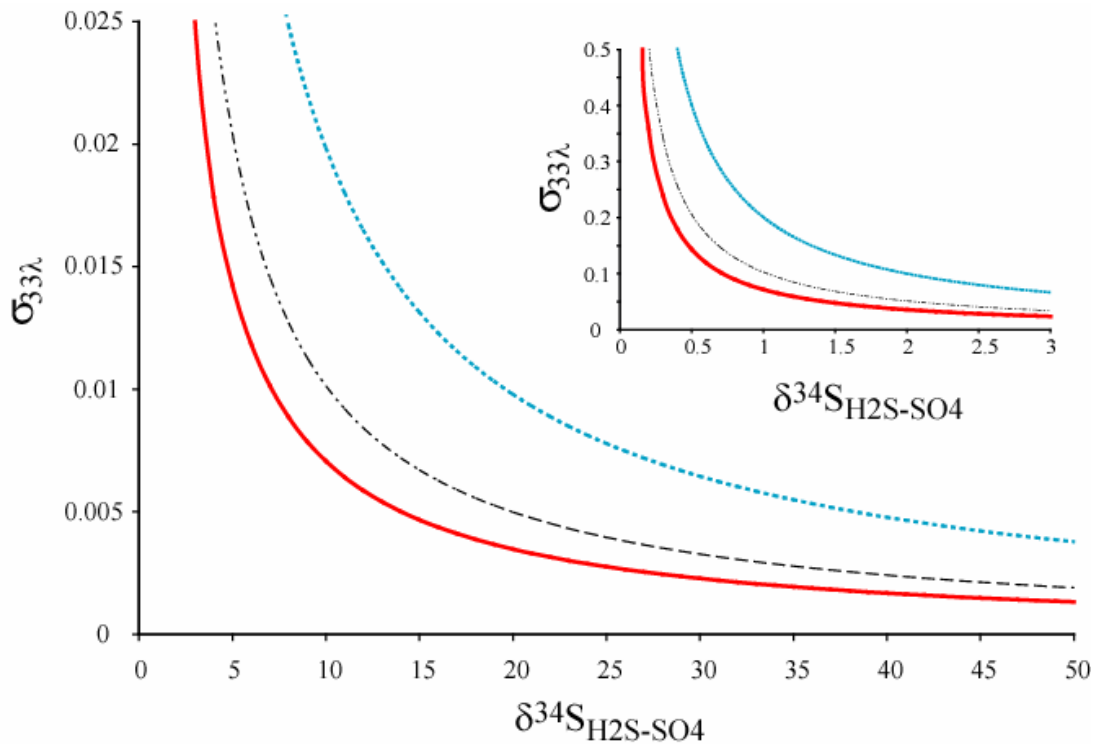**Figure A2: Uncertainties in slope (λ) and a function of the magnitude of fractionation (δ^{34}S). As can be seen, as the magnitude of the fractionation gets larger, the uncertainties associated with the measurements decreases. This allows for precise measures of slope (λ) when the δ^{34}S is large, but also indicates the difficulty in measuring λ when δ^{34}S is small.**

Appendix 5: The isotopic consequences of mass-balance and Rayleigh distillation:

The isotope effects presented in this study are the result of either mass-balance or changes in the process imparting isotopic fractionations. All of these signals can be fully explained with mass-dependent principles, and do not require any non mass-dependent isotope effects. For this reason, this study does not consider isotope effects associated with magnetics (coupled or uncoupled spins), self-shielding, or consequences of changing nuclear geometry. Below, a brief discussion of mass-balance is presented, both as an open and closed (Rayleigh) system. The open system discussion is pedagogic, whereas the Rayleigh discussion is directed at the biological studies presented in Chapters 2 and 3.

Open system: The isotope signatures (Δ^{33}S and Δ^{36}S) discussed throughout this study can be generated as a function of mixing (ie. mass-balance between two, or a series of pools) and/or variability within the processes responsible for the transfer of material between the pools. A simple example of two component mixing is presented in Figure A3. The compositions were solved for by assuming two pools with δ^{34}S values of -50 and +50 ‰. In the case of the blue circles, the values of δ^{33}S were calculated according to $\lambda = 0.515$ ($^{33}\alpha = {}^{34}\alpha^{0.515}$). For the red and gray fields, values of 0.510 ($^{33}\alpha = {}^{34}\alpha^{0.510}$) and 0.520 ($^{33}\alpha = {}^{34}\alpha^{0.520}$) were used. The fundamental point that should be taken from this figure is that even when $\lambda = 0.515$, non-zero Δ^{33}S (and Δ^{36}S) can be produced just through simple mixing. Mathematically, this is because 'δ' values are defined linearly and 'Δ' values are defined exponentially. If the relationship between the pools is not 0.515 (as is the case for the red and gray circles),

an additional signal can be contributed. At present, and for a majority of the material

presented in this study, it is difficult to distinguish between the products of mixing

and the role of different intrinsic processes.
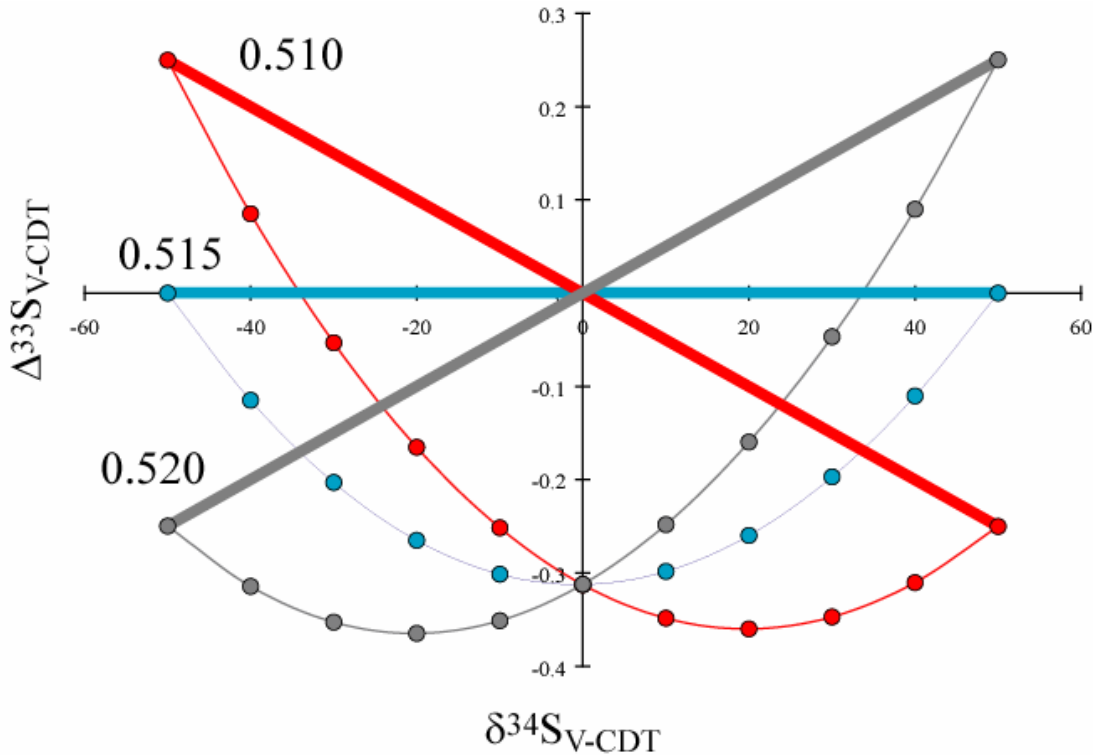
Figure A3: A mixing diagram for δ^{34}S and Δ^{33}S. Circles represent 10% increments in a simple two component mixing model. The original relationship between δ^{34}S and δ^{33}S was varied from 0.510 to 0.520. Since Δ^{33}S is defined using a 0.515 relationship, the tie line between 0% and 100% material transfer is flat.

Closed system: These microbial experiments were run in batch mode, meaning that

they are subject to closed system effects, which I model using typical Rayleigh

fractionation equations (Appendix 2). Below, I examine the effects of closed system

dynamics in terms of both λ and Δ values. If the observed data (V-CDT corrected) is

interpreted and compared to the data that has been processed and the Rayleigh effects

removed, λ values would not significantly shift and do not result in a significant

modification of the overall field represented in Figure 16. Conversely, if I evaluate

the data in terms of Δ values, I see a significant shift in the slope of the Δ^{33}S vs. Δ^{36}S

relationship. The initial observation would then suggest that λ values, which are

calculated independent of δ^{34}S, might be less susceptible to closed system (mass

balance) overprinting. I test this premise with a simple one step Rayleigh

fractionation model with slopes that deviate from 0.5145 and 1.90. I note that the

choice of 0.5145 over 0.515 introduces an inherent deviation on its own. This allows

for a model system with significant mass balance effects (distillation from 0% to

100%), which I use to test the hypothesis derived from the data. When non-

equilibrium values are placed into a Rayleigh fractionation equation, the result is

significant deviation from the case with 0.515 and 1.90. This holds true both when

plotting the results as a function of λ and Δ, and thus differs from the initial

observation of the experimental data. The cause of this inconsistency (between

theory and observation) is significant, and requires further investigation. I suggest,

however, that the variability between theory and observation could be in part

attributable to intra-cellular mass-balance effects, and again points to the need for

further constraints on the internal cycling of sulfur.

References

Abbott S. T. and Sweet I. P. (2000) Tectonic control on third-order sequences in a siliciclastic ramp-style basin: an example from the Roper Superbasin (Mesoproterozoic), northern Australia. *Australian Journal of Earth Sciences* **47**(3), 637-657.

Addison W. D., Brumpton G. R., Vallini D. A., McNaughton N. J., Davis D. W., Kissin S. A., Fralick P. W., and Hammond A. L. (2005) Discovery of distal ejecta from the 1850 Ma Sudbury impact event. *Geology* **33**(3), 193-196.

Akagi, J.M. (1995) Respiratory sulfate reduction. In: Barton, L.L. (Ed.), Sulfate-Reducing Bacteria. Plenum Press, New York, pp. 89–109.

Albert D. B., Taylor C., and Martens C. S. (1995) Sulfate Reduction Rates and Low Molecular-Weight Fatty-Acid Concentrations in the Water Column and Surficial Sediments of the Black-Sea. *Deep-Sea Research Part I-Oceanographic Research Papers* **42**(7), 1239-1260.

Angert, A., Rachmilevitch, S., Barkan, E., and Luz, B., 2003, Effects of photorespiration, the cytochrome pathway, and the alternative pathway on the triple isotopic composition of atmospheric O_2. *Global Biogeochemical Cycles* **17**, Art. No. 1030.

Arnold G. L., Anbar A. D., Barling J., and Lyons T. W. (2004) Molybdenum isotope evidence for widespread anoxia in mid-proterozoic oceans. *Science* **304**(5667), 87-90.

Bak, F., and Pfennig, N. (1987) Chemolithotrophic growth of Desulfovibrio-Sulfodismutans sp-nov by disproportionation of inorganic sulfur-compounds. *Archives of Microbiology* **147**, 184-189.

Bekker A., Holland H. D., Wang P. L., Rumble D., Stein H. J., Hannah J. L., Coetzee L. L., and Beukes N. J. (2004) Dating the rise of atmospheric oxygen. *Nature* **427**(6970), 117-120.

Berner, R. A., Lasaga, A. C., and Garrels, R. M. (1983) The carbonate-silicate geochemical cycle and its effect on atmoshperic carbon dioxide over teh past 100 million years. *American Journal of Science* **283**(7), 641-683.

Berner R. A. (1991) A Model for Atmospheric CO2 over Phanerozoic Time. *American Journal of Science* **291**(4), 339-376.

Berner R. A. and Canfield D. E. (1989) A New Model for Atmospheric Oxygen over Phanerozoic Time. *American Journal of Science* **289**(4), 333-361.

Berner R. A., Lasaga A. C., and Garrels R. M. (1983) The Carbonate-Silicate Geochemical Cycle and Its Effect on Atmospheric Carbon-Dioxide over the Past 100 Million Years. *American Journal of Science* **283**(7), 641-683.

Bevington, P. and Robinson, K. (2003) Data Reduction and Error Analysis for the Physical Sciences. McGraw-Hill Press, New York, pp. 300.

Bigeleisen, J., and Mayer, M. G. (1947) Calculation of Equilibrium Constants for Isotopic Exchange Reactions. *Journal of Chemical Physics* **15**, 261-267.

Bigeleisen, J., and Wolfsberg, M. (1958) Theoretical and experimental aspects of isotope effects in chemical kinetics. *Advances in Chemical Physics* **1**, p. 15-76.

Blunier, T., Barnett, B., Bender, M. L., and Hendricks, M. B. (2002) Biological oxygen productivity during the last 60,000 years from triple oxygen isotope measurements. *Global Biogeochemical Cycles* **16**, art. no. 1029.

Brewer P. G., Spencer D. W., and Bender M. L. (1974) Elemental Composition of Suspended Matter from Northern Argentine Basin. *Transactions-American Geophysical Union* **55**(4), 308-308.

Brocks J. J., Love G. D., Summons R. E., Knoll A. H., Logan G. A., and Bowden S. A. (2005) Biomarker evidence for green and purple sulphur bacteria in a stratified Palaeoproterozoic sea. *Nature* **437**(7060), 866-870.

Brunner B. and Bernasconi S. M. (2005) A revised isotope fractionation model for dissimilatory sulfate reduction in sulfate reducing bacteria. *Geochimica et Cosmochimica Acta* **69**(20), 4759-4771.

Burdett J. W., Arthur M. A., and Richardson M. (1989) A Neogene Seawater Sulfur Isotope Age Curve from Calcareous Pelagic Microfossils. *Earth and Planetary Science Letters* **94**(3-4), 189-198.

Canfield, D. E. (1998) A new model for Proterozoic ocean chemistry. *Nature* **396**, 450-453.

Canfield, D. E. (2001) Biogeochemistry of sulfur isotopes, in J.W. Valley, D.R. Cole eds., *Stable Isotope Geochemistry: Reviews in Mineralogy & Geochemistry* **43**, 607-636.

Canfield, D. E. (2001b) Isotope fractionations by natural populations of sulfate reducing bacteria. *Geochimica et Cosmochimica Acta* **65**(7), 1117-1124.

Canfield D. E. (2004) The evolution of the Earth surface sulfur reservoir. *American Journal of Science* **304**(10), 839-861.

Canfield D. E. (2005) The early history of atmospheric oxygen: Homage to Robert A. Garrels. *Annual Review of Earth and Planetary Sciences* **33**, 1-36.

Canfield, D.E., Raiswell, R., Westrich, JT., Reaves, C.M., and Berner, R.A. (1986) The use of chromium reduction in the anaysis of reduced inorganic sulfur in sediments and shales. *Chemical Geology* **54**, 149-155.

Canfield, D. E., and Thamdrup, B. (1994) The production of ^{34}S depleted sulfide during bacterial disproportionation of elemental sulfur. *Science* **266**, 1973-1975.

Canfield, D. E., and Teske, A. (1996) Late Proterozoic rise in atmospheric oxygen concentration inferred from phylogenetic and sulphur-isotope studies. *Nature* **382**, 127-132.

Canfield, D. E., and Thamdrup, B. (1996) Fate of elemental sulfur in an intertidal sediment. *FEMS Microbiology Ecology* **19**, 95-103.

Canfield, D. E., Thamdrup, B., and Fleischer, S. (1998) Isotope fractionation and sulfur metabolism by pure and enrichment cultures of elemental sulfur-disproportionating bacteria. *Limnology and Oceanography* **43**, 253-264.

Canfield D. E., Habicht K. S., and Thamdrup B. (2000) The Archean sulfur cycle and the early history of atmospheric oxygen. *Science* **288**(5466), 658-661.

Canfield D. E., Olesen C. A., and Cox R. P. (2006) Temperature and its control of isotope fractionation by a sulfate-reducing bacterium. *Geochimica et Cosmochimica Acta,* **70**(3), 548-561.

Canfield, D. E., Poulton, S. W., and Narbonne, G. M. (2007) Late-Neoproterozoic deep-ocean oxygenation and the rise of animal life. *Science* **315**(5808), 92-95.

Castro, H. F., Williams, N. H., and Ogram, A. (2000) Phylogeny of sulfate-reducing bacteria. *FEMS Microbiology Ecology* **31**, 1-9.

Cates N. L. and Mojzsis S. J. (2006) Chemical and isotopic evidence for widespread Eoarchean metasedimentary enclaves in southern West Greenland. *Geochimica et Cosmochimica Acta* **70**(16), 4229-4257.

Chambers, L. A., Trudinger, P. A., Smith, J. W., and Burns, M. S. (1976) Possible boundary-condition in bacterial sulfur isotope fractionation. *Geochimica et Cosmochimica Acta* **40**, 1191-1194.

Claypool G. E., Holser W. T., Kaplan I. R., Sakai H., and Zak I. (1980) The Age Curves of Sulfur and Oxygen Isotopes in Marine Sulfate and Their Mutual Interpretation. *Chemical Geology* **28**(3-4), 199-260.

Cline, J. D. (1969) Spectrophotometric determination of hydrogen sulfide in natural waters. *Limnology and Oceanography* **14**, 454-458.

Coplen T. B., Bohlke J. K., De Bievre P., Ding T., Holden N. E., Hopple J. A., Krouse H. R., Lamberty A., Peiser H. S., Revesz K., Rieder S. E., Rosman K. J. R., Roth E., Taylor P. D. P., Vocke R. D., and Xiao Y. K. (2002) Isotope-abundance variations of selected elements - (IUPAC Technical Report). *Pure and Applied Chemistry* **74**(10), 1987-2017.

Craig H., Horibe Y., Sowers T. (1988) Gravitational separation of gases and isotopes in polar ice caps. *Science* **242**, 1675-1678.

Cypionka, H. (1995) Solute transport and cell energetics. In: Barton, L.L. (Ed.), Sulfate-Reducing Bacteria. Plenum Press, New York, pp. 151–184.

Cypionka, H., Smock, A. M., and Bottcher, M. E. (1998) A combined pathway of sulfur compound disproportionation in Desulfovivrio desulfuricans. *FEMS Microbiology Letters* **166**, 181-186.

Derry L. A., Kaufman A. J., and Jacobsen S. B. (1992) Sedimentary Cycling and Environmental-Change in the Late Proterozoic - Evidence from Stable and Radiogenic Isotopes. *Geochimica et Cosmochimica Acta* **56**(3), 1317-1329.

DesMarais D. J. (1994) Tectonic Control of the Crustal Organic-Carbon Reservoir During the Precambrian. *Chemical Geology* **114**(3-4), 303-314.

Detmers, J., Bruchert, V., Habicht, K. S., and Kuever, J. (2001) Diversity of sulfur isotope fractionations by sulfate-reducing prokaryotes. *Applied and Environmental Microbiology* **67**, 888-894.

Ding T., Valkiers S., Kipphardt H., De Bievre P., Taylor P. D. P., Gonfiantini R., and Krouse R. (2001) Calibrated sulfur isotope abundance ratios of three IAEA sulfur isotope reference materials and V-CDT with a reassessment of the atomic weight of sulfur. *Geochimica et Cosmochimica Acta* **65**(15), 2433-2437.

Evans, D. A. D. (2006) Proterozoic low orbital obliquity and axial-dipolar geomagnetic field from evaporite palaeolatitudes *Nature* **444**(7115), 51-55.

Farquhar, J., Bao, H. M., and Thiemens, M. (2000) Atmospheric influence of Earth's earliest sulfur cycle. *Science* **289**, 756-758.

Farquhar J., Savarino J., Airieau S., and Thiemens M. H. (2001) Observation of wavelength-sensitive mass-independent sulfur isotope effects during SO2 photolysis: Implications for the early atmosphere. *Journal of Geophysical Research-Planets* **106**(E12), 32829-32839.

Farquhar J., Wing B. A., McKeegan K. D., Harris J. W., Cartigny P., and Thiemens M. H. (2002) Mass-independent sulfur of inclusions in diamond and sulfur recycling on early earth. *Science* **298**(5602), 2369-2372.

Farquhar, J., and Wing, B. A. (2003) Multiple sulfur isotopes and the evolution of the atmosphere. *Earth and Planetary Science Letters*, **213**, 1-13.

Farquhar, J., Johnston, D. T., Wing, B. A., Habicht, K. S., Canfield, D. E., Airieau, S. A., and Thiemens, M. H. (2003) Multiple sulfur isotopic interpretations of biosynthetic pathways: Implications for biological signatures in the sulfur isotope record. *Geobiology* **1**, 15-27.

Farquhar, J., and Wing, B. A. (2005) The terrestrial record of stable sulphur isotopes: a review of the implications for the evolution of Earth's sulphur cycle. In Mineral Deposits and Earth Evolution. *Geological Society, London, Special publication*, 167-177.

Fike, D. A., Grotzinger, J. P., Pratt, L. M. and Summons, R. E. (2006) Oxidation of the ediacaran ocean. *Nature* **444**, 744-747.

Finster, K., Liesack, W., and Tindall, B. J. (1997) Desulfospira joergensenii, gen. nov, sp. nov, a new sulfate-reducing bacterium isolated from marine surface sediment. *Systematic and Applied Microbiology* **20**, 201-208.

Finster, K., Liesack, W., and Thamdrup, B., 1998, Elemental sulfur and thiosulfate disproportionation by *Desulfocapsa sulfoexigens* sp. nov., a new anaerobic bacterium isolated from marine surface sediment. *Applied and Environmental Microbiology* **64**, 119-125.

Fitz R. M. and Cypionka H. (1990) Formation of Thiosulfate and Trithionate During Sulfite Reduction by Washed Cells of Desulfovibrio-Desulfuricans. *Archives of Microbiology* **154**(4), 400-406.

Forrest, J., and Newman, L. (1977) Ag-110 microgram sulfate analysis for short time resolution of ambient levels of sulfur aerosol. *Analytical Chemistry* **49**, 1579-1584.

Fralick, P.W. (1988) Microbial bioherms, Lower Proterozoic Gunflint Formation, Thunder Bay, Ontario. *in*, ed. Geldsetzer, H.H.J., James, N.P. and Tebbut, G.E., Reefs. Canada and Adjacent Areas. *Canadian Society of Petroleum Geologists Memoir* **13**, 24-29.

Fralick, P.W. and Barrett, T.J. (1995) Depositional controls on iron formation associations in Canada. In, ed. A.G. Plint, Sedimentary Facies Analysis, *International Association of Sedimentologists Special Publication* **22**, 137-156.

Fralick, P.W., Davis, D.W. and Kissin, S.A. (2002) The age of the Gunflint Formation, Ontario, Canada: single zircon U-Pb age determinations from reworked volcanic ash. *Canadian Journal of Earth Sciences* **39**, 1085-1091.

Fralick, P.W. and Miall, A.D. (1989) Sedimentology of the Lower Huronian Supergroup (Early Proterozoic), Elliot Lake, Ontario, Canada. *Sedimentary Geology* **63**, 127-153.

Frank T. D., Kah L. C., and Lyons T. W. (2003) Changes in organic matter production and accumulation as a mechanism for isotopic evolution in the Mesoproterozoic ocean. *Geological Magazine* **140**(4), 397-420.

Frederiksen, T. M., and Finster, K. (2003) Sulfite-oxido-reductase is involved in the oxidation of sulfite in *Desulfocapsa sulfoexigens* during the disproportionation of thiosulfate and elemental sulfur. *Biodegredation* **14**, 189-198.

Fry, B. (2003) Steady state models of stable isotope distributions. *Isotopes in Environmental and Health Studies* **39**, p. 219-232.

Fry B., Cox J., Gest H., and Hayes J. M. (1986) Discrimination between S-34 and S-32 During Bacterial Metabolism of Inorganic Sulfur-Compounds. *Journal of Bacteriology* **165**(1), 328-330.

Fry B., Ruf W., Gest H., and Hayes J. M. (1988) Sulfur Isotope Effects Associated with Oxidation of Sulfide by O-2 in Aqueous-Solution. Chemical Geology 73(3), 205-210.

Fry B., Jannasch H. W., Molyneaux S. J., Wirsen C. O., Muramoto J. A., and King S. (1991) Stable Isotope Studies of the Carbon, Nitrogen and Sulfur Cycles in the Black-Sea and the Cariaco Trench. *Deep-Sea Research Part a-Oceanographic Research Papers* **38**, S1003-S1019.

Gao X. and Thiemens M. H. (1993) Isotopic Composition and Concentration of Sulfur in Carbonaceous Chondrites. *Geochimica et Cosmochimica Acta* **57**(13), 3159-3169.

Garrels R. M. and Lerman A. (1981) Phanerozoic Cycles of Sedimentary Carbon and Sulfur. *Proceedings of the National Academy of Sciences of the United States of America-Physical Sciences* **78**(8), 4652-4656.

Gellatly, A. M. and Lyons, T. W. (2005) Trace sulfate in mid proterozoic carbonates and the sulfur isotope record biospheric evolution. *Geochim. Cosmochim. et Acta* **69**(15), 3813-3829.

Goldhaber M. B. and Kaplan, I. R. (1975) Controls and consequences of sulfate reduction rates in recent marine sediments. *Soil Science* **119** (1), 42-55.

Goldman S. D. D., Kasting, J., Johnston, D. T. And Farquhar, J. (in press)

Habicht, K. S., Canfield, D. E., and Rethmeier, J. (1998) Sulfur isotope fractionation during bacterial reduction and disproportionation of thiosulfate and sulfite. *Geochimica et Cosmochimica Acta* **62**, 2585-2595.

Habicht, K. S., and Canfield, D. E. (2001) Isotope fractionation by sulfate-reducing natural populations and the isotopic composition of sulfide in marine sediments. *Geology* **29**, 555-558.

Habicht, K. S., Gade, M., Thamdrup, B., Berg, P., and Canfield, D. E. (2002) Calibration of sulfate levels in the Archean Ocean. *Science* **298**, 2372-2374.

Harrison, A. G., and Thode, H. G. (1958) Mechanism of the bacterial reduction of sulphate from isotope fractionation studies. *Transactions of the Faraday Society* **54**, 84-92.

Hayes, J.M., Lambert, I.B., and Strauss, H. (1992) The Sulfur Isotopic Record, in J.W. Schopf, C. Klein eds., *The Proterozoic Biosphere, a multidisciplinary study*, 129-132.

Hayes J. M. (1993) Factors Controlling C-13 Contents of Sedimentary Organic-Compounds - Principles and Evidence. *Marine Geology* **113**(1-2), 111-125.

Hayes, J. M. (2001) Fractionation of carbon and hydrogen isotopes in biosynthetic processes, in J.W. Valley, D.R. Cole eds., *Stable Isotope Geochemistry: Reviews in Mineralogy & Geochemistry* **43**, 225-277.

Heamen, L., Easton, R.M., Hart, T.R., MacDonald, C.A., Fralick, P.W. and Hollings, P. (2005) Proterozoic history of the Lake Nipigon area, Ontario: Constraints from U-Pb zircon and baddelyite dating. *Ontario Exploration and Geoscience Symposium, Toronto, Ontario*, 12-14.

Hemming, S.R., McLennan, S.M. and Hanson, G.N. (1995) Geochemical and Nd/Pb isotopic evidence for the provenance of the Early Proterozoic Virginia Formation, Minnesota. Implications for tectonic setting of the Animikie Basin. *Journal of Geology* **103**, 147-168.

Hoek, J., Reysenbach, A. L., Habicht, K. S., Canfield, D. E. (2006) Effect of hydrogen limitation and temperature on the fractionation of sulfur isotopes by a deep-sea hydrothermal vent sulfate-reducing bacterium. *Geochimica et Cosmochimica Acta*, **70**, 5831-5841.

Hoffman, P.F. (1987) Early Proterozoic foredeeps, foredeep magmatism and Superior-type iron-formations of the Canadian shield. In, ed. Kroner, A., Proterozoic Lithospheric Evolution, *American Geophysical Union Series* **17**, 85-98.

Hoffman P. F., Kaufman A. J., Halverson G. P., and Schrag D. P. (1998) A Neoproterozoic snowball earth. *Science* **281**(5381), 1342-1346.

Holland, H. D. (2006) The oxygenation of the atmosphere and oceans. *Philosophical Translations of the Royal Society.* **361**(1470), 903-915.

Holser W. T., Kaplan, I. R. Sakai, H., and Zak, I. (1979) Isotope geochemistry of oxygen in the sedimentary sulfate cycle. *Chemical Geology* **25** (1-2), 1-17.

Hu G. X., Rumble D., and Wang P. L. (2003) An ultraviolet laser microprobe for the in situ analysis of multisulfur isotopes and its use in measuring Archean sulfur isotope mass-independent anomalies. *Geochimica et Cosmochimica Acta* **67**(17), 3101-3118.

Hulston, J. R., Thode, H. G. (1965) Cosmic Ray Produced ^{36}S and ^{33}S in Metallic Phase of Iron Meteorites. *Journal of Geophysical Research* **70**, 4435-4442.

Hurtgen, M. T., Arthur, M. A., Suits, N. S., and Kaufman, A. J. (2002) The sulfur isotopic composition of Neoproterozoic seawater sulfate: implications for a snowball Earth? *Earth and Planetary Science Letters* **203**, 413-429.

Hurtgen, M. T., Arthur, M. A., and Galverson, G. P. (2005) Neoproterozoic sulfur isotopes, the evolution of microbial sulfur species, and the burial efficiency of sulfide as sedimentary pyrite. *Geology* **33** (1), 41-44.

Il'chencko, S.V., and Sorokin, Y.I. (1991) K otsenke intensivnosti obrazovaniya serovodoroda v Chernom more (To the estimate of hydrogen sulfide production in the Black Sea). *in* Ed. Vinogradov, M.E., The Black Sea ecosystem variability: natural and anthropogenic factors. Nauka, Moscow, 73-77 (in Russian).

Jackson, M. J., Muir, M. D., and Plumb, K. A.(1987) Geology of the southern McArthur Basin, Northern Territory. *Bureau of Mineral Resources Bulletin* **220**.

Johnston, D.T., Wing, B.A., Farquhar, J., Kaufman, A.J., Strauss, H., Lyons, T.W., Kah, L.C., Canfield, D.E. (2005a) Active microbial sulfur disproportionation in the Mesoproterozoic. *Science* **310**, 1477-1479.

Johnston, D.T., Farquhar, J., Wing, B.A., Kaufman, A.J., Canfield, D.E., Habicht, K. S. (2005b) Multiple sulfur isotope fractionation in biological systems. *American Journal of Science* **305**, 645-660.

Johnston D. T., Poulton S.W., Farquhar J., Wing B. A., Fralick P.W., and Canfield D. E. (2006) Evolution of the oceanic sulfur cycle in the late Paleoproterozoic. *Geochimica et Cosmochimica Acta* **70**(23), 5723-5739.

Jørgensen, B.B. (1977) Sulfur cycle of coastal marine sediments. *Limno and Ocean* **22**(5) 814-832.

Jørgensen, B. B. (1982) Mineralization of organic-matter in the sea bed - the role of sulfate reduction. *Nature* **296**, 643-645.

Jørgensen, B. B. (1990a) The sulfur cycle of fresh-water sediments - role of thiosulfate. *Limnology and Oceanography* **35**, 1329-1342.

Jørgensen, B. B. (1990b) A thiosulfate shunt in the sulfur cycle of marine-sediments. *Science* **249**, 152-154.

Jørgensen, B. B., and Bak, F. (1991) Pathways and microbiology of thiosulfate transformations and sulfate reduction in a marine sediment (Kattegat, Denmark). *Applied and Environmental Microbiology* **57**, 847-856.

Jørgensen B. B., Fossing H., Wirsen C. O., and Jannasch H. W. (1991) Sulfide Oxidation in the Anoxic Black-Sea Chemocline. *Deep-Sea Research Part a-Oceanographic Research Papers* **38**, S1083-S1103.

Jorgensen, B. B. and Kasten, S. 2006 (2006) Sulfur cycling and methane oxidation, in H.D. Shultz, Z. Mattias eds., *Marine Geochemistry*, 271-309.

Kah L. C., Lyons T. W., and Frank T. D. (2004) Low marine sulphate and protracted oxygenation of the proterozoic biosphere. *Nature* **431**(7010), 834-838.

Kampschulte A. and Strauss H. (2004) The sulfur isotopic evolution of Phanerozoic seawater based on the analysis of structurally substituted sulfate in carbonates. *Chemical Geology* **204**(3-4), 255-286.

Kaplan, I. R., and Rittenberg, S. C. (1964) Microbiological fractionation of sulphur isotopes. *Journal of General Microbiology* **34**, 195-212.

Kaplan, I.R. (1975) Stable isotopes as a guide to biogeochemical processes. *Proceedings of the Royal Society of London. Series B, Biological Sciences* **189**, 183-211.

Karhu J. A. and Holland H. D. (1996) Carbon isotopes and the rise of atmospheric oxygen. *Geology* **24**(10), 867-870.

Kaufman A. J., Jacobsen S. B., and Knoll A. H. (1993) The Vendian Record of Sr and C-Isotopic Variations in Seawater - Implications for Tectonics and Paleoclimate. *Earth and Planetary Science Letters* **120**(3-4), 409-430

Kaufman A. J. and Knoll A. H. (1995) Neoproterozoic Variations in the C-Isotopic Composition of Seawater - Stratigraphic and Biogeochemical Implications. *Precambrian Research* **73**(1-4), 27-49.

Kaufman A. J., Knoll A. H., and Narbonne G. M. (1997) Isotopes, ice ages, and terminal Proterozoic earth history. *Proceedings of the National Academy of Sciences of the United States of America* **94**(13), 6600-6605.

Kemp, A. L. W., and Thode, H. G. (1968) Mechanism of bacterial reduction of sulphate and of sulphite from isotope fractionation studies. *Geochimica et Cosmochimica Acta* **32**, 71-91.

Knoll A. H. (1994) Proterozoic and Early Cambrian Protists - Evidence for Accelerating Evolutionary Tempo. *Proceedings of the National Academy of Sciences of the United States of America* **91**(15), 6743-6750.

Kobayash.K, Takahash.E, and Ishimoto M. (1972) Biochemical Studies on Sulfate-Reducing Bacteria .11. Purification and Some Properties of Sulfite Reductase, Desulfoviridin. *Journal of Biochemistry* **72**(4), 879-.

Kopp R. E., Kirschvink J. L., Hilburn I. A., and Nash C. Z. (2005) The paleoproterozoic snowball Earth: A climate disaster triggered by the evolution of oxygenic photosynthesis. *Proceedings of the National Academy of Sciences of the United States of America* **102**(32), 11131-11136

Krogh,T.E., Davis, D.W. and Corfu, F. (1984) Precise U-Pb zircon and baddeleyite ages for the Sudbury area. In, ed. E.G. Pye, The geology and ore deposits of the Sudbury structure. *Ontario Geological Survey Special Volume* **1**, 431-446.

Krouse H. R. and Coplen T. B. (1997) Reporting of relative sulfur isotope-ratio data (technical report). *Pure and Applied Chemistry* **69**(2), 293-295.

Kump L. R., Pavlov A., and Arthur M. A. (2005) Massive release of hydrogen sulfide to the surface ocean and atmosphere during intervals of oceanic anoxia. *Geology* **33**(5), 397-400.

Logan G. A., Hayes J. M., Hieshima G. B., and Summons R. E. (1995) Terminal
Proterozoic Reorganization of Biogeochemical Cycles. *Nature* **376**(6535), 53-56.

Lucente, M.E. and Morey, G.B. (1983) Stratigraphy and sedimentology of the lower
Proterozoic Verginia Formation, northern Minnesota. *Minnesota Geological
Survey Report of Investigations* **28**, 28.

Luepke J. J. and Lyons T. W. (2001) Pre-Rodinian (Mesoproterozoic)
supercontinental rifting along the western margin of Laurentia: geochemical
evidence from the Belt-Purcell Supergroup. *Precambrian Research* **111**(1-4),
79-90.

Luther G. W., Church T. M., and Powell D. (1991) Sulfur Speciation and Sulfide
Oxidation in the Water Column of the Black-Sea. *Deep-Sea Research Part a-
Oceanographic Research Papers* **38**, S1121-S1137.

Lyons, T.W., Walter, L.M., Gellatly, A.M., Martini, A.M., and Blake, R.E. (2004)
Sites of anomalous organic remineralization in the carbonate sediments of
South Florida, U.S.A.: The sulfur cycle and carbonate-associated sulfate, *in*
Amend, J., Edwards, K., and Lyons, T. (eds.), Sulfur Biogeochemistry—Past
and Present: *Geological Society of America Special Paper* **379**, p. 161-176.

Maric, M. and Fralick, P.W. (2005) Sedimentology of the Rove and Virginia
Formations and their tectonic significance. *Institute on Lake Superior Geology*
51, 41-42.

Matsuhisa, Y., Goldsmith, J. R., and Clayton, R. N. (1978) Mechanisms of
Hydrothermal Crystallization of Quartz at 250-Degrees-C and 15 Kbar.
Geochimica et Cosmochimica Acta **42**, 173-182.

Miller, M. F. (2002) Isotopic fractionation and the quantification of ^{17}O anomalies in
the oxygen three-isotope system: an appraisal and geochemical significance.
Geochimica et Cosmochimica Acta **66**, 1881-1889.

Millero F. J., Hubinger S., Fernandez M., and Garnett S. (1987) Oxidation of H_2S in
Seawater as a Function of Temperature, Ph, and Ionic-Strength.
Environmental Science & Technology **21**(5), 439-443.

Mook, W. G. (2000) Environmental isotopes in the hydrological cycle principles and
applications, V I: Introduction- Theory, Methods, Review, **1**: Paris,
UNESCO/IAEA.

Morey, G.B. (1973) Stratigraphic framework of middle Proterozoic rocks in Minnesota. In, ed. G.M. Young, Huronian Stratigraphy and Sedimentation. *Geological Association of Canada Special Paper* **12**, 211-249.

Mojzsis S. J., Coath C. D., Greenwood J. P., McKeegan K. D., and Harrison T. M. (2003) Mass-independent isotope effects in Archean (2.5 to 3.8 Ga) sedimentary sulfides determined by ion microprobe analysis. *Geochimica et Cosmochimica Acta* **67**(9), 1635-1658.

Muramoto J. A., Honjo S., Fry B., Hay B. J., Howarth R. W., and Cisne J. L. (1991) Sulfur, Iron and Organic-Carbon Fluxes in the Black-Sea - Sulfur Isotopic Evidence for Origin of Sulfur Fluxes. *Deep-Sea Research Part a-Oceanographic Research Papers* **38**, S1151-S1187.

Murray J. W., Top Z., and Ozsoy E. (1991) Hydrographic Properties and Ventilation of the Black-Sea. *Deep-Sea Research Part a-Oceanographic Research Papers* **38**, S663-S689.

Neretin L. N., Volkov, II, Bottcher M. E., and Grinenko V. A. (2001) A sulfur budget for the Black Sea anoxic zone. *Deep-Sea Research Part I-Oceanographic Research Papers* **48**(12), 2569-2593.

Neretin L. N., Bottcher M. E., and Grinenko V. A. (2003) Sulfur isotope geochemistry of the Black Sea water column. *Chemical Geology* **200**(1-2), 59-69.

Ohmoto H. (1986) Stable Isotope Geochemistry of Ore-Deposits. *Reviews in Mineralogy* **16**, 491-559.

Ohmoto H., Watanabe Y., Ikemi H., Poulson S. R., and Taylor B. E. (2006) Sulphur isotope evidence for an oxic Archaean atmosphere. *Nature* **442**(7105), 908-911.

Ojakangas, R.W. (1983) Tidal deposits in the Early Proterozoic basin of the Lake Superior region - The Palms and Pokegama Formations: Evidence for subtidal-shelf deposition of Superior-type banded iron-formation. In, ed. Medaris, L.G., *Early Proterozoic Geology of the Great Lakes Region, Geological Society of America Memoir* **160**, 49-66.

Ojakangas, R.W., Morey, G.B. and Southwick, D.L. (2001) Palaeoproterozoic basin development and sedimentation in the Lake Superior region, North America. *Sedimentary Geology* **141**, 319-341.

Ono, S., Eigenbrode, J. L., Pavlov, A. A., Kharecha, P., Rumble, D., Kasting, J. F., Freeman, K. H. (2003) New insights into Archean sulfur cycle from mass-independent sulfur isotope records from the Hamersley Basin, Australia.

Earth and Planetary Science Letters **213**, 15-30.

Ono S., Wing B., Johnston D., Farquhar J., and Rumble D. (2006) Mass-dependent fractionation of quadruple stable sulfur isotope system as a new tracer of sulfur biogeochemical cycles. *Geochimica et Cosmochimica Acta* **70**(9), 2238-2252.

Ono S., Beukes N. J., Rumble D., and Fogel M. L. (2006) Early evolution of atmospheric oxygen from multiple-sulfur and carbon isotope records of the 2.9 Ga Mozaan Group of the Pongola Supergroup, Southern Africa. *South African Journal of Geology* **109**(1-2), 97-108.

Ono, S., Shanks, W. C., Rouxel, O. J., and Rumble, D. (2007) S-33 constraints on the seawater sulfate contribution in modern seafloor hydrothermal vent sulfides. *Geochimica et Cosmochimica Acta* **71**(5), 1170-1182.

Page R. W. and Sweet I. P. (1998) Geochronology of basin phases in the western Mt Isa Inlier, and correlation with the McArthur Basin. *Australian Journal of Earth Sciences* **45**(2), 219-232.

Papineau D., Mojzsis S. J., Coath C. D., Karhu J. A., and McKeegan K. D. (2005) Multiple sulfur isotopes of sulfides from sediments in the aftermath of Paleoproterozoic glaciations. *Geochimica et Cosmochimica Acta* **69**(21), 5033-5060.

Papineau, D., Mojzsis, S. J., and Schmitt, A. K. (2007) Multiple sulfur isotopes from Paleoproterozoic Huronian interglacial sediments and the rise of atmospheric oxygen. *Earth and Planetary Science Letters* **255**, 188-212.

Pavlov A. A. and Kasting J. F. (2002) Mass-independent fractionation of sulfur isotopes in Archean sediments: Strong evidence for an anoxic Archean atmosphere. *Astrobiology* **2**(1), 27-41.

Paytan, A., Kastner, M. Campbell, D. and Thiemens, M. H. (1998) The sulfur isotopic composition of Cenozoic seawater sulfate. *Science* **282** (5393), 1459-1462.

Paytan, A., Kastner, M. Campbell, D. and Thiemens, M. H. (2004) Seawater sulfate isotope fluctuation is the cretaceous. *Science* **304** (5677), 1663-1665.

Peck, H. D. (1959) The ATP-dependent reduction of sulfate with hydrogen in extracts of Desulfovibrio desulfuricans. *Proceedings of the National Academy of Sciences of the United States of America* **45**, 701-708.

Peck, H. D. (1961) Evidence for reversibility of reaction catalyzed by Adenosine 5'-Phosphosulfate reductase. *Biochimica et Biophysica Acta* **49**, 621-624.

Poulton S. W., Fralick P. W., and Canfield D. E. (2004) The transition to a sulphidic ocean ~ 1.84 billion years ago. *Nature* **431**(7005), 173-177.

Poulton, S.W., and Canfield, D.E. (2005) Development of a sequential extraction procedure for iron: implications for iron partitioning in continentally derived particulates. *Chemical Geology* **214** (3-4), 209-221.

Pufahl, P.K. and Fralick, P.W. (1995) Paleogeographic reconstruction of the Gunflint-Mesabi-Cuyuna depositional system: a basin analysis approach. *Proceedings of the Institute on Lake Superior Geology* **41**, 59-60.

Pufahl, P.K. and Fralick, P.W. (2004) Depositional controls on Paleoproterozoic iron formation accumulation, Gogebic Range, Lake Superior region, USA. *Sedimentology* **51**, 791-808.

Pufahl, P.K., Fralick, P.W. and Scott, J. (2000) Depositional environments of the Palaeoproterozoic Gunflint Formation. *in*, ed. P.W. Fralick, *Institute of Lake Superior Geology Field Guide* **46**, 46.

Rabus R., Bruchert V., Amann J., and Konneke M. (2002) Physiological response to temperature changes of the marine, sulfate-reducing bacterium Desulfobacterium autotrophicum. *Fems Microbiology Ecology* **42**(3), 409-417.

Rees, C. E. (1973) Steady-state model for sulfur isotope fractionation in bacterial reduction processes. *Geochimica et Cosmochimica Acta* **37**, 1141-1162.

Rees, C. E. (1978) Sulphur isotope measurements using SO_2 and SF_6. *Geochimica et Cosmochimica Acta* **42**, 383-389.

Ross D. A., Degens E. T., and Macilvai.J. (1970) Black Sea - Recent Sedimentary History. *Science* **170**(3954), 163-165.

Rouxel O. J., Bekker A., and Edwards K. J. (2005) Iron isotope constraints on the Archean and Paleoproterozoic ocean redox state. *Science* **307**(5712), 1088-1091.

Rudnicki M. D., Wilson P. A., and Anderson W. T. (2001) Numerical models of diagenesis, sediment properties, and pore fluid chemistry on a paleoceanographic transect: Blake Nose, Ocean Drilling Program Leg 171B. *Paleoceanography* **16**(6), 563-575.

Schauble, E. A. (2004) Applying stable isotope fractionation theory to new systems, in C.M. Johnson, B.L. Beard, and F. Albarede, eds., *Geochemistry of Non-Traditional Stable Isotopes: Reviews in Mineralogy & Geochemistry* **54**, 65-111.

Scherer, S., Neuhaus, K. (2002) Life at low temperatures. In: Balows, A., Truper, H.G., Dworkin, M., Harder, W., Schleifer, K.H. (Eds.), The Prokaryotes: An Evolving Electronic Resource for the Microbiological Community, third edition, release 3.9, April 1 2002, Springer, New York. Available from: <http://link.springer-ny.com/link/service/books/10125>.

Scott D. L., Rawlings D. J., Page R. W., Tarlowski C. Z., Idnurm M., Jackson M. J., and Southgate P. N. (2000) Basement framework and geodynamic evolution of the Palaeoproterozoic superbasins of north-central Australia: an integrated review of geochemical, geochronological and geophysical data. *Australian Journal of Earth Sciences* **47**(3), 341-380.

Shen, Y. A., Buick, R., and Canfield, D. E. (2001) Isotopic evidence for microbial sulphate reduction in the early Archaean era. *Nature* **410**, 77-81.

Shen Y. N., Canfield D. E., and Knoll A. H. (2002) Middle Proterozoic ocean chemistry: Evidence from the McArthur Basin, northern Australia. *American Journal of Science* **302**(2), 81-109.

Shen Y., Knoll A. H., and Walter M. R. (2003) Evidence for low sulphate and anoxia in a mid-Proterozoic marine basin. *Nature* **423**(6940), 632-635.

Shen Y. N. and Buick R. (2004) The antiquity of microbial sulfate reduction. *Earth-Science Reviews* **64**(3-4), 243-272.

Sims, P.K., Van Schmus, W.R., Schulz, K.J. and Peterman, Z.E. (1989) Tectonostratigraphic evolution of the Early Proterozoic Wisconsin magmatic terranes of the Penokean orogen. *Canadian Journal of Earth Sciences* **26**, 2145-2158.

Sørensen K. B. and Canfield D. E. (2004) Annual fluctuations in sulfur isotope fractionation in the water column of a euxinic marine basin. *Geochimica et Cosmochimica Acta* **68**(3), 503-515.

Southwick, D.L. and Morey, G.B. (1991) Tectonic imbrication and foredeep development in the Penokean Orogen, east-central Minnesota - an interpretation based on regional geophysics and the results of test-drilling. *United States Geological Survey Bulletin*, **1904-C**, 17.

Strauss H. (1993) The Sulfur Isotopic Record of Precambrian Sulfates - New Data and a Critical-Evaluation of the Existing Record. *Precambrian Research* **63**(3-4), 225-246.

Strauss H. (1997) The isotopic composition of sedimentary sulfur through time. *Palaeogeography Palaeoclimatology Palaeoecology* **132**(1-4), 97-118.

Strauss, H. (2004) 4 Ga of seawater evolution. *in* Amend, J., Edwards, K., and Lyons, T. (eds.), Sulfur Biogeochemistry—Past and Present: *Geological Society of America Special Paper* **379**, 195-210.

Sweeney R. E. and Kaplan I. R. (1980) Stable Isotope Composition of Dissolved Sulfate and Hydrogen-Sulfide in the Black-Sea. *Marine Chemistry* **9**(2), 145-152.

Thamdrup, B., Canfield, D. E., Ferdelman, T. G., Glud, R. N., and Gundersen, J. K. (1996) A biogeochemical survey of the anoxic basin Golfo Dulce, Costa Rica. *Revista De Biologia Tropical* **44**, 19-33.

Thamdrup, B., Finster, K., Fossing, H., Hansen, J. W., and Jorgensen, B. B. (1994) Thiosulfate and sulfite distributions in porewater of marine-sediments related to manganese, iron, and sulfur geochemistry. *Geochimica et Cosmochimica Acta* **58**, 67-73.

Thamdrup, B., Finster, K., Hansen, J. W., and Bak, F. (1993) Bacterial disproportionation of elemental sulfur coupled to chemical-reduction of iron or manganese. *Applied and Environmental Microbiology* **59**, 101-108.

Thiemens M. H. (1999) Atmosphere science - Mass-independent isotope effects in planetary atmospheres and the early solar system. *Science* **283**(5400), 341-345.

Thiemens M. H. (2006) History and applications of mass-independent isotope effects. *Annual Review of Earth and Planetary Sciences* **34**, 217-262.

Thode, H. G Kleerekoper, H., McElcheran, D.E. (1951) Sulphur isotope fractionation in the bacterial reduction of sulphate. *Res. London* **4**, 581–582.

Thode, H. G., Monster, J., and Dunford, H. B. (1961) Sulphur isotope geochemistry. *Geochimica et Cosmochimica Acta* **25**, 159-174.

Tolmazin D. (1985) Changing Coastal Oceanography of the Black-Sea .1. Northwestern Shelf. *Progress in Oceanography* **15**(4), 217-276.

Troelsen, H., and Jørgensen, B. B. (1982) Seasonal dynamics of elemental sulfur in 2 coastal sediments. *Estuarine Coastal and Shelf Science* **15**, 255-266.

Turchyn, A. V. and Schrag, D. P. (2004) Oxygen isotope constraints on the sulfur cycle over the past 10 million years. *Science* **303**(5666), 2004-2007.

Urey, H. C. (1947) The thermodynamic properties of isotopic substances. *Journal of the Chemical Society*, 562-581.

Van Wyck, N. and Johnson, C.M. (1997) Common lead, Sm-Nd, and U-Pb constraints on petrogenesis, crustal architecture and tectonic setting of the Penokean Orogen (Paleoproterozoic) in Wisconsin, U.S.A. *Geological Society of America Bulletin* **109**, 799-808.

Walker, J.C.G., and Bimblecombe, P. (1985) Iron and sulfur in the pre-biologic ocean. *Precambrian Research* **28**(3-4), 205-222.

Wentzien S. W. and Sand W. (2004) Tetrathionate disproportionation by Thiomonas intermedia K12. *Engineering in Life Sciences* **4**(1), 25-30.

Whitehouse M. J., Kamber B. S., Fedo C. M., and Lepland A. (2005) Integrated Pb- and S-isotope investigation of sulphide minerals from the early Archaean of southwest Greenland. *Chemical Geology* **222**(1-2), 112-131.

Williams, J. S. (1967) Variance of weighted regression estimators. *Journal of the American Statistical Association* **62**, 1290-1301.

Wing, B.A, Lyons, J.R., and Farquhar, J. (2004) Experimental constraints on anomolous S-isotopic fractionation during UV irradiation of SO_2. *Geochimica et Cosmochimica Acta* **68**(11), A781-A781.

Wortmann U. G., Bernasconi S. M., and Bottcher M. E. (2001) Hypersulfidic deep biosphere indicates extreme sulfur isotope fractionation during single-step microbial sulfate reduction. *Geology* **29**(7), 647-650.

Young, E. D., and Galy, A. (2004) The isotope geochemistry and cosmochemistry of magnesium, in C.M. Johnson, B.L. Beard, and F. Albarede, eds., *Geochemistry of Non-Traditional Stable Isotopes: Reviews in Mineralogy & Geochemistry* **54**, 197-230.

Young, E. D., Galy, A., and Nagahara, H. (2002) Kinetic and equilibrium mass-dependent isotope fractionation laws in nature and their geochemical and cosmochemical significance. *Geochimica et Cosmochimica Acta* **66**, 1095-1104.

Zhao G.C., Sun M., Wilde S.A., and Li S.Z. (2004) A Paleo-Mesoproterozoic supercontinent: assembly, growth and breakup. *Earth Science Reviews* **67** (1-2), 91-123.

Zmolek P., Xu X. P., Jackson T., Thiemens M. H., and Trogler W. C. (1999) Large mass independent sulfur isotope fractionations during the photopolymerization of (CS2)-C-12 and (CS2)-C-13. *Journal of Physical Chemistry A* **103**(15), 2477-2480.